GRWD1 mediates Kaposi's sarcoma-associated herpesvirus epigenetic reprogramming in cellular transformation

by

Shan Wei

B.S., University of Calgary, 2014

M.S., University of Southern California, 2016

Submitted to the Graduate Faculty of the

School of Medicine in partial fulfillment

of the requirements for the degree of

Doctor of Philosophy

University of Pittsburgh

2022

UNIVERSITY OF PITTSBURGH

SCHOOL OF MEDICINE

This dissertation was presented

by

Shan Wei

It was defended on

March 28, 2022

and approved by

Yuan Chang, M.D., Distinguished Professor, Department of Pathology

Lin Zhang, Ph.D., Professor, Department of Pharmacology and Chemical Biology

Kathy H.Y. Shair, Ph.D., Assistant Professor, Department of Microbiology and Molecular Genetics

Nara Lee, Ph.D., Assistant Professor, Department of Microbiology and Molecular Genetics

Dissertation Director: Shou-Jiang Gao, Ph.D., Professor, Department of Microbiology and Molecular Genetics

GRWD1 mediates Kaposi's sarcoma-associated herpesvirus epigenetic reprogramming in cellular transformation

Shan Wei, Ph.D.

University of Pittsburgh, 2022

Kaposi's sarcoma-associated herpesvirus (KSHV) infection is causally associated with numerous cancers. The mechanism of KSHV-induced oncogenesis remains unclear. By performing a CRISPR-Cas9 screening in a model of KSHV-induced cellular transformation of primary cells, we identified epigenetic regulators that were essential for KSHV-induced cellular transformation. Examination of TCGA data sets of the top 9 genes, including glutamate-rich WD repeat containing 1 (GRWD1), a WD40 family protein upregulated by KSHV, that had positive effects on cell proliferation and survival of KSHV-transformed cells (KMM) but not the matched primary cells (MM), uncovered the predictive values of their expressions for patient survival in numerous types of cancer. We revealed global epigenetic remodeling including H3K4me3 epigenetic active mark in KMM cells compared to MM cells. Knockdown of GRWD1 inhibited cell proliferation, cellular transformation, and tumor formation and caused downregulation of the global H3K4me3 mark in KMM cells. GRWD1 interacted with WD repeat domain 5 (WDR5), the core protein of the H3K4 methyltransferase complex, and several H3K4me3 methyltransferases, including myeloid leukemia 2 (MLL2). Knockdown of WDR5 and MLL2 phenocopied GRWD1 knockdown, caused the global reduction of the H3K4me3 mark and altered the expression of similar sets of genes. Transcriptome sequencing (RNA-seq) and chromatin immunoprecipitation sequencing (ChIP-seq) analyses further identified common and distinct cellular genes and

pathways that were regulated by GRWD1, WDR5, and MLL2. These results indicate that KSHV hijacks the GRWD1-WDR5-MLL2 epigenetic complex to regulate H3K4me3 methylation of specific genes, which is essential for KSHV-induced cellular transformation. Our work has identified an epigenetic complex as a novel therapeutic target for KSHV-induced cancers.

Table of Contents

List of Tables

List of Figures

Acknowledgments

Foremost, I would like to express my sincere gratitude to my mentor and thesis committee chair Dr. Shou-Jiang Gao for his continuous guidance and support of my Ph.D. study and my research. I have been amazingly fortunate to have an advisor who provided me the outstanding opportunities in research training and gave me the freedom to choose my research projects. I am grateful for his patience, motivation, enthusiasm, immense knowledge, and all the valuable discussions about my experiments.

Besides my mentor, I would like to thank the rest of my dissertation committee: Dr. Yuan Chang, Dr. Lin Zhang, Dr. Kathy Shair, and Dr. Nara Lee, for their kind support and insightful knowledge, as well as for their wonderful suggestions I had taken.

My sincere thanks also go to Dr. Robert Binder and Dr. Jennifer Bomberger as the Directors of the Program in Microbiology and Immunology for guiding me through my Ph.D. study and for all their valuable and helpful advice.

I would like to express my appreciation to all the current and former Gao lab members as well as our bioinformatic collaborators Dr. Xinghua Lu, Dr. Songjian Lu, and Dr. Lifan Liang for all the help they have given me and for all the good time we have had together.

Additionally, I would like to especially thank Dr. Amy Lee and Dr. Zoltan Tokes at the University of Southern California for their continued support during my master's study and the process of my Ph.D. program application.

Last but not the least, I would like to thank my parents and my grandma for their unconditional love and support throughout my life.

1.0 Introduction

1.1 Epigenetics and histone modifications

1.1.1 The concept of epigenetics

The term epigenetics was introduced by Conrad Waddington in 1942 to describe the heritable changes that regulate phenotype but do not alter the DNA sequences (1-3). The pattern of epigenetics is critical to regulating multiple important biological processes, including imprinted X-inactivation, genomic imprinting, and gene expression in embryonic development (1, 4). The changes in epigenetics can be reversed, and the most common epigenetic processes that regulate the dynamic structure of the chromatin are DNA methylation, post-translational modifications of the histones, nucleosome positioning, and epigenetic changes regulated by noncoding RNAs (1, 3-5). More than 700 proteins have been reported to participate in epigenetic regulation (6); however, how these proteins are involved in this process remains largely unclear, and additional novel epigenetic factors remain to be discovered. Dysregulation of the epigenetic process results in abnormal gene expression leading to a variety of diseases, including cancers, cardiovascular diseases, Alzheimer's disease, etc. (3, 5, 7, 8). Revealing the underlying mechanism of epigenetic regulation and investigating the functions of epigenetic factors are important for understanding the control of gene expression and identifying novel therapies.

1.1.2 Histone methylation

Histone modification is one of the most important epigenetic processes regulating the chromatin structure. Eukaryotic DNA is packaged into condensed chromatin structures called nucleosomes around octamers of double subunits of histone proteins, H2A, H2B, H3, and H4 (9-11). Multiple marks of covalent post-translational modification can be found on these histone proteins, including methylation, acetylation, phosphorylation, ubiquitination, ADP-ribosylation, and glycosylation (9-11). Most of these modifications occur in the N-terminal histone tails (9-11). Accordingly, specific enzymes are responsible for adding or removing these histone modifications, including histone methyltransferases (HMTs) and histone demethylases (HDMs), histone acetyltransferase (HATs) and histone deacetylase (HDACs), kinases and phosphatases, ubiquitin ligases and deubiquitinases (DUBs), and SUMO ligases and proteases (3, 5, 11). Different modifications on the histone tails alter the nucleosome dynamics and the accessibility of the DNA by transcription factors, thus regulating the activation or repression of gene expression (Fig.1) (3, 5, 11). In general, histone acetylation is relevant to transcription activation, and histone methylation is associated with transcription repression (9). However, histone methylation on some lysine and arginine leads to transcription activation as well, such as histone H3 methylation at lysine 4 (H3K4) and histone H4 at arginine 3 (H4R3) (9, 12).

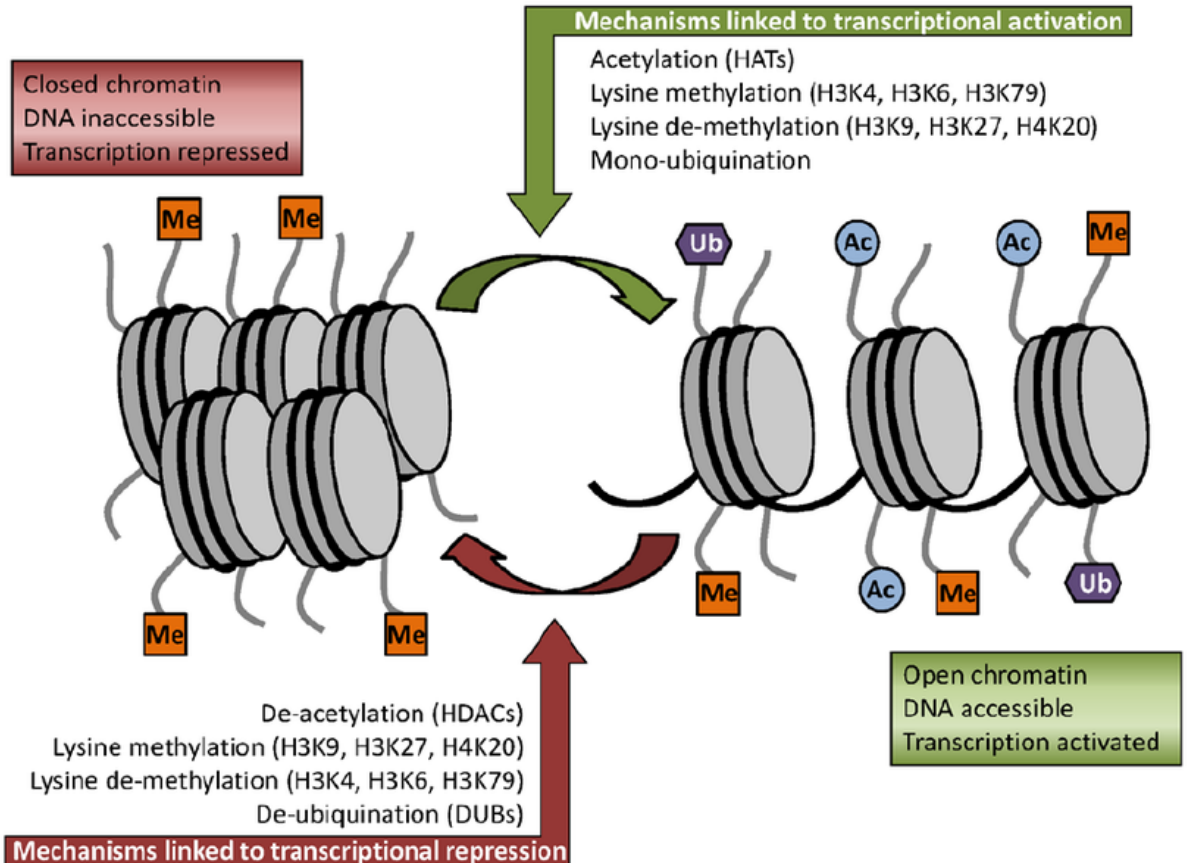

Figure 1: The key histone modifications influencing gene expression (5). The dynamic chromatin incudes active and repressive states. During the repressive state, chromatin is supercoiled and enriched for DNA and histone methylation marks (H3K9, H3K27, H3K20), thus DNA is inaccessible to the transcriptional machinery. The active state of Chromatin is accessible to transcription factors (TFs) and enriched for histone marks (H3K4, H3K6, H3K79), leading to transcriptional activation.

1.1.2.1 Histone lysine methylation

Histone lysine methylation has been recognized as a key mark among different histone modifications. Based on the location and methylation status (mono-, di-, or tri-), the methylation of histone lysine leads to transcriptional activation or repression (3, 9, 10). Five lysine residues on

histone H3 (K4, K9, K27, K36, and K79) and one lysine on histone H4 (K20) have been reported to be methylated by their corresponding histone lysine methyltransferases (HKMTs) (9), which play important roles in regulating critical biological processes, such as cell cycle control, RNA transcription and DNA repair (13). Besides H3K79 methylation catalyzed by the DOT1 family enzymes, all other lysine methylations are performed by the SET domain family methyltransferases (13, 14).

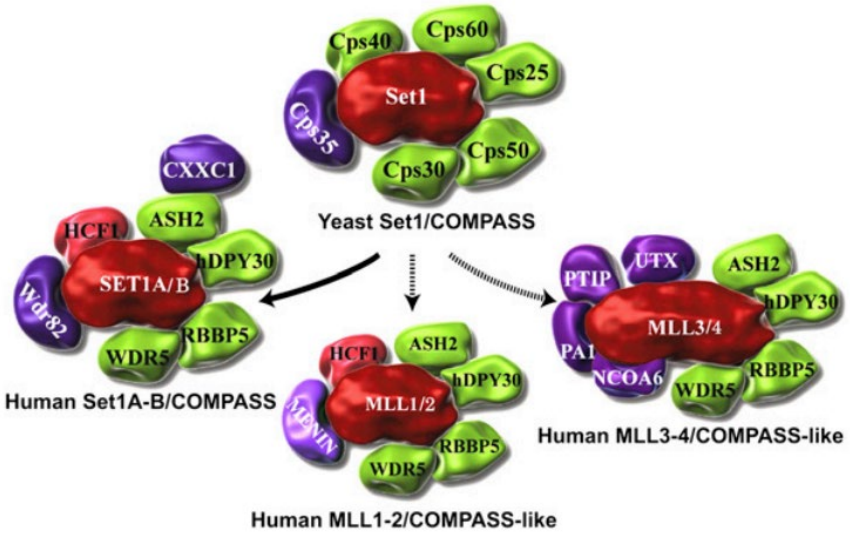

Figure 2: COMPASS and COMPASS-like complexes from yeast to human (15).

The MLL/SET1 family methyltransferases which catalyze histone H3K4 methylation are required to assemble into complexes with multiple proteins called COMPASS (complex of proteins associated with Set1) to reach their maximal catalytic and biological activities (13-15). The highly conserved COMPASS methyltransferase complex is capable of catalyzing mono-, di- and trimethylation of H3K4 (13). In humans, there are at least six multi-protein complexes belonging to the MLL/SET1 family, including SET1A, SET1B, and Mixed Lineage Leukemia

(MLL) 1-4 (Fig. 2) (14-16). In general, SET1A and SET1B are responsible for most H3K4me3 marks on gene promoters (16); MLL1 regulates important genes during development (16, 17); MLL2 regulates H3K4me3 marks at bivalent promoters (18); MLL3 and MLL4 act as major H3K4 mono-methylases at the enhancers (16, 19, 20). Besides the complex-specific subunits, four common subunits shared by all six complexes largely stimulate the catalytic activity, including WD repeat containing protein 5 (WDR5), Retinoblastoma Binding Protein 5 (RbBP5), Absent-Small-Homeotic-2- Like protein (ASH2L) and Dumpy-30 protein (DPY30) (14, 16).

1.1.2.2 WDR5, the core protein of H3K4 methyltransferase complexes

The WD40 repeat domain protein WDR5 is one of the core subunits of the human MLL/SET1 H3K4 methyltransferase complexes (16, 21). As one of the four common subunits, WDR5 greatly enhances the catalytic activity of the MLL/SET1 complex together with RbBP5, ASH2L, and DPY30 (16, 21-23). WDR5 also mediates the assembly of MLL/SET1 histone methyltransferase complexes by recognizing and binding an arginine-containing motif (21, 23). WDR5 knockdown results in the reduction of total H3K4 methylation level (24, 25). Besides its function in H3K4 methylation, WDR5 has also been described as a cellular multitasker such as by acting as a histone tail reader and being part of the nucleosome remodeling and deacetylase (NuRD) complex (21, 23).

WDR5 plays a critical role in the tumorigenesis of several cancers (26). As a well-known oncogenic factor for MLL-rearranged leukemia, WDR5 recruits MLLs to the enhancers that are enriched for binding sites of E-twenty-six (ETS) family transcription factors, resulting in leukemogenic gene activation and leukemia (26, 27). WDR5 also induces the transcriptional activation of critical oncogenes, such as the oncogenic transcription factor Myc (28, 29). WDR5

overexpression is observed in gastric and colon cancer and is associated with poor prognosis in patients (26).

1.1.2.3 The Mixed Lineage Leukemia 2

The Mixed Lineage Leukemia 2 (MLL2), also known as KMT2B, is a member of the mammalian H3K4 methyltransferase family (16, 30). Composed of 2,715 amino acids, MLL2 is a paralog of MLL1 and is widely expressed in human tissues (30). Besides the four core subunits WDR5, RbBP5, ASH2L, and DPY30, MLL1 and MLL2 contain Menin, host cell factors 1/2 (HCF1/2), and the lens epithelium-derived growth factor (LEDGF) as additional unique subunits to increase their functional diversity (30).

Chromatin immunoprecipitation sequencing (ChIP-seq) shows MLL2 can establish narrow H3K4me3 peaks close to active promoter regions of developmentally-related genes and at bivalent promoters of genes with low expression levels in embryonic stem cells (18, 30, 31). About 70% of the identified MLL2 binding sites are localized to promoter regions, but MLL2 also establishes H3K4me3 peaks at non-transcriptional start site (TSS) regions (30). Some studies showed that MLL2 depletion did not cause global bulk reduction of H3K4 methylation in mouse embryonic stem cells or fibroblast (31, 32). However, other studies revealed the downregulation of H3K4me3 marks by ChIP-seq and the reduction of total H3K4me3 levels by Western-blotting after MLL2 knockdown (18, 33, 34).

The KMT2 family members are among the most frequently mutated genes in several human cancers (35). For MLL2 (KMT2B), 236 mutations were found in the Catalogue of Somatic Mutations in Cancer (COSMIC) database (cancer.sanger.ac.uk), including cancers in the endometrium, large intestine, lung, glioma and liver, and most of the mutations were affecting the SET domain (35). As a positive regulator of cell growth, the deficiency of MLL2 in embryonic

stem cells (ESCs) and germline knockout mice would increase apoptosis, resulting in proliferation defects and embryonic lethality (35-39).

1.2 Kaposi's sarcoma-associated herpesvirus

1.2.1 Human tumor-associated viruses

The first tumor-associated virus, Rous sarcoma virus (RSV), was discovered from a solid chicken tumor that could be transmitted to other healthy chickens through cell-free tumor extracts by Peyton Rous in 1911 (40-43). Later on, in 1970, the first confirmed oncogene, RSV-encoded Src, was discovered, leading to the identification of the first cellular counterpart of a cancer-causing gene in avian cellular sequences in 1976 (42-45). These discoveries provide insights into the idea that human tumor cells can be developed from alterations in normal cells, building up the foundation of current cancer biology (42, 43). At least seven human viruses have been causally linked to human malignancies, Epstein–Barr virus (EBV), hepatitis B virus (HBV), hepatitis C virus (HCV), human papillomavirus (HPV), human T-cell lymphotropic virus (HTLV-1), Kaposi's associated sarcoma virus (KSHV) and Merkel cell polyomavirus (MCV), together contribute to 10–15% of the cancers worldwide (42, 43, 46, 47).

Besides the oncogenic mechanism of HBV and HCV promoting chronic inflammation, other viruses induce cancers through their oncogenic activities during their latency (42, 43, 46). The latent membrane protein 1 (LMP1) of EBV mimics a constitutively active CD40 receptor, which belongs to the family of tumor necrosis factor receptors, inducing signaling pathways such as NF-κB thus contributing to B-cell proliferation and transformation (48, 49). The expression of

two viral oncoproteins in HPV, E6, and E7, interferes with the functions of cellular tumor suppressors, p53 and retinoblastoma (Rb), respectively (42, 50). HTLV-1 encodes a protein called Tax, which activates the pathways of NF-κB, AP-1, and CRE and interacts with several chromatin remodeling regulators, such as HDAC1 and SWI/SNF, resulting in the instability of the genome and transformation (42, 51, 52). KSHV encodes a list of viral oncoproteins, including vGPCR, vIL-6, vBcl-2, vMIPs, vFLIP, vCyclin, LANA, and Kaposin B (42, 53-55). The activity of the large T (LT) of MCV inhibits LT inhibits Rb, and the small T (sT) expression alone is sufficient to induce cellular transformation in immortalized rodent fibroblast cell lines, through its interactions with Protein Phosphatase 2A (PP2A), SKP1-CUL1-FBOX (SCF) Complexes, MYCL/MAX and TIP60 (KAT5)/P400 (EP400) complex, etc (46, 56-59). Like in non-viral related cancers, the hallmarks of cancer are acquired by oncogene activation and tumor suppressor inactivation (60-63). Human tumor-associated viruses encode oncogenic proteins to establish persistence in the host, avoid or inactivate host defense and promote host cell survival, resulting in the inhibition of tumor suppressors pathways, changes to the microenvironment, and genomic instability, which accelerate cancer formation (43, 47, 60, 64, 65).

By identifying the mechanism of tumorigenesis of the human tumor-associated virus, new treatments can be developed to target their associated malignancies. Furthermore, understanding the role of viral oncoproteins during the transformation can provide insights into uncovering the mechanisms of tumor initiation, maintenance, and dissemination for both viral-related and non-viral related cancers (42).

1.2.2 Background of Kaposi's sarcoma-associated herpesvirus

Kaposi's sarcoma, a usually low-grade vascular tumor before the AIDS epidemic, is the first tumor identified to be associated with human immunodeficiency virus (HIV) infection (53, 66, 67). It is the second most common cancer among AIDS patients and remains one of the most common cancers in sub-Saharan Africa (53, 67, 68). Four different subtypes of KS are defined by the clinical and epidemiologic characteristics, including classic KS (Mediterranean), endemic KS (African), epidemic KS (AIDS-associated), and iatrogenic KS (transplant-related) (54, 66, 69, 70). KS tumors usually develop on the skin or the subcutaneous tissue and are known to be of endothelial origin (54, 66). Its etiological agent, KSHV, was first identified by Chang and Moore in 1994 (71). The majority of KS tumor cells are latently infected by KSHV (55).

Kaposi's sarcoma-associated herpesvirus (KSHV), also known as human herpesvirus 8 (HHV8), is a member of the gamma herpesvirus family, and the etiological agent of several human diseases, including Kaposi's sarcoma (KS), primary effusion lymphoma (PEL) and multicentric Castleman's disease (MCDs) (53, 54, 66, 72-75). KSHV has a large double-stranded DNA genome with a complex gene organization of more than 90 genes that encode for viral proteins and noncoding RNAs (53, 76). Like other herpesviruses, its viral life cycle has both lytic and latent replication phases (Fig. 3) (53, 76, 77). Following primary infection, KSHV turns into a latent state and establishes a life-long persistent infection in the host. During the latency, KSHV only expresses a few viral products, including latency-associated nuclear antigen (LANA) encoded by ORF73, KSHV-encoded vCyclin encoded by ORF72, KSHV-encoded FLICE inhibitory protein (vFLIP) encoded by ORF71, and 12 viral precursor microRNAs (miRNAs) (55, 78-80). These viral latent products repress KSHV lytic replication, mediate the viral episome replication and

promote the survival of host cells (55, 78). Therefore, KSHV latent products are critical to maintaining KSHV latency and are directly responsible for KSHV-induced tumorigenesis (81, 82).

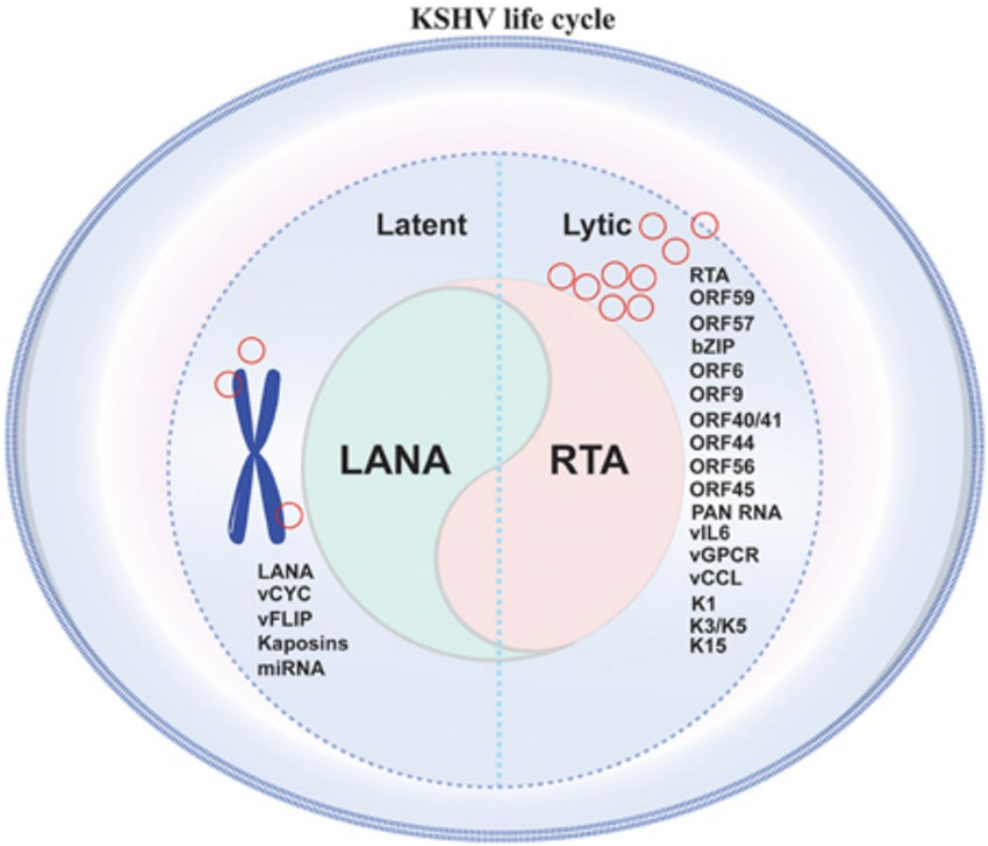

Figure 3: Schematic representation of KSHV life cycle in the host cell (77).

1.2.3 KSHV infection systems and a model for KSHV-induced cellular transformation

Despite extensive studies, the mechanism of KSHV-induced oncogenesis remains unclear partially due to the lack of an experimental model of KSHV-induced cellular transformation of primary cells. Several KSHV-infected cell lines were derived from PEL, including KSHV-infected BC3, BCBL1, BCP-1, etc. (83-87). KSHV is predominantly latent but can be induced into lytic replication in these PEL cell lines (83-87). Hence, they are useful tools for studying KSHV lytic

replication and PEL biology and for producing infectious KSHV virions, albeit at low titer, for infecting other cells (83, 86, 87). However, PEL cells are transformed cancer cells, and there is a lack of non-cancer primary cell control for PEL cell lines.

KSHV can infect a variety of human primary cells including multiple lineages of endothelial cells, epithelial cells, fibroblasts, macrophages, B-cells, dendritic cells, etc. (87-96). However, KSHV does not transform these cells and these cells undergo senescence after multiple passages (87-96). Thus, these systems are only useful for studying the early stage of KSHV infection. Multiple immortalized cells are also susceptible to KSHV infection (88-90). Among them, KSHV-infected telomerase-immortalized dermal microvascular endothelial cells (TIME) are not transformed, they cannot form colonies in soft agar or form tumors *in vivo* (89). Immortalized KSHV-infected telomerase-immortalized umbilical vein endothelial cells (TIVE) cells are transformed, acquire the ability of anchorage-independent growth, and induce tumor in nude mice (88). However, these cells are already immortalized before KSHV infection, and the transformed cells contain genetic alterations that are important for cellular transformation (88-90). Hence, their utility is limited.

Our lab has previously discovered that KSHV can efficiently infect and transform primary rat embryonic metanephric mesenchymal precursor (MM) cells (97). The KSHV-transformed MM (KMM) cells express hallmark KS tumor cells markers including vascular endothelial, lymphatic endothelial, precursor, and mesenchymal markers (97). KMM cells are immortalized, proliferate at a faster rate, lose contact inhibition, and are capable of inducing tumors *in vivo* (97). The transformation phenotype was not restricted to a specific viral isolate since both BAC36 KSHV and virions from BCP-1 cells can efficiently infect and transform MM cells (97). We and others have subsequently found that KSHV can also infect primary human mesenchymal stem cells and

hematopoietic precursor cells. While these KSHV-infected mesenchymal stem cells can form colonies in soft agar, the efficiency is low, and they do not induce any tumor following inoculation into nude mice (97-99). Hence, the utility of this system is low.

This unique system of MM and KMM cells has been used to identify viral and cellular factors mediating KSHV-induced tumorigenesis (100-109). A genome-wide CRISPR-Cas9 screening was performed to discover novel growth-promoting and growth-repressive genes in this system (110). A library of CRISPR genome-wide sgRNAs to target cellular genes specifically was transduced into MM and KMM cells with the expression of Cas9 (110). On days 1, 4, 11, and 21 post-transductions, DNA from the surviving MM and KMM cells was sequenced and analyzed based on the abundance of sgRNA (110). A group of genes that was essential for the survival of primary cells but not transformed cells was identified (110). Several pathways enriched in KMM cells but not MM cells were also determined, such as the hypoxia signaling pathway and the p38 mitogen-activated protein kinase (MAPK) pathway (110). By comparing cancer cells with their untransformed counterparts, oncogenic viruses are useful models for genome-wide screenings to identify novel therapeutic targets.

1.2.4 Epigenetic regulation in KSHV life cycles and KSHV-induced tumorigenesis

KSHV episome is subjected to a variety of epigenetic modifications, including DNA methylation, histone methylation, and histone acetylation (111-116). Following the entry into cells, KSHV generally establishes latency in the majority of the infected cells (113, 117). The KSHV genome undergoes epigenetic modifications to ensure the expression of viral latent products while repressing lytic gene expression (113, 117, 118). Upon reactivation, the KSHV genome undergoes

extensive epigenetic changes to ensure the cascade expression of the viral lytic genes (118). Thus, KSHV hijacks the host epigenetic machinery to fine-tune its life cycle (113-115, 119).

The epigenetic regulation in KSHV latent and lytic phases has been extensively studied (113, 117, 118). Following KSHV primary infection, the latent-to-lytic switch protein RTA is expressed (113, 120). Lysine-specific demethylase 2B (KDM2B) is then recruited to the RTA promoter, which limits the enrichment of the activating marks to repress the expression of RTA, and the binding of KDM2B to the viral episome may facilitate the recruitment of Polycomb repressive complexes (PRCs) (121). The repressive histone mark H3K27me3 is deposited by PRC2 and H2AK119-Ub is deposited by Polycomb repressive complex 1 (PRC1) (113, 122). As a result, the expression of KSHV lytic genes is repressed, leading to the establishment of latency. After these processes, the expression of KSHV's major latent product LANA helps the recruitment of PRC2 and SET1 onto KSHV episome to form bivalent chromatin at specific sites (111, 123). The deposition of DNA methylation and heterochromatin-associated mark H3K9me3 may be facilitated by KSHV miRNAs (124). To reactivate the virus, the formation of viral genome heterochromatin is prevented by H3K9me3 demethylase JMJAD2A, which is SUMOylated by a basic region-leucine zipper (bZIP) protein encoded by KSHV (125, 126). During the early stages of viral reactivation, the enzymatic catalytic subunit of PRC2, enhancer of zeste homolog 2 (EZH2), dissociates from the immediate-early and delayed-early promoters thus decreasing the histone repressive mark H3K27me3 (127). The KSHV-encoded long noncoding RNA, polyadenylated nuclear RNA (PAN RNA), is expressed and recruits the histone demethylases UTX and JMJD3 as well as lysine methyltransferase 2D (KMT2D) to the chromatin to decrease the repressive marks and increase the active marks, leading to the production of RTA and activation of the lytic gene expression (114, 115, 127).

Similarly, in KSHV transformed PEL and KMM cells, the host cell genome undergoes epigenetic remodeling (34, 111). However, whether epigenetic remodeling is a driving factor or the effect of KSHV-induced cellular transformation remains unknown, and the underlying mechanism remains largely unrevealed.

Numerous KSHV latent products have been shown to regulate epigenetic remodeling (111, 119, 123, 128-131). KSHV LANA associates with the promoters of multiple cellular genes, and it can interact with DNA and histone methyltransferase complexes, including PRC2, SET1, MLL1, and DNA methyltransferase 3A (DNMT3A), and facilitates their recruitment (111, 119, 123, 131). In the meanwhile, the KSHV latent products vFLIP and LANA regulate EZH2 through the NF-κB pathway and promote KSHV-induced angiogenesis (128). These results indicate that KSHV might reprogram the cellular epigenetic modifications to induce cellular transformation.

1.3 The WD40 repeat protein: Glutamate Rich WD Repeat Containing 1

1.3.1 WD40 repeat domain proteins

The WD40 repeat domain is abundant in all major eukaryotic proteins (132, 133). It was first described as a repetitive sequence motif with the amino acids Gly-His and Trp- Asp in the Gβ subunit of the heterotrimeric G proteins and the CDC4 protein (132, 134). The repeating motifs are mostly 36-46 amino acids, and the WD40 repeat proteins on average contain four to seven of these repeating domains (133, 135). This family of proteins functions as a protein-protein interaction adaptor involved in many cellular functions, such as cell cycle regulation, mRNA splicing, and vesicular fusion (133, 135-137).

1.3.2 Glutamate Rich WD Repeat Containing 1

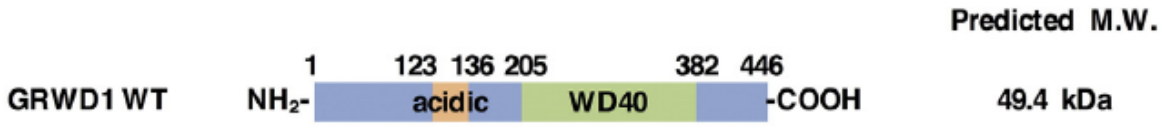

Figure 4: Schematic representation of wild type GRWD1. Figure modified from Figure 1A, Aizawa *et al.* 2016 (139).

Glutamate Rich WD Repeat Containing 1 (GRWD1) was initially identified as an early vitamin D3 inducible gene since its partial cDNA fragment was identified in a screening (136, 138). The structure of this 62 kDa protein contains two domains, a glutamate-rich acidic domain at its N-terminal and multiple WD40 repeat domains at its C-terminal (Fig. 4) (136, 139, 140). GRWD1 was first described as a protein involved in ribosome biogenesis because of the function of its yeast homolog Rrb1 (136, 141, 142), and later on reported to be a Cdt1-binding protein with function in nucleosome assembly and disassembly (139, 140). GRWD1 is also a histone-binding protein, its N-terminal domain can interact with both H2A/H2B and H3-H4 to facilitate the loading of MCM2 helicase (140). The function of p53 can be repressed by GRWD1 via the RPL11-MDM2 pathway, together with constitutively active KRAS and HPV E7, it can transform a telomerase-immortalized cell line HFF2/T, suggesting that GRWD1 is a potential oncoprotein (143-146). Furthermore, GRWD1 has been predicted to function in the regulation of H3K4 methylation through the interaction with CUL4-DDB1 ubiquitin ligase (25). Taken together, as a multifunctional protein, GRWD1 participates in multiple cellular processes. Dysregulation of GRWD1 is associated with poor prognosis of patients in a variety of cancers, such as lower grade glioma (LGG), mesothelioma (MESO), and skin cutaneous melanoma (SKCM) (147).

1.3.2.1 GRWD1 with ribosome biogenesis

GRWD1 is evolutionary conservative. Human GRWD1 has functions similar to its yeast homolog Rrb1 (136). Rrb1 is an essential WD40 repeat protein in yeast (141, 142). It regulates the gene expression of ribosomal protein (RP) and 60S ribosomal subunits assembly (141, 142). Rrb1 interacts with rpL3 to regulate its localization and gene expression (141, 142). Because of the ribosomal regulation function of its yeast homolog, GRWD1 is also postulated to be involved in ribosome biogenesis.

Most of the GRWD1 protein is located in the nucleus, including the nucleolus, which suggests its similar ribosomal function to the yeast homolog (34, 136). Indeed, GRWD1 was co-sedimented with pre-ribosomal ribonucleoprotein particles (RNPs) in cellular fractionation (136). Importantly, the knockdown of GRWD1 decreased the total level of *de novo* synthesized proteins (136). Furthermore, mass spectrometry data has shown that human ribosomal protein RPL3 is one of the major binding partners of GRWD1 (unpublished data), which further supports the functional conservation of GRWD1. Future experiments are needed to investigate the functions of the GRWD1-RPL3 complex in humans and how they regulate ribosome biogenesis. Since GRWD1 is essential for cell proliferation (34, 136), the underlying mechanisms of this protein may reveal how ribosome biogenesis regulates the cell cycle and other cellular functions.

1.3.2.2 GRWD1 with DNA replication and nucleosome assembly

In eukaryotes, it is critical to precisely control the DNA replication licensing process to ensure accurate duplication of genome DNA and that it occurs only once during each replication cycle (148, 149). To control the initiation of DNA replication and chromatin licensing, DNA replication factor 1 (CDT1) is one of the most important regulating targets (148-150). CDT1 is recruited to replication origins after the binding of origin recognition complexes (ORC), and as a

key licensing factor, it promotes the assembly of the pre-replication complex (pre-RC) together with the cell division cycle 6 (CDC6), as well as the recruitment of minichromosome maintenance (MCM) 2-7 (148-150).

To identify CDT1-binding proteins, a proteomics approach was applied including CDT1 affinity chromatography, liquid chromatography, and tandem mass spectrometry analysis (151). GRWD1 was one of the CDT1-binding proteins identified by this study, and it physically interacted with CDC6 as well (140, 151). Interestingly, the yeast homolog Rrb1 also interacts with the yeast pescadillo homologue 1 (YPH1), which is one of the ORC-binding proteins in yeast (142, 152). In humans, GRWD1 has been identified as a histone-binding protein, which regulates chromatin dynamics and the loading of MCM (139, 140). Using ChIP-qPCR, it has been shown that GRWD1 binds to replication origins during the G1 phase of the cell cycle, and the binding depends on the presence of CDT1 and CDC6 (140). The loading of MCM was suppressed by GRWD1 depletion, and GRWD1 overexpression compromised the reduction bindings of GRWD1 and MCM7 to the replication origins caused by CDT1 silencing (140). Furthermore, GRWD1 is globally associated with pre-RC and its depletion has been shown to alter the chromatin structure (140). The ability of GRWD1 to maintain chromatin openness is conducted by its N-terminal acidic domain (139, 140).

GRWD1 has also been shown to have nucleosome assembly and disassembly activity (139). Recombinant GRWD1 can act as histone chaperones to remove H2A-H2B dimers from nucleosomes and form hexasomes by their acidic domain (139). This ability of GRWD1 partially explains the mechanism of how it regulates the chromatin structures, and therefore promotes the loading of MCM at the origins of replication.

1.3.2.3 GRWD1, an oncogenesis related protein

As the "guardian of the genome", p53 is one of the most important tumor suppressors regulating a variety of cellular functions, such as cell cycle arrest and apoptosis (153). The impairment of ribosome biogenesis will cause defects in the key process of protein synthesis, and the repression of ribosomal biogenesis has been reported to activate p53 through the ribosomal protein (RP)-mouse double minute 2 homolog (MDM2)-p53 pathway (146, 154, 155). MDM2 is a RING-type E3 ubiquitin ligase, which negatively regulates p53 by promoting p53 ubiquitination and its subsequent degradation (146, 154, 156). When ribosomal stress occurs, the nucleolus is disrupted, leading to the release of ribosomal proteins such as RPL11 and RPL5, which interact with MDM2 to inhibit its ability to degrade p53 (144, 146, 154, 156) (Fig. 3). As a result, the cellular level of p53 is stabilized. The induction of p53 leads to cell cycle arrest and apoptosis (146, 154, 156). Through its ability to directly interact with RPL11, GRWD1 can inhibit the function of RPL11 to silence MDM2 (144-146). When GRWD1 is overexpressed, MDM2 continues to degrade p53 during ribosomal stress, resulting in a low p53 level (144-146). Therefore, the regulatory machinery of p53 cannot function properly. Furthermore, GRWD1 has been demonstrated to directly interact with p53, thus negatively regulating the transcriptional activity of p53 (Fig. 5) (143, 144, 146). Taken together, GRWD1 is a negative regulator of p53 and functions in both direct and indirect manners. Thus, it is proposed that GRWD1 is an oncogenesis-related ribosomal protein and that any dysregulations during this process might promote oncogenesis (144, 146). Importantly, overexpression of GRWD1 is associated with poor prognosis of patients among many types of cancer (147).

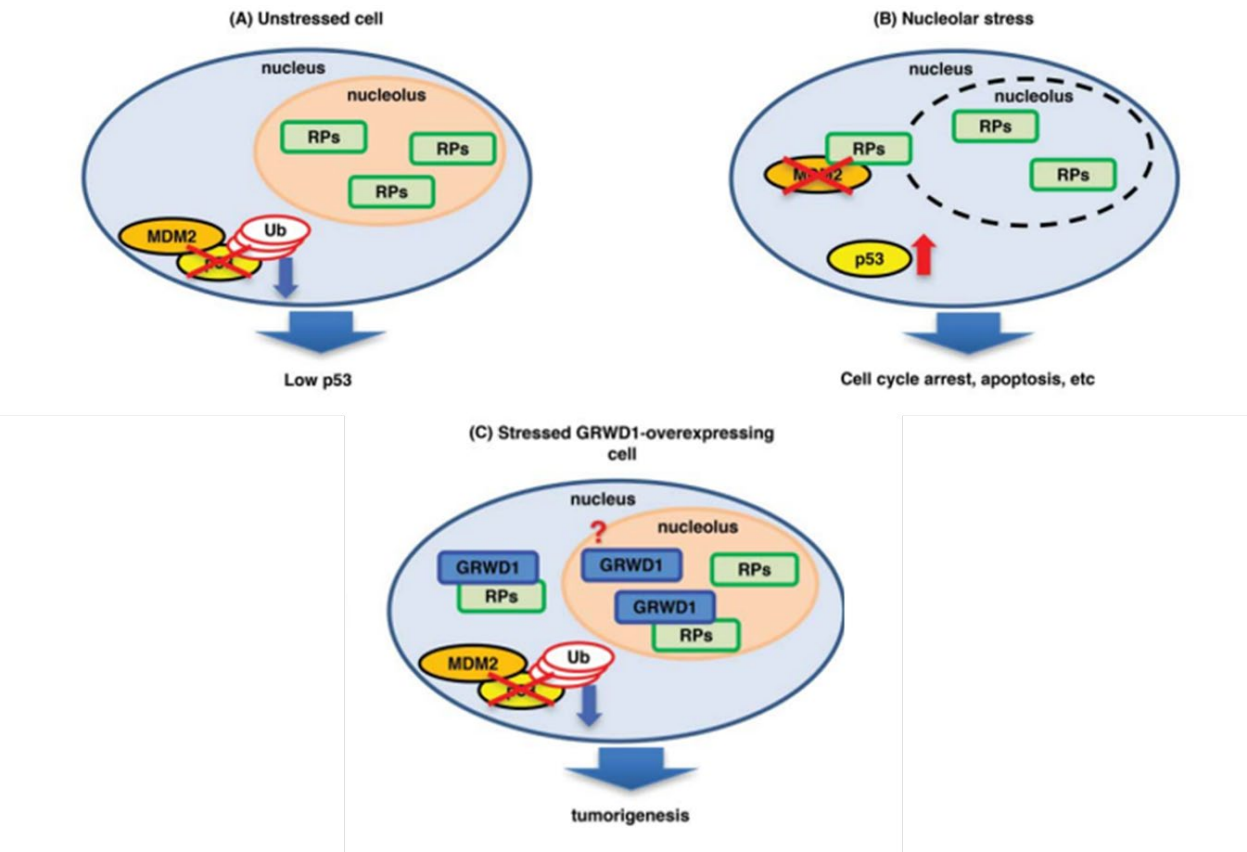

Figure 5: A model for p53 regulation by ribosomal proteins and GRWD1.(A) Ribosome proteins (RPs) such as RPL11 stay inside the nucleolus in unstressed condtion, MDM2 binds to and ubiquitinates p53 to keep it at low level. (B) During nucleolar stress, RPs are released into the nucleoplasm and interact with MDM2 to inhibit its function to ubiquitinate p53. (C) When GRWD1 is overexpressed, it binds to RPL11 and inhibits its ability to silence MDM2, leading to the downregulation of p53, thus promotes tumorgenesis. Figure modified from Figure 1, Takafuji *et al.* 2017 (146).

2.0 GRWD1-WDR5-MLL2 epigenetic complex mediates the H3K4me3 mark and is essential for Kaposi's sarcoma-associated herpesvirus-induced cellular transformation

This is the author's version of the work. Sections of this chapter have been adapted from the original work published in mBio and are posted here with permission from the journal.

Shan Wei[a], Songjian Lu[b], Lifan Liang[b], Xian Wang[a], Wan Li[a], Tingting Li[a], Luping Chen[a], Enguo Ju[a], Xinquan Zhang[a], Zhao Lai[c], Yufei Huang[a,d], Xinghua Lu[b], Shou-Jiang Gao[a]

[a]Cancer Virology Program, UPMC Hillman Cancer Center, and Department of Microbiology and Molecular Genetics, University of Pittsburgh, Pittsburgh, PA, USA

[b]Department of Biomedical Informatics, University of Pittsburgh, Pittsburgh, PA, USA

[c]Greehey Children's Cancer Research Institute, University of Texas Health Science Center at San Antonio, San Antonio, TX, USA

[d]Department of Medicine, University of Pittsburgh, Pittsburgh, PA, USA

2.1 Introduction

Epigenetics is the study of heritable changes that regulate gene expression without affecting the sequence of DNA (1). The most common epigenetic processes that regulate the dynamic structure of chromatin are DNA methylation and posttranslational modifications of histones (1, 3). Histone lysine methylation has been recognized as a key mark among histone

modifications (3, 9). The methylation of lysine side chains of the histone tails leads to activation or repression of transcription, depending on the location and methylation status (mono-, di-, or tri-) (3, 9). Over 700 proteins have been reported to participate in epigenetic remodeling (9); however, the functions of many of these proteins remain unclear, and additional novel epigenetic factors remain to be discovered. Epigenetic dysregulation is involved in many human diseases, including cancers, cardiovascular diseases, Alzheimer's disease, etc. (3, 7). Understanding the mechanism of epigenetic regulation and the functions of epigenetic factors is essential for identifying novel therapies.

Kaposi's sarcoma-associated herpesvirus (KSHV) is a human tumor virus causally linked to Kaposi's sarcoma (KS) and primary effusion lymphomas (PEL) (53). As KSHV is a member of the herpesvirus family, its life cycle has both latent and lytic replication phases. The majority of KS tumor cells are latently infected by KSHV expressing only a few viral latent products, including LANA, vCyclin, vFLIP, and 12 viral precursor microRNAs (miRNAs) (55, 78). These proteins and miRNAs repress KSHV lytic replication, mediate the replication of viral episome, and promote the survival of cells (55, 78). Hence, KSHV latent products are required to maintain KSHV latency and are directly responsible for the development of KSHV-induced tumors (81). Despite extensive studies, the mechanism of KSHV-induced oncogenesis remains unclear in part due to the lack of an experimental model of KSHV-induced cellular transformation of primary cells. We have succeeded in transforming primary rat embryonic metanephric mesenchymal precursor (MM) cells with KSHV (97). Compared to untransformed primary cells, KSHV-transformed MM (KMM) cells are immortalized, have a higher proliferation rate, show no contact inhibition, and gain the ability to form tumors in vivo (97). This unique system has been used to identify viral and cellular genes mediating KSHV-induced tumorigenesis (100-109). For this purpose, a genome-wide

CRISPR-Cas9 screening was performed with matched MM and KMM cells, which led to the identification of a group of genes that were essential for the survival of KMM but not MM cells (110).

Numerous KSHV latent products regulate epigenetic remodeling (111, 128). However, whether epigenetic remodeling is critical for KSHV-induced cellular transformation and the underlying mechanisms remain unknown. To investigate the epigenetic factors that are essential for KSHV-transformed cells, we have combined the results of the CRISPR-Cas9 screening (110) with those of the EpiFactors database (6) and the TCGA survival data (147) and identified a set of epigenetic regulators that are potentially important for the survival of KSHV-transformed cells. Among them, glutamate-rich WD repeat containing 1 (GRWD1) is a highly conserved protein belonging to the WD40 family functionally involved in ribosome biogenesis (136, 139). GRWD1 has two domains, an N-terminal glutamate-rich acidic domain and a C-terminal WD40 repeat domain (139). GRWD1 is a histone-binding protein interacting with both H2A/H2B and H3-H4 through its N-terminal domain. It regulates chromatin dynamics and the loading of MCM2 helicase (139) and is predicted to regulate H3K4 methylation (25). Furthermore, overexpression of GRWD1 represses the function of tumor suppressor p53 and, together with constitutively active oncogene KRAS and human papillomavirus (HPV) oncogene E7, transforms a telomerase-immortalized cell line, HFF2/T (145), suggesting that GRWD1 is a potential oncogene. Indeed, our results show that GRWD1 dysregulation is associated with poor prognosis of patients in several types of cancer (147), including brain lower-grade glioma (LGG), mesothelioma (MESO), and skin cutaneous melanoma (SKCM). Taken together, GRWD1 is a strong candidate epigenetic regulator that might be involved in KSHV-induced tumorigenesis.

In this study, we have hypothesized that GRWD1 might function as an essential epigenetic factor mediating KSHV-induced cellular transformation by regulating the expression of specific cellular genes. We have found that GRWD1 recruits an H3K4 methyltransferase complex to the promoters of growth-promoting genes to increase their expression and enhance KSHV-induced cell proliferation and cellular transformation. We have demonstrated that GRWD1 forms a complex with the core protein of the H3K4 methyltransferase complex, WD repeat domain 5 (WDR5), and the H3K4 methyltransferase myeloid/lymphoid or mixedlineage leukemia 2 (MLL2), also known as MLL4 or histone-lysine N-methyltransferase 2B (KMT2B). By ChIP-seq and transcriptome sequencing (RNA-seq) study, we have determined that GRWD1 functions as an essential regulator of histone H3 lysine 4 (H3K4) trimethylation (H3K4me3) through the GRWD1-WDR5- MLL2 complex.

2.2 Materials and methods

2.2.1 Cell culture

MM cells and 293T cells were cultured in Dulbecco modified Eagle medium (DMEM) (25-500; Genesee) with 10% fetal bovine serum (F2442; Sigma-Aldrich). KMM cells were cultured under the same condition as MM cells except with 250 mg/mL of hygromycin. MM and KMM cells between 5 and 15 passages were used for the experiment, MM cells would undergo crisis after about 25 passages. MM and KMM cells with stable GRWD1 knockdown by lentivirus infection were cultured in their respective media with 1 mg/mL and 5 mg/mL of puromycin, respectively. Cells were cultured in a medium without selection for 1 week before any experiments.

2.2.2 Plasmids, shRNAs, and siRNAs.

The shRNA plasmid was constructed by inserting the shRNA oligonucleotides (Integrated DNA Technologies) into the pLKO.1 lentiviral vector. The shRNA oligonucleotide sequences were designed by BLOCK-iT™ RNAi Designer (Thermo Fisher Scientific) and shown as follows:

GRWD1 shRNA1 (F: 5'-CCGGGGAGCTGGTAATGGATGAAGACTCGAGTCTTCATCCATTACCAGCTCCTTTTTG-3', R: 5'-AATTCAAAAAGGAGCTGGTAATGGATGAAGACTCGAGTCTTCATCCATTACCAGCTCC-3')

GRWD1 shRNA2 (F: 5'- CCGGGGATGGTGGTTCCTGGAATGTCTCGAGACATTCCAGGAACCACCATCCTTTTTG-3', R: 5'- AATTCAAAAAGGATGGTGGTTCCTGGAATGTCTCGAGACATTCCAGGAACCACCATCC-3')

GRWD1 shRNA3 (F: 5'- CCGGGCAGTTGCTGTTCGTGCATCACTCGAGTGATGCACGAACAGCAACTGCTTTTTG-3', R: 5'- AATTCAAAAAGCAGTTGCTGTTCGTGCATCACTCGAGTGATGCACGAACAGCAACTGC-3')

WDR5 shRNA1 (F: 5'- CCGGGCTCATTGATGACGACAATCCCTCGAGGGATTGTCGTCATCAATGAGCTTTTTG-3', R: 5'- AATTCAAAAAGCTCATTGATGACGACAATCCCTCGAGGGATTGTCGTCATCAATGAGC-3')

WDR5 shRNA2 (F: 5'- CCGGGGGAAGTTCCTGGTCTGTTCTCTCGAGAGAACAGACCAGGAACTTCCCTTTTTG-3', R: 5'- AATTCAAAAAGGGAAGTTCCTGGTCTGTTCTCTCGAGAGAACAGACCAGGAACTTCCC-3')

WDR5 shRNA3 (F: 5'- CCGGGCAGCTTGCGAGGTCAATACTCTCGAGAGTATTGACCTCGCAAGCTGCTTTTTG-3', R: 5'- AATTCAAAAAGCAGCTTGCGAGGTCAATACTCTCGAGAGTATTGACCTCGCAAGCTGC-3')

MLL2 shRNA1 (F: 5'- CCGGGCGGCTGTGACAATCCCTAAACTCGAGTTTAGGG

ATTGTCACAGCCGCTTTTTG-3', R: 5'- AATTCAAAAAGCGGCTGTGACAATCCCTAAA CTCGAGTTTAGGGATTGTCACAGCCGC-3')

MLL2 shRNA2 (F: 5'- CCGGGCAGAATGAGTGGACACATGTCTCGAGACATGTG TCCACTCATTCTGCTTTTTG-3', R: 5'- AATTCAAAAAGCAGAATGAGTGGACACATGT CTCGAGACATGTGTCCACTCATTCTGC-3')

MLL2 shRNA3 (F: 5'- CCGGGGTCTGAAGATGAATCCATGGCTCGAGCCATGGA TTCATCTTCAGACCTTTTTG-3', R: 5'- AATTCAAAAAGGTCTGAAGATGAATCCATGG CTCGAGCCATGGATTCATCTTCAGACC-3')

The siRNAs against GRWD1 were obtained from Sigma-Aldrich (SASI_Rn01_00060441, SASI_Rn01_00060442, SASI_Rn01_00060443).

The overexpression plasmid was constructed by cloning the coding sequence from the cDNA of 293T cells with an N-terminal FLAG tag into the pCDH vector using the following primers:

GRWD1 (F, 5'-TGC TTATCTAGACGGCCACCATGGATTACAAGGATGACGACG ATAAGGCGGCGCGCAAGG-3'; R, 5'-TGCTTAGAAT TCTCAGACGCTGATGGTGCG-3') and WDR5 (F, 5'-TGCTTATCTAGACGGCCACCATGGATTACAAGGATGACG ACGATA AGGCGACGGAGGAGAAGAAGC-3'; R, 5'-TAAGCAGAATTCTTAGCAGTCACTCTTCC ACAGTTTAATTG-3').

The FLAG tag MLL2 C-terminal plasmid pcDNA3 MLL2 653 was a gift from Matthew Meyerson (Addgene plasmid no. 11017; http://n2t.net/addgene:11017; RRID: Addgene_11017).

2.2.3 Lentiviral infection

Supernatants of 293T cells transfected with p8.74 and pMDG packaging vectors as well as the shRNA vectors were collected and filtered at 48 or 72 h after the transfection. Viral transduction was performed by spinning infection at 1,500 rpm for 1 h with Polybrene at 10mg/mL. The knockdown efficiency was examined at 48 or 72 h post transduction.

2.2.4 Soft agar assay

The soft agar assay was performed as previously described (10). Briefly, 2 × 104 cells suspended in 1 mL of 0.3% top agar (A5431; Sigma-Aldrich) were plated onto 0.5% base agar in one well of 6-well plates and covered by cultured medium. After 3 weeks, the plates were photographed with a microscope under a 2× lens objective, and colonies with diameters of .50mm were counted.

2.2.5 Cell cycle and apoptosis assays

Cell cycle analysis was performed by propidium iodide (PI) staining, and flow cytometry was conducted with a FACSCanto II flow cytometry system (BD Biosciences). The fixable viability dye eFluor 660 kit (650864; eBioscience) and phycoerythrin (PE)-Cy7 annexin V apoptosis detection set (88810374; eBioscience) were used to detect apoptotic cells following the instructions of the manufacturer. The data were analyzed with the FlowJo software (BD Biosciences).

2.2.6 GST pulldown assay

Purified recombinant glutathione S-transferase (GST), GST-GRWD1, and WDR5 proteins were purchased from Abcam (ab81793, ab164438, and ab98079). Recombinant WDR5 protein was incubated with GST-GRWD1 or GST protein and then bound with glutathione Sepharose 4B (GE17-0756-01; Sigma-Aldrich). The beads were washed five times, and the pulldown proteins were eluted and analyzed by Western blotting.

2.2.7 Immunofluorescence assay, co-IP, and Western blotting

For immunofluorescence assay, cells were fixed with 4% paraformaldehyde (P6148; Sigma-Aldrich) for 12 min at room temperature, permeabilized with 100% methanol at 220°C for 12 min and blocked with 1% bovine serum albumin (BSA) and 0.1% Tween 20 in phosphate-buffered saline (PBS) for 1 h. The cells were stained with primary antibodies for 1 h followed by 1 h of incubation with Alexa Fluor-labeled secondary antibodies (Invitrogen, Themo Fisher Scientific) at room temperature. Primary and secondary antibodies were diluted in 3% BSA in PBS. 49,6-Diamidino-2-phenylindole (DAPI) (D9542; Sigma-Aldrich) was used for the nuclear counterstaining.

Co-IP experiments were performed with the anti-FLAG M2 affinity gel (A2220; Sigma-Aldrich) according to the manufacturer's instructions. Cell lysates were treated with Benzonase Nuclease (E1014; Sigma-Aldrich) for 1 h with rotation at 4°C. Before adding the affinity gel, the lysates were precleared with mouse IgG-agarose (A0919; Sigma-Aldrich) with rotation at 4°C for 4 h.

For Western blotting, protein samples were resolved by SDS-PAGE and transferred to nitrocellulose membranes (10600004; GE Healthcare). Protein signals were detected with chemiluminescent substrate (34096; Thermo Scientific) after the incubation with primary and secondary antibodies.

Mouse monoclonal antibodies against GRWD1 (sc-514125; Santa Cruz), histone H3 (sc-517576; Santa Cruz), and b-actin (sc-376421; Santa Cruz) **and rabbit monoclonal antibodies against WDR5 (catalog no.13105; Cell Signaling Technology)**, MLL2 C-terminal sequence (catalog no. 38058; Cell Signaling Technology), H3K4me3 (catalog no. 9751; Cell Signaling Technology), FLAG tag (catalog no. 14793; Cell Signaling Technology), and GST tag (catalog no. 2625; Cell Signaling Technology) were used for the experiments.

2.2.8 Proximity ligation assay (PLA)

PLA was performed with Duolink® In Situ Red Starter Kit Mouse/Rabbit (catalog no. DUO92101-1KT; Sigma-Aldrich) according to the manufacturer's instructions. Mouse monoclonal antibodies against GRWD1 (sc-514125; Santa Cruz) and rabbit monoclonal antibodies against WDR5 (catalog no.13105; Cell Signaling Technology) were used for the assay.

2.2.9 Real-time quantitative reverse transcription-PCR (RT-qPCR) and RNA-seq

Cells were collected and lysed in TRI reagent (T9424; Sigma-Aldrich), and the total RNA was isolated following the manufacturer's instructions. Reverse transcription was performed with the isolated total RNA with the Maxima H Minus first-strand cDNA synthesis kit (K1652; Thermo Scientific). The SsoAdvanced universal SYBR green supermix kit (172-5272; Bio-Rad) was used

for the quantitative PCR. The primers used for these experiments were as follows (for Rattus norvegicus):

GRWD1 (F,5'-GTGAGGGCTTTGCTCTTGAC-3'; R, 5'-CACTGCAGATCCTCCACAGA-3')

WDR5 (F, 5'-GG TGCACCTCCTCTCTGAAG-3'; R, 59-TGTGCACTGGGCAATACAAT-3')

MLL2 (F, 5'-TGCTCAGTGGAGACAACAGG- 3'; R, 5'-ACCAAATGGCACAGTTGACA-3').

ADAR: (F, 5'-GGGGACCCACAGGGGTG -3'; R, 5'-CGGTTGTTTTCCTTGGGCAG -3')

OAS1A: (F, 5'-GGGAAGTGCCGGTGGATG-3'; R, 5'-CCGCCCCTTCTGAATCTGTT-3')

IL1A: (F, 5'-TCGGGAGGAGACGACTCTAA-3'; R, 5'-TTTCCGGAATCTCCTTCAGCA-3')

BST2: (F, 5'-GACCCAATAGTTGGCAGGTCA-3'; R, 5'-AGATGCAATCTGGGCTCCAC-3')

SOHLH1: (F, 5'-CCAACTTGGTCTTGGCATCT-3'; R, 5'-GGCTCAGGGTCTCCAATGTA-3')

ZFP112: (F, 5'-GTGTAGTCCGGGCTGCTAAT-3'; R, 5'-AAAGGCTGATGTGCCACTGA-3')

ADAMTS19: (F, 5'-AGGACTGCATGACGTGCTC-3'; R, 5'-CTCACCTTGGACCAGTCACC-3')

HS3ST3B1: (F, 5'-TTCGCCATGCTTTGCATCTG-3'; R, 5'-GGGCATCAGGTCCCGGT-3')

CDK1: (F, 5'-CTGGCCAGTTCATGGATTCT-3'; R, 5'-CCGAAATCTGCCAGTTTGAT-3')

CDK2: (F, 5'-CATTCCTCTTCCCCTCATCA-3'; R, 5'-GTACGGACAGGGACTCCAAA-3')

CDT1: (F, 5'-CGCACTTAAGCTTCCCTGTC-3'; R, 5'-CAGTTTGTGGAAAGGGCATT-3')

PCNA: (F, 5'-AGGACGGGGTGAAGTTTTCT-3'; R, 5'-CAGTGGAGTGGCTTTTGTGA-3')

The isolated mRNA was used to prepare the RNA-seq library using the Illumina TruSeq stranded mRNA-seq sample preparation guide (Illumina, San Diego, CA, USA) and subjected to sequencing using a 50-bp single-read sequencing module with a HiSeq 3000 sequencing system from Illumina.

2.2.10 ChIP-seq and ChIP-qPCR

ChIP experiments were conducted using the SimpleChIP enzymatic chromatin IP kit (magnetic beads) (catalog no. 9003; Cell Signaling Technology) according to the manufacturer's instructions. The ChIP DNA was used for the ChIP-seq library preparation by using the Swift Biosciences Accel-NGS 2S Plus DNA library kit (Swift Biosciences, Ann Arbor, MI, USA) and subjected to sequencing using a 50-bp single-read sequencing module with the HiSeq 3000 sequencing system from Illumina. ChIP DNA was analyzed by quantitative PCR with the SsoAdvanced universal SYBR green supermix kit and the following primers (for Rattus norvegicus promoters):

ADAR (F: 5'-GTAGCCTTCAGGAGAGTCGG-3', R: 5'-GGACCAGAGCAGGTAACAACA-3')

OAS1A (F: 5'-TCGACTGGATTGATGGACCC-3', R: 5'-AATGCGATTCGAAGGACCAGT-3')

IL1A (F: 5'-TGCTGATAGACTCGCTCACG-3', R: 5'-GAGAACTTAGGGAGCAGCTGAA-3')

BST2 (F: 5'-TCAAGTTCCTTGATGCGGGC-3', R: 5'-TAACAGCCAGCCCATGTTTCT-3')

SOHLH1 (F: 5'-GGGCACTACTGCCTCAGTTT-3', R: 5'-AGCTAGGATCCATGCTGTGG-3')

ZFP112 (F: 5'-CAGTCACCTGGATGGAGGAT-3', R: 5'-TTTGAGCCTTGCAGGAAACT-3')

ADAMTS19 (F: 5'-CCCTTTGCAGAGCGTGTACT-3', R: 5'-ACCAGAGGAGCAGTCCAGT

C-3’)

HS3T3B1 (F: 5’-AGAAGCTCGAGATGGGACTG-3’, R: 5’-TGATCACAGCTCCGAATGAG-3’)

2.2.11 Bioinformatic analysis

We performed patients’ survival analysis using the Kaplan-Meier Survival Analysis for selected epigenetic genes based on their gene expression data to partition tumors. For expression values of each gene in a particular tumor type, we use $\mu-\delta$ and $\mu+\delta$ to partition tumors into three groups, where μ and δ are the mean and standard deviation of the expression values of the gene in tumors, respectively.

For the RNA-seq data processing, we first used Partek Flow to process raw RNA-seq data and matched sequenced RNA segments into genes to obtain expression values of genes. Then the gene expression data were normalized with dChip (157). For each gene g, we obtained a set of expression values for all control samples and a set of expression values for test samples with shRNA each of GRWD1, WDR5, or MLL2. We decided that the gene g was differentially expressed if 1) fold change of mean values for control samples and test samples was at least 1.3; 2) t-test p-Value for control samples and test samples was at most 0.05.

For ChIP-seq analysis, quality control, read mapping, and signal track visualization were performed by deploying the ChIP-seq pipeline developed in ENCODE project (158). Specifically, we used Bowtie2 (159) to align the single-end read fragments to the Rattus Norvegicus genome (Rn6). Bowtie2 was configured with default parameters. Signal tracks of fold change and P values were generated from MACS2 by comparing each immunoprecipitation profile with its corresponding background/input profile.

Within each peak set generated by MACS2, the peak regions were restricted to 150 bps downstream and upstream to the peak summit. Hence the width of peak regions was fixed as 301 bps. To generate the consensus peak set across samples, the peak summits were recentered to the optimal enrichment across samples within the same condition. We used DiffBind (160) to quantify read counts in consensus peak sets. Read counts were then normalized with TMM (161) and minus the full library size of the input. We visualized the similarity among samples with heatmap and multi-dimensional scaling (MDS). Samples were removed before differential analysis if they were not consistent with other repeats (i.e., H3K4me3 of the 2nd replicate of GRWD1 knockdown in KMM cells; and H3K27me3 of the 1st replicate of control cells).

With the read counts of the remaining samples, we used EdgeR (161) to perform differential analysis on GRWD1 knockdown versus vehicle control within each cell line and each histone position. Peak regions with P values < 0.05 and absolute log fold change > 0.5 were selected as differential binding sites. Heatmaps were also plotted to verify the effect size. We then used ChIPseeker (162) to annotate the binding sites with their closest genes.

2.2.12 Tumor growth in mice

The mice experiment complied with IACUC protocol 21079422 approved by the University of Pittsburgh. The growth of subcutaneous tumors was performed as previously described (107). Cells at 5×10^6 were injected into both flanks of the nude mice. Tumor volumes were measured twice a week using 0.2 cm^3 as a threshold. The experiment was terminated at week 21 following inoculation. Mice were terminated by carbon dioxide (CO2) inhalation followed by cervical dislocation when the tumor volume reached 1.5 cm^3. Tumor analysis was performed as previously described (107).

2.2.13 Statistical analysis

Data are shown as mean ± SD (standard deviations) where appropriate. The two-tailed Student t test or one-way analysis of variance (ANOVA) was used to compare data between the experimental groups. Statistical significance was considered at P values less than 0.05, 0.01, or 0.001, represented by *, **, or ***, respectively.

2.2.14 Data availability

All the RNA-seq and ChIP-seq results are available at GenBank, Project ID PRJNA781746.

2.3 Results

2.3.1 Alterations of global epigenetic modifications in KSHV-transformed cells

To determine alterations in the epigenetic landscape of KSHV-transformed cells, we performed ChIP-seq to identify the common active mark H3K4me3 and H3 lysine 27 trimethylation (H3K27me3) repressive mark in MM and KMM cells. Compared to MM cells, there were significant changes in H3K4me3 and H3K27me3 marks in KMM cells (Fig. 6), which were consistent with alterations of gene expression in these cells (107).

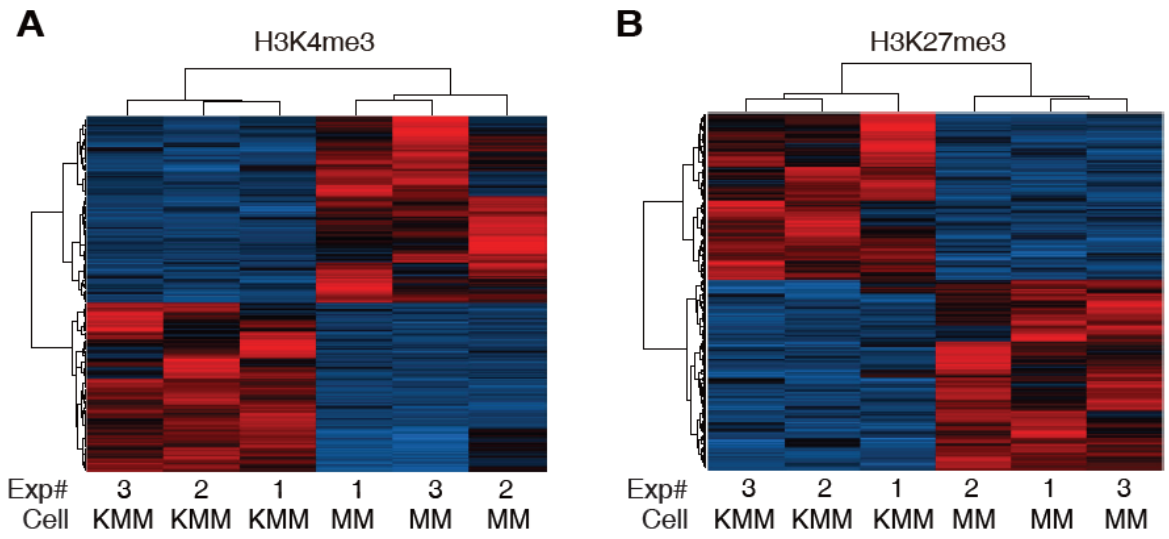

Figure 6: Heatmaps of H3K4me3 (A) and H3K27me3 (B) peaks of MM and KMM cells. Red indicates upregulation and blue indicates downregulation.

We have previously performed a CRISPR-Cas9 screening with MM and KMM cells and identified genes that promote or suppress cell proliferation and survival (110). By combining the EpiFactors database (6) and the epigenetic factors newly described between 2015 and 2021 (139, 163-167), we identified 701 epigenetics-related genes that had differential effects on cell proliferation and survival between MM and KMM cells following their knockout (Fig. 7). Of the 6 groups of genes identified, group 2 (17 genes) had negative and group 8 (109 genes) had positive effects on cell proliferation and survival of KMM but not MM cells, respectively (110) (Fig. 5). The top 9 genes in group 8 with the most differences in CRISPR scores between KMM and MM cells on day 21 following knockout were CXXC1, NFYB, GRWD1, KAT8, PRMT5, EXOSC9, EXOSC5, TADA3, and RUVBL1 (Fig. 8 and 9). These genes are likely essential for the proliferation of KMM but not MM cells.

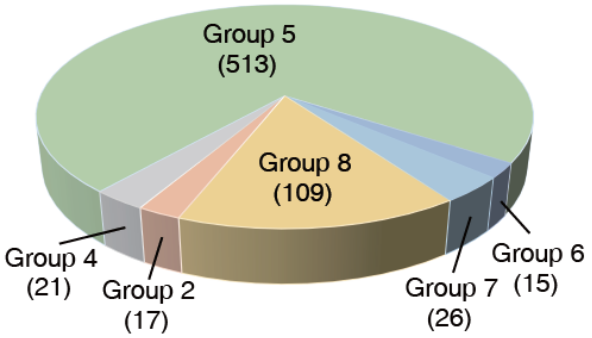

Group 2 (negative effects on KMM survival)	
Histone acetylation	5
Histone methylation	2
Histone phosphorylation	2
Histone ubiquitination	1
TF activator	1
TF repressor	1
N/A	5
Total	17

Group 4 (postive effects on MM survival)	
Histone acetylation	6
Histone methylation	2
Histone ubiquitination	4
Histone deubiquitination	1
TF activator	1
TF repressor	1
Histones / Replication-dependent	1
N/A	8
Total	21

Group 6 (negative effects on MM survival)	
Histone methylation	2
Histone phosphorylation	2
Histone ubiquitination	1
Histone deubiquitination	1
Histones / Replication-dependent	1
N/A	9
Total	15

Group 7 (postive effects on both cells)	
Histone acetylation	4
Histone methylation	3
Histone phosphorylation	1
Histone ubiquitination	5
RNA degradation	3
Histones / Replication-dependent	3
N/A	8
Total	26

Group 5 (no sigificant effects on both cells)	
DNA methylation	4
DNA demethylation	4
DNA hydroxymethylation	5
Histone acetylation	90
Histone methylation	92
Histone phosphorylation	41
Histone ubiquitination	38
Histone deubiquitination	3
Histone deacetylation	4
Histone citrullination	4
Histone sumoylation	2
RNA degradation	1
RNA deamination	1
TF activator	15
TF repressor	21
mRNA editing	3
Histones / Replication-dependent	19
Histones / Replication-independent	9
N/A	215
Total	513

Group 8 (postive effects on KMM survival)	
DNA methylation	2
Histone acetylation	20
Histone GlcNAcylation	1
Histone methylation	16
Histone phosphorylation	8
Histone ubiquitination	11
RNA degradation	5
TF activator	1
TF repressor	2
Histones / Replication-dependent	2
Histones / Replication-independent	3
N/A	39
Total	109

Figure 7: Distribution of epigenetic factors in 9 groups identified in CRISPR-Cas9 screening of MM and KMM cells. Functional classification of epigenetic factors in the 9 groups identified in CRISPR-Cas9 screening of MM and KMM cells are shown in the table.

Group	Gene	KMM-MM
Group8	CXXC1	-5.44
Group8	NFYB	-4.67
Group8	GRWD1	-4.00
Group8	KAT8	-3.67
Group8	PRMT5	-3.41
Group8	EXOSC9	-2.84
Group8	EXOSC5	-2.84
Group8	TADA3	-2.63
Group8	RUVBL1	-2.61

Figure 8: Top 9 epigenetic factors with the largest differences in CRISPR score between MM and KMM cells in Group 8 identified in CRISPR-Cas9 screening. CRISPR score is defined as the average (log2(final sgRNA abundance/initial sgRNA abundance)).

To determine the likely involvement of these genes in other types of cancer, we examined their prognostic values using the TCGA database (Fig. 10; see also Fig. S1 and Table 1). Patients with a higher expression level of CXXC1 had a worse prognosis for liver hepatocellular carcinoma (LIHC) but a better prognosis for bladder urothelial carcinoma (BLCA) and uterine corpus endometrial carcinoma (UCEC). Patients with a higher expression level of NFYB had a worse prognosis for kidney renal clear cell carcinoma (KIRC) and kidney renal papillary cell carcinoma (KIRP) but a better prognosis for BLCA, cervical squamous cell carcinoma, and endocervical adenocarcinoma (CESC), brain lower-grade glioma (LGG), LIHC, sarcoma (SARC), and skin cutaneous melanoma (SKCM). Patients with a higher expression level of GRWD1 had a worse prognosis for LGG, lung adenocarcinoma (LUAD), breast cancer (BC), SARC, and SKCM.

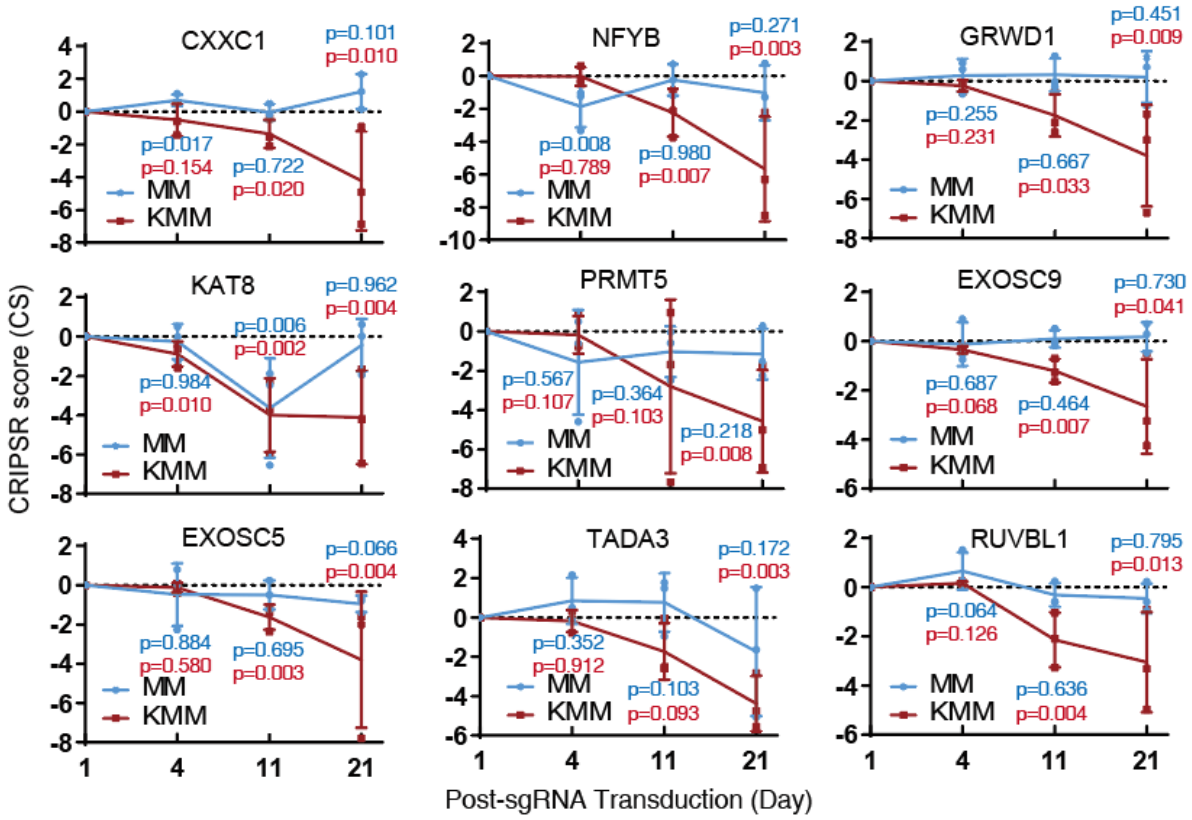

Figure 9: CRISPR scores on days 4, 11, and 21 of the top 9 epigenetic regulators with the largest CRISPR score (CS) differences between MM and KMM cells. The p-values of three sgRNAs for MM and KMM were listed for each time point.

Patients with a higher expression level of KAT8 had a better prognosis for BC. Patients with a higher expression level of PRMT5 had a worse prognosis for BLCA, head and neck squamous cell carcinoma (HNSC), LIHC, and SARC but a better prognosis for glioblastoma multiforme (GBM) and KIRC. Patients with a higher expression level of EXOSC9 had a worse prognosis for BC. Patients with a higher expression level of EXOSC5 had a worse prognosis for KIRC, KIRP, BC, and prostate adenocarcinoma (PRAD). Patients with a higher expression level of TADA3 had a worse prognosis for KIRC but a better prognosis for BLCA. Patients with a higher expression level of RUVBL1 had a worse prognosis for LGG, LIHC, BC, and SARC. Since

a higher expression level of GRWD1 is associated with a worse prognosis for 5 types of cancer, especially SARC, which is similar to KS and the KMM tumor, and its epigenetic role in cancer is largely unknown, we chose to further investigate GRWD1's role in KSHV-induced cellular transformation.

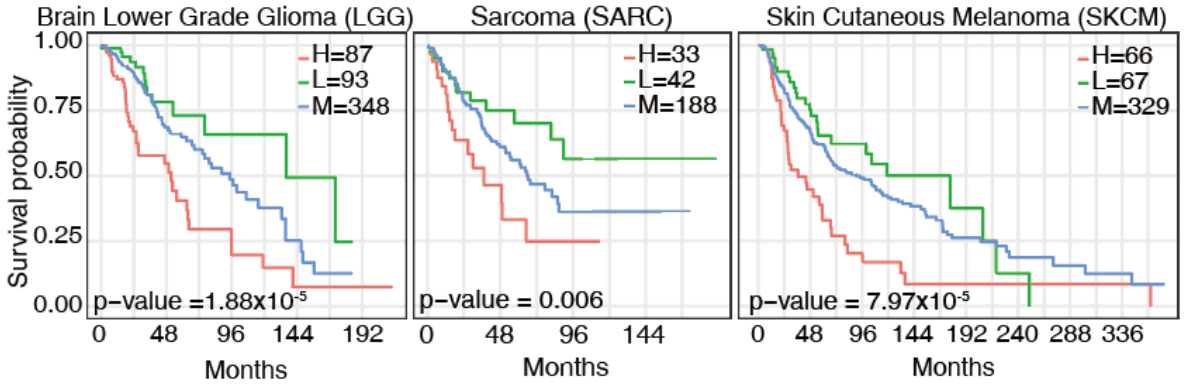

Figure 10: Survival analysis of GRWD1 expression in brain lower grade glioma (LGG), sarcoma (SARC), and skin cutaneous melanoma (SKCM). H, L, and M, high, low, and medium, respectively.

Table 1: Summary of survival analysis of top 9 epigenetic genes in group 8 identified by CRISPR-Cas9 screening of MM and KMM cells.

Gene	Disease Type	ID	P-Value
CXXC1	Bladder Urothelial Carcinoma	BLCA	0.033
	Kidney Renal Clear Cell Carcinoma	KIRC	0.021
	Kidney Renal Papillary Cell Carcinoma	KIRP	0.004
	Liver Hepatocellular Carcinoma	LIHC	0.091
	Breast Cancer	MetaBric	0.010
	Sarcoma	SARC	0.001
	Uterine Corpus Endometrial Carcinoma	UCEC	0.039
EXOSC5	Glioblastoma Multiforme	GBM	0.094
	Kidney Renal Clear Cell Carcinoma	KIRC	0.001
	Kidney Renal Papillary Cell Carcinoma	KIRP	0.001
	Lung Squamous Cell Carcinoma	LUSC	0.043
	Breast Cancer	MetaBric	0.049
	Prostate Adenocarcinoma	PRAD	0.070
EXOSC9	Breast Cancer	MetaBric	0.006
GRWD1	Glioblastoma Multiforme	GBM	0.086
	Brain Lower Grade Glioma	LGG	0.000
	Lung Adenocarcinoma	LUAD	0.008
	Breast Cancer	MetaBric	0.008
	Sarcoma	SARC	0.006
	Skin Cutaneous Melanoma	SKCM	0.000
KAT8	Breast Cancer	MetaBric	0.012
NFYB	Bladder Urothelial Carcinoma	BLCA	0.033
	Cervical Squamous Cell Carcinoma and Endocervical Adenocarcinoma	CESC	0.038
	Kidney Renal Clear Cell Carcinoma	KIRC	0.000
	Kidney Renal Papillary Cell Carcinoma	KIRP	0.022
	Brain Lower Grade Glioma	LGG	0.001
	Liver Hepatocellular Carcinoma	LIHC	0.002
	Sarcoma	SARC	0.057
	Skin Cutaneous Melanoma	SKCM	0.002
PRMT5	Bladder Urothelial Carcinoma	BLCA	0.001
	Glioblastoma Multiforme	GBM	0.010
	Head-Neck Squamous Cell Carcinoma	HNSC	0.027
	Kidney Renal Clear Cell Carcinoma	KIRC	0.025
	Brain Lower Grade Glioma	LGG	0.000
	Liver Hepatocellular Carcinoma	LIHC	0.007
	Breast Cancer	MetaBric	0.000
	Ovarian Serous Cystadenocarcinoma	OV	0.067
	Sarcoma	SARC	0.033
RUVBL1	Kidney Renal Papillary Cell Carcinoma	KIRP	0.039
	Brain Lower Grade Glioma	LGG	0.032
	Liver Hepatocellular Carcinoma	LIHC	0.000
	Breast Cancer	MetaBric	0.006
	Sarcoma	SARC	0.046
TADA3	Bladder Urothelial Carcinoma	BLCA	0.037
	Kidney Renal Clear Cell Carcinoma	KIRC	0.018
	Kidney Renal Papillary Cell Carcinoma	KIRP	0.001
	Breast Cancer	MetaBric	0.083
	Sarcoma	SARC	0.012
	Uterine Corpus Endometrial Carcinoma	UCEC	0.021

2.3.2 GRWD1 is essential for cell proliferation and cellular transformation of KSHV transformed cells

To confirm the essential role of GRWD1 in the proliferation of KSHV transformed cells, we performed a lentivirus-mediated short hairpin RNA (shRNA) knockdown of GRWD1. At day 3 posttransduction, GRWD1 RNA and protein levels were reduced by >70% and >60% in MM and KMM cells, respectively (Fig. 11A and 11B). Interestingly, the protein level of GRWD1 was higher in untransduced KMM than in MM cells (Fig. 11B). As expected, KMM cells proliferated at a much higher rate than MM cells did (97). Compared to untransduced cells or cells transduced with scrambled shRNA, both MM and KMM cells transduced with the shRNAs had significantly reduced proliferation rates with a more profound effect observed in KMM than MM cells (Fig. 12). GRWD1 knockdown induced cell cycle arrest by increasing the G1 phase and reducing S phase cell numbers of both MM and KMM cells, respectively (Fig. 13A), but had minimal effect on the numbers of apoptotic cells for both types of cells (Fig. 13B). Importantly, GRWD1 knockdown completely abolished colony formation of KMM cells in soft agar (Fig. 14). As expected, no colony was observed with MM cells with or without GRWD1 knockdown.

We further examined the effect of GRWD1 knockdown on tumor formation of KMM cells in nude mice. GRWD1 knockdown significantly reduced the number of tumors as well as the progression of tumors (Fig. 15-18 and Table 2) (168). At the endpoint of week 21, the average volume of tumors induced by KMM cells transduced with scrambled shRNA was 233.03 mm^3 while the values for those transduced with the three shRNAs were 93.28 mm^3, 120.27 mm^3, and 56.76 mm^3, respectively, excluding the excessive large tumors terminated in advance (Fig. 18 and Table 2).

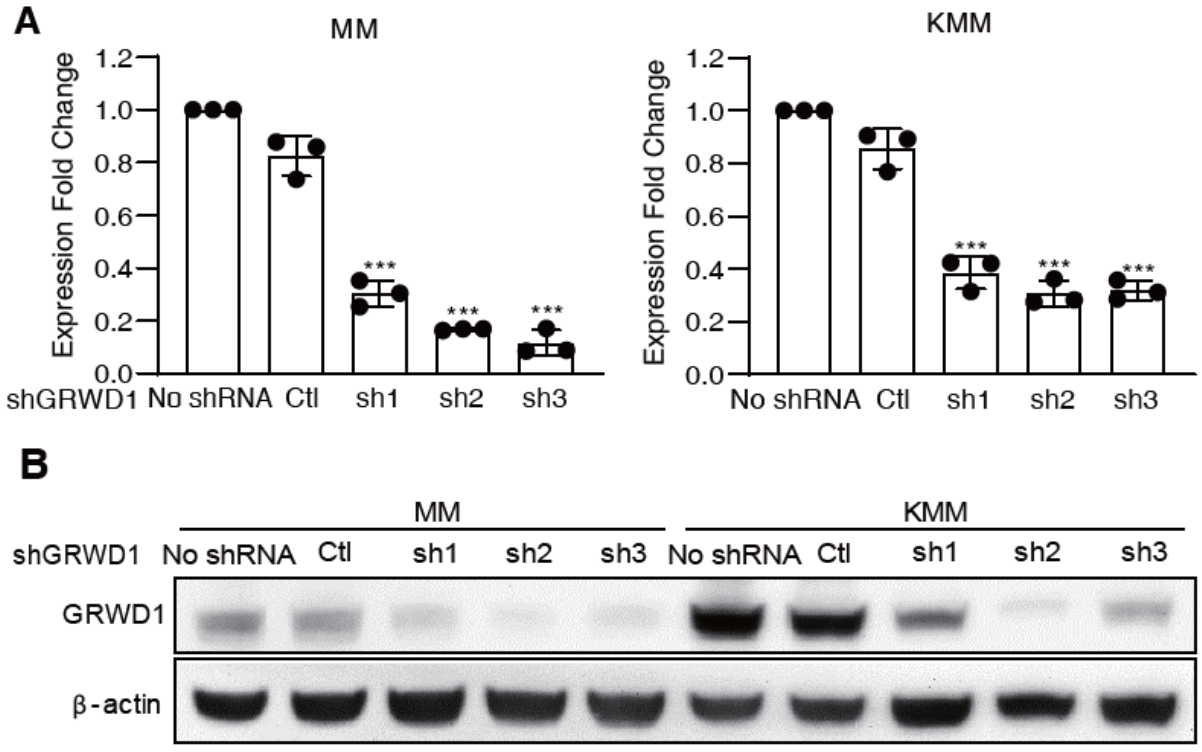

Figure 11: Knockdown efficiencies of GRWD1 shRNAs examined by RT-qPCR (A) and Western-blotting (B). GRWD1 knockdown greater than 60% was confirmed after 48hrs post-transduction.

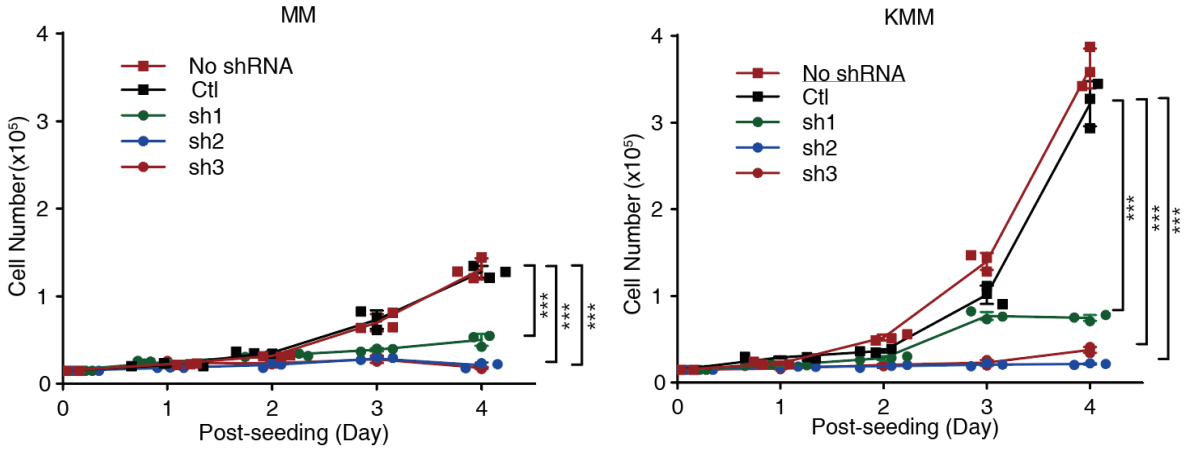

Figure 12: The effects of GRWD1 knockdown on cell proliferation. Growth curve was calculated from day 1 to day 4 post-transduction. The data of three or more independent biological replicates were calculated. The values which are statistically significant are indicated with asterisks.

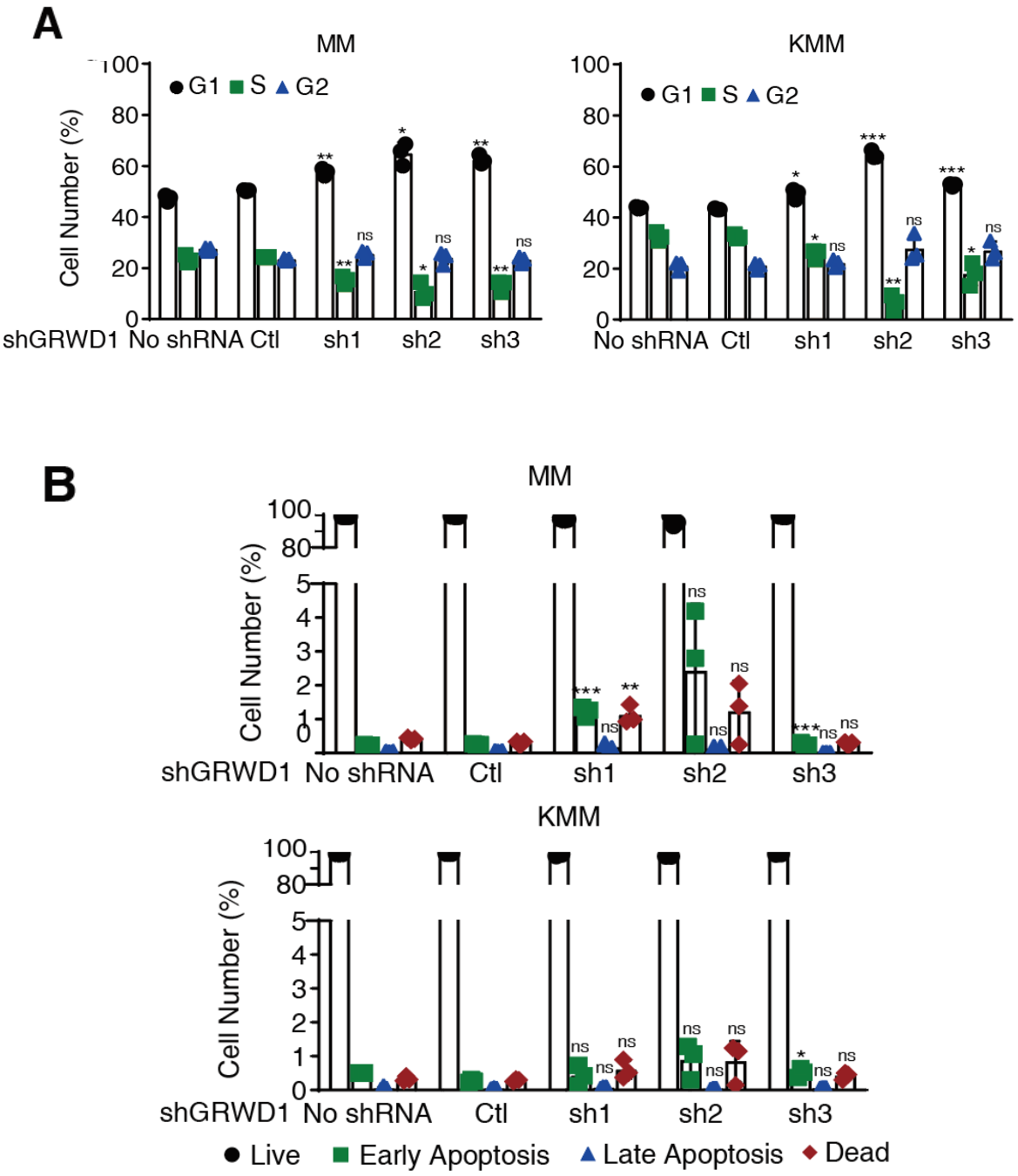

Figure 13: The effects of GRWD1 knockdown on cell cycle progression (A) and apoptosis (B). (A) Bar graph representing the percentage of cells in G1, S and G2. (B) Bar graph representing the percentage of cells in live, early apoptosis, late apoptosis and dead. Bars represent an average of three measurements. Asterisks represent significant results.

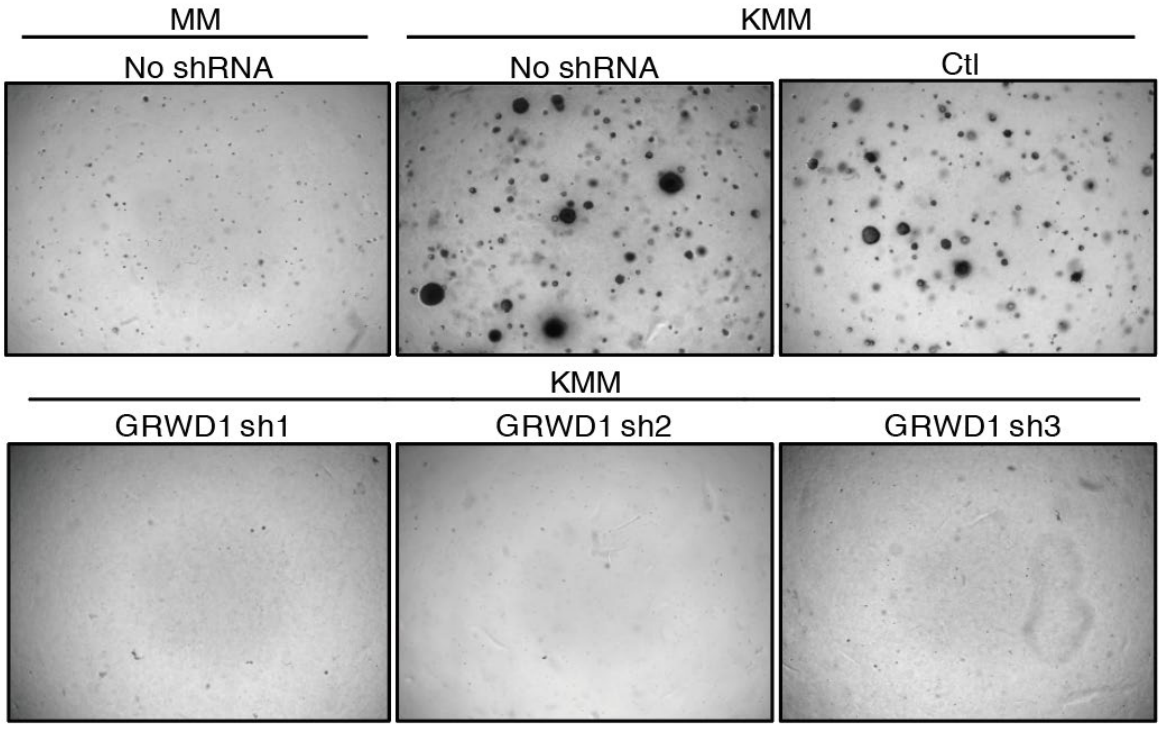

Figure 14: GRWD1 knockdown reduced the efficiency of colony formation on soft agar of KMM cells. Picture showed the representative images of colonies in soft agar.

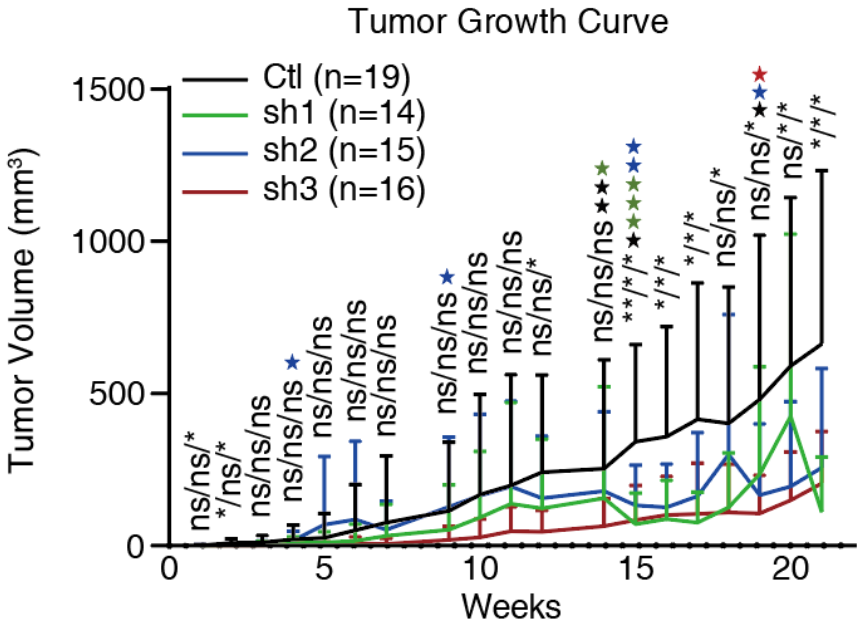

Figure 15: GRWD1 knockdown inhibited the progression of KMM tumors in nude mice. Tumor growth curves obtained by measuring the volumes of the tumors in the four treatment groups. Mice with tumors exceeding the 1.5 cm^3 volume limit were terminated before the final day of the experiment and labeled with stars.

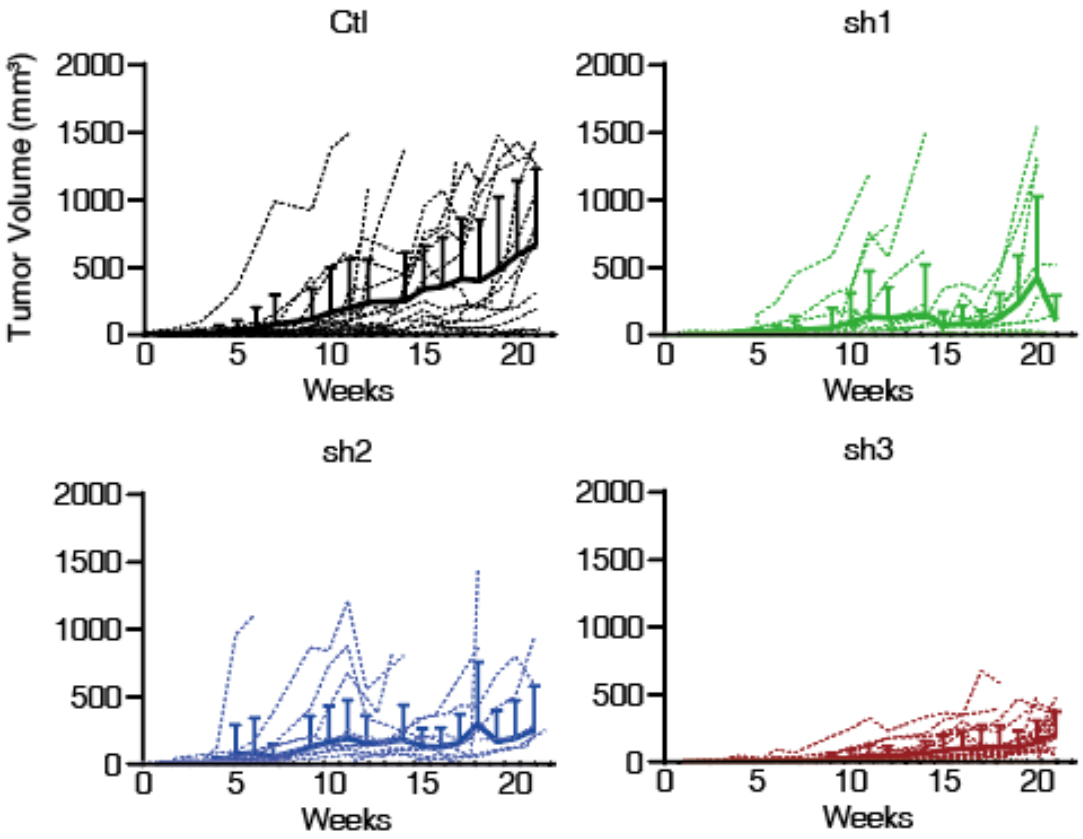

Figure 16: The tumor volumes of individual tumors from each group showing that GRWD1 knockdown inhibited the progression of KMM tumors. Thicker lines are the averages of the tumor volumes. Mice with tumors exceeding the 1.5 cm^3 volume limit were terminated before the final day of the experiment.

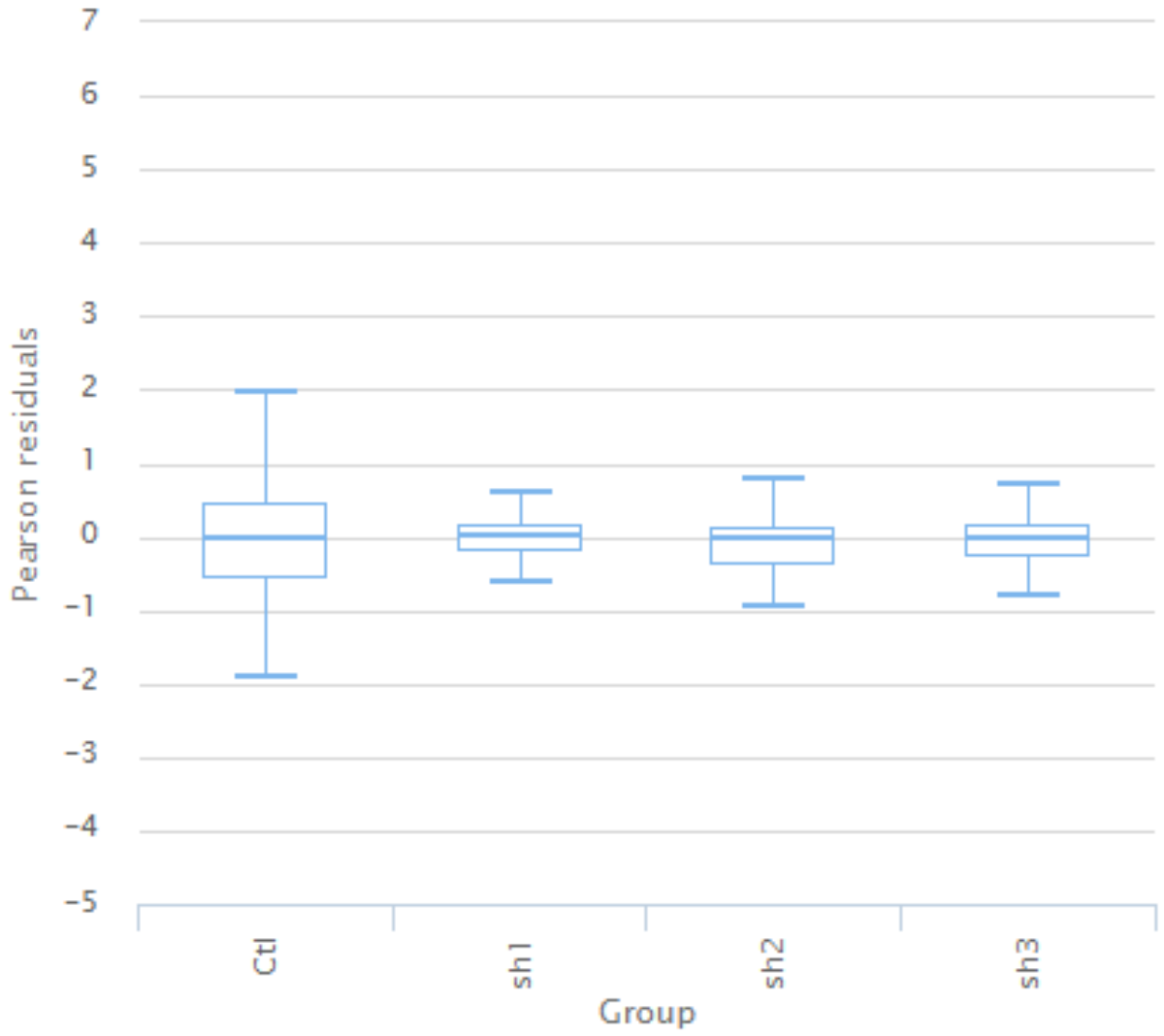

Figure 17: Longitudinal analysis of the distribution of tumor growth across time points and mice. Figure created with TumGrowth (168).

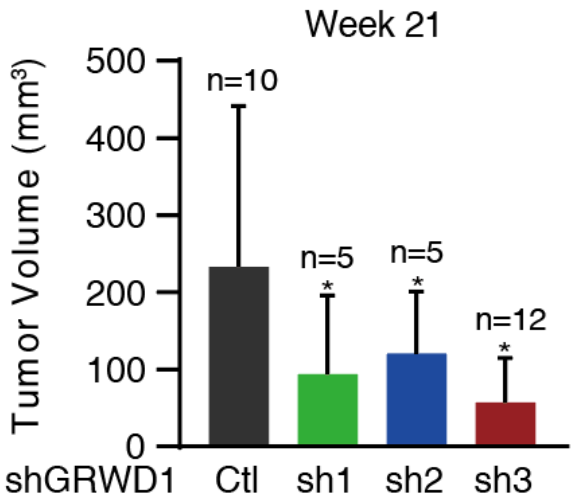

Figure 18: At the endpoint of week 21, GRWD1 knockdown reduced the volume of KMM tumors in nude mice. Mice with tumors exceeding the 1.5 cm^3 volume limit were terminated before the final day of the experiment.

Table 2: Tumor incidence of each treatment group.

Group	Tumor incidence in total	Tumor incidence at week 21 (End)	Tumor incidence at week 15
Ctl	90%(18/20)	91%(10/11)	74%(14/19)
sh1	70%(14/20)	56%(5/9)	30%(6/20)
sh2	75%(15/20)	56%(5/9)	56%(9/16)
sh3	75%(15/20)	71%(12/17)	30%(6/20)

Taken together, these results indicate that GRWD1 is essential for cell cycle progression, cell proliferation, and cellular transformation of KSHV-transformed cells and that GRWD1 is also required for the proliferation of primary cells.

2.3.3 GRWD1 maintains H3K4me3 mark at specific loci of KSHV-transformed cells

GRWD1 regulates chromatin architecture (139, 140) and is potentially involved in histone methylation (25). Thus, we examined GRWD1's role in epigenetic remodeling in KSHV transformed cells. Transient GRWD1 knockdown was sufficient to reduce the overall H3K4me3 level but not those of H3K27me3, H3K4me2, and H3K4me in both MM and KMM cells (Fig. 19 and 20). To identify the specific H3K4me3 loci that were regulated by GRWD1, we performed ChIP-seq in cells with stable GRWD1 knockdown. We achieved high efficiency of GRWD1 knockdown with shRNA2. Because of GRWD1's essential role, we failed to generate stable knockdown KMM cells with this shRNA (Fig. 11 and 12). However, we were able to generate GRWD1 stable knockdown cells with shRNA1 and shRNA3. GRWD1 knockdown differentially altered the H3K4me3 peaks in MM and KMM cells (Fig. 21).

To identify the GRWD1-regulated H3K4me3 peaks, we defined differential peaks between GRWD1 and scrambled shRNA knockdown cells with a P-value <0.05 and a fold change >0.5. We identified 8,501 and 1,765 differential H3K4me3 peaks for MM and KMM cells, respectively (Appendix Table S1A and B). The altered H3K4me3 peaks were annotated to 5,076 and 1,546 genes in MM and KMM cells, respectively, of which 861 genes were shared in the two types of cells (Fig. 22), indicating both common and distinct epigenetic regulations between MM and KMM cells. Among the top distinct representative genes regulated by GRWD1 in MM cells, we

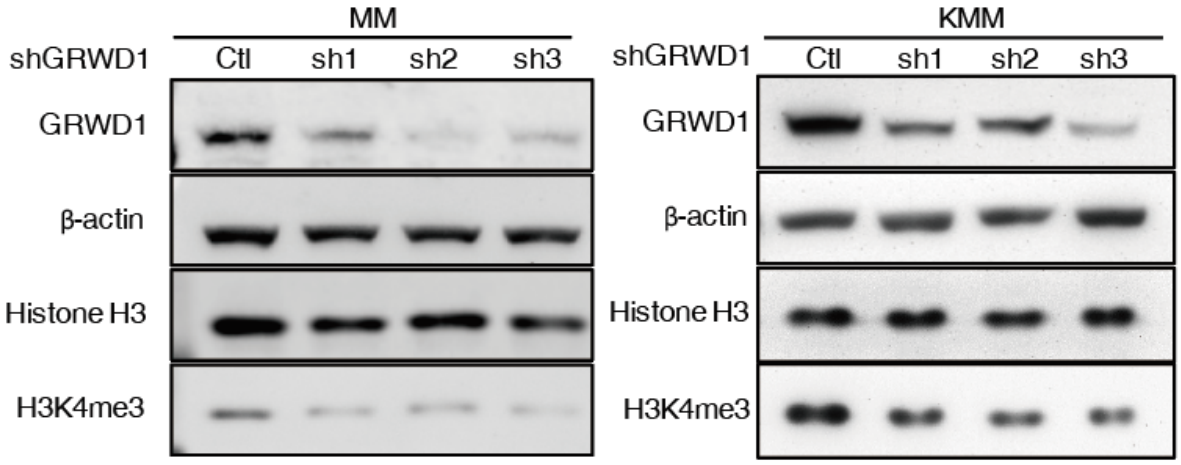

Figure 19: Western-blots showed the signal of H3K4me3 marks were decreased after GRWD1 knockdown in MM and KMM cells.

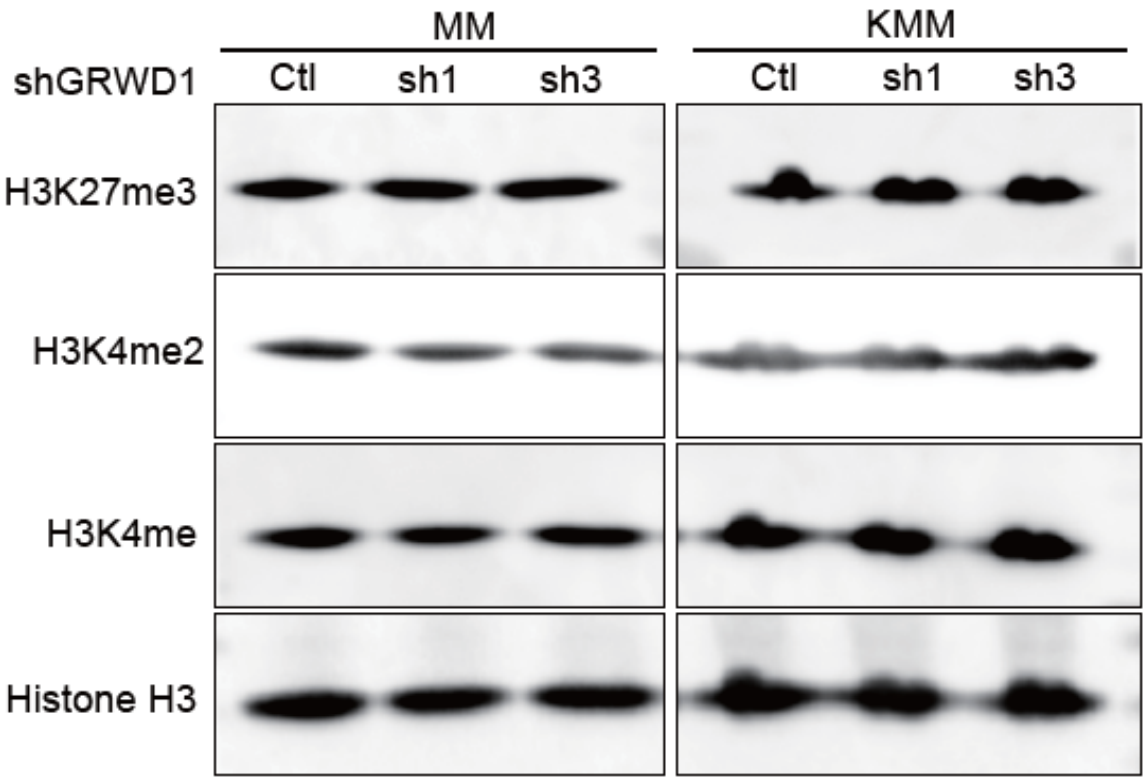

Figure 20: Western blots showing that H3K27me3, H3K4me2, and H3K4me epigenetic marks and total histone H3 remain unchanged after GRWD1 knockdown in MM and KMM cells.

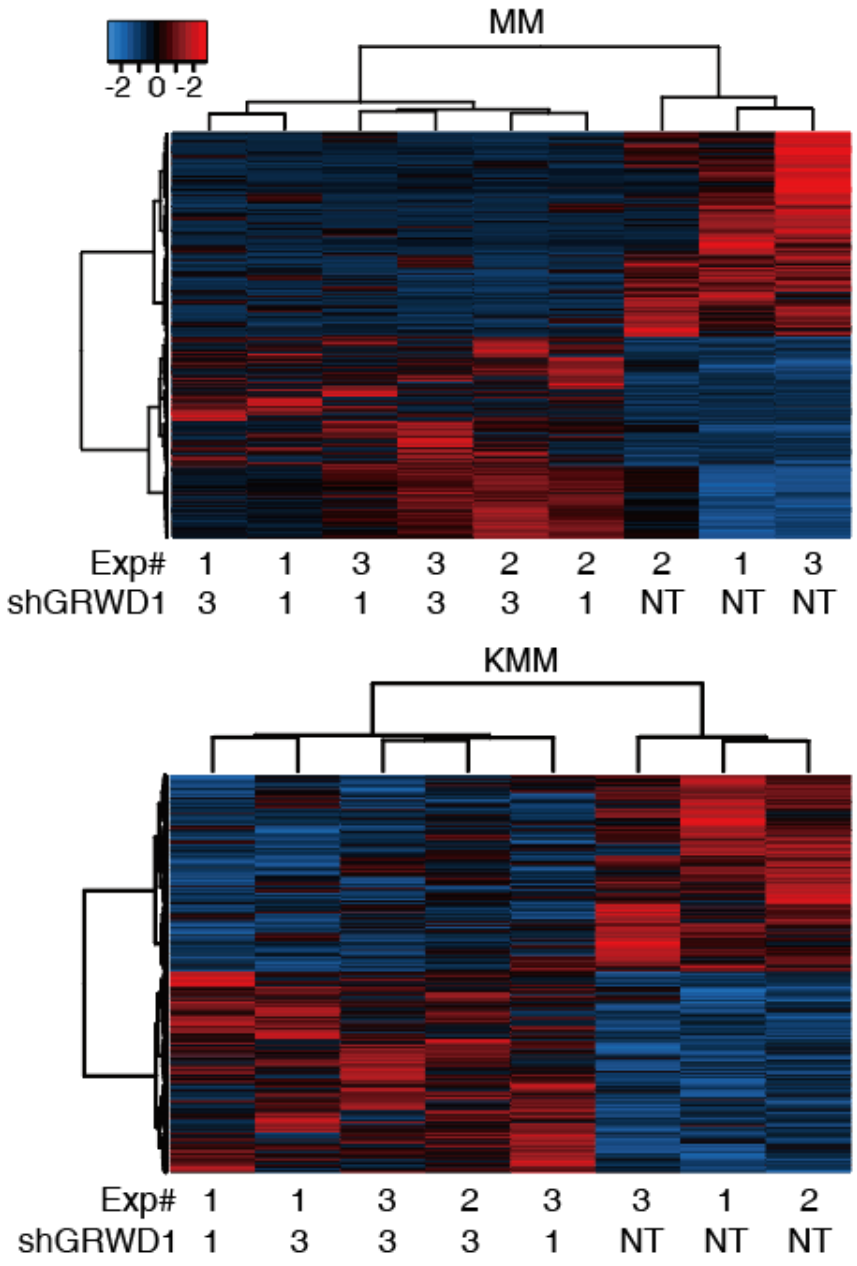

Figure 21: Heatmaps showing alterations of H3K4me3 marks after GRWD1 knockdown in MM and KMM cells Red indicates upregulation and blue indicates downregulation.

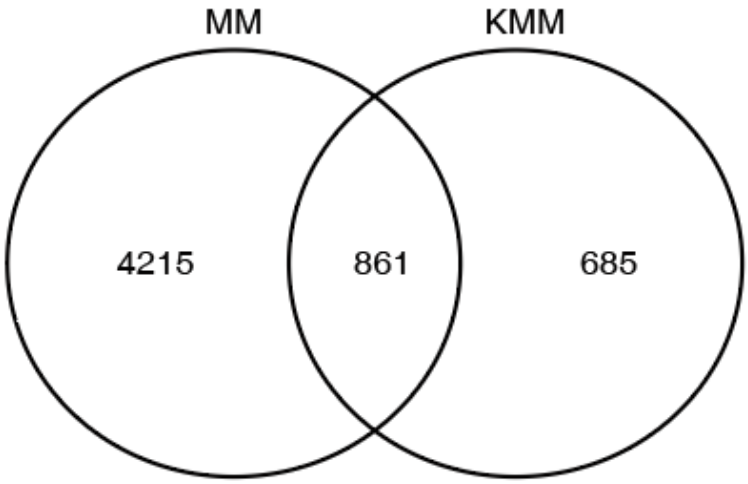

Figure 22: Differential alterations of H3K4me3 marks between MM and KMM cells after GRWD1 knockdown. The numbers of peaks which were unique for MM, unique for KMM, shared between MM and KMM cells were labelled.

validated ADAR, OAS1A, IL1A, and BST2 by ChIP-qPCR, which had minimal changes in KMM cells following GRWD1 knockdown (Fig. 23A). Indeed, there were significant reductions of H3K4me3 peaks for all four genes in MM cells in ChIP-Seq analysis (Fig. 24A and 25). In contrast, there was no change in the H3K4me3 peak for the ADAR gene while there was only a minor or no peak for the OAS1A, IL1A, or BST2 gene in KMM cells (Fig. 24A). In agreement with these results, the expression levels of OAS1A, IL1A, and BST2 genes were significantly reduced in MM cells following GRWD1 knockdown (Fig. 26A). However, only one shRNA marginally reduced the expression of the ADAR gene in MM cells while the second one had no effect (Fig. 26A), suggesting that the expression of the ADAR gene might also be regulated by other epigenetic factors and marks. No significant expression level change was found for these four genes in KMM cells following GRWD1 knockdown (Fig. 26A). Interestingly, the expression levels of OAS1A,

IL1A, and BST2 genes were 2.2-, 10-, and 5-fold lower in KMM cells than MM cells, respectively (Fig. 26A), suggesting that KSHV might downregulate the expression of these genes. Similarly, we validated SOHLH1, ZFP112, ADAMTS19, and HS3ST3B1 as the top representative genes regulated by GRWD1 in KMM cells by ChIP-qPCR (Fig. 23B). ZFP112 and ADAMTS19 genes had no significant changes in H3K4me3 while reductions for SOHLH1 and HS3ST3B1 genes were observed in MM cells following GRWD1 knockdown (Fig. 23B). Consistent with these results, significant reductions of H3K4me3 peaks for ZFP112 and ADAMTS19 were observed in KMM cells in ChIP-Seq analysis, which were not observed in MM cells, while SOHLH1 and HS3ST3B1 peaks were reduced significantly in both cell types (Fig. 24B). In addition, SOHLH1 and HS3ST3B1 had both H3K4me3 and H3K27me3 marks at the promoters in MM cells, indicating the bivalent nature of these promoters (Fig. 25). In agreement with these results, the expression levels of these four genes were significantly reduced in KMM cells following GRWD1 knockdown (Fig. 26B). However, no significant changes were observed in MM cells following GRWD1 knockdown (Fig. 26B), suggesting they were regulated by another mechanism. In addition, the expression levels of SOHLH1 and HS3ST3B1 were 9.4- and 3.2-fold higher, respectively, in KMM than MM cells, while ZFP112 gene expression was 6-fold lower in KMM than MM cells (Fig. 26B), suggesting KSHV regulation of these genes. Together, these results indicate that GRWD1 is required for sustaining specific H3K4me3 peaks in both MM and KMM cells, and the epigenetic landscapes were distinct between the primary and transformed cells.

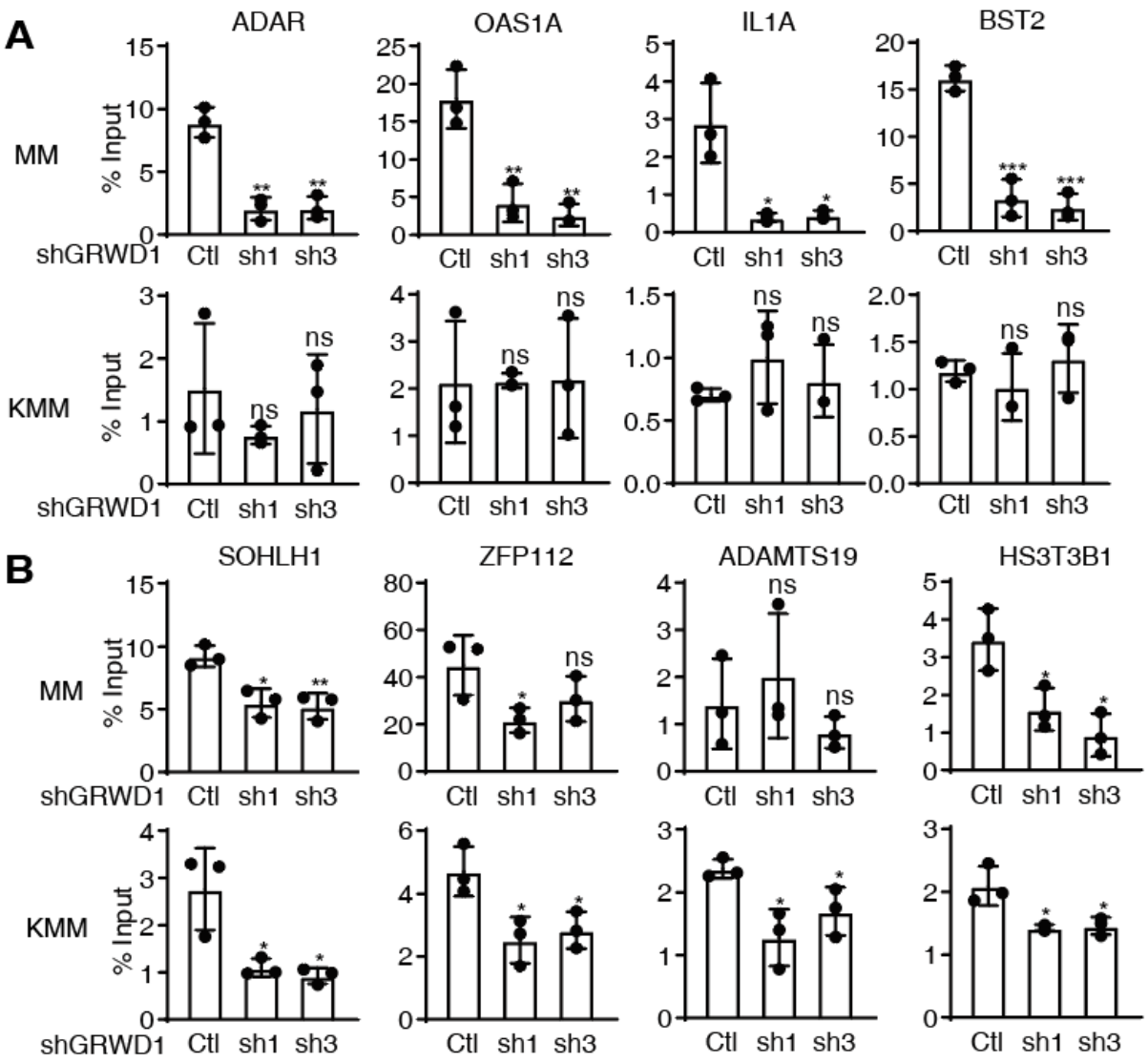

Figure 23: ChIP-qPCR validation of reduction of H3K4me3 peaks at specific gene loci in MM (A) and KMM (B) cells. The same H3K4me3 peaks were also examined in the other cells for comparison. Asterisks represent significant results.

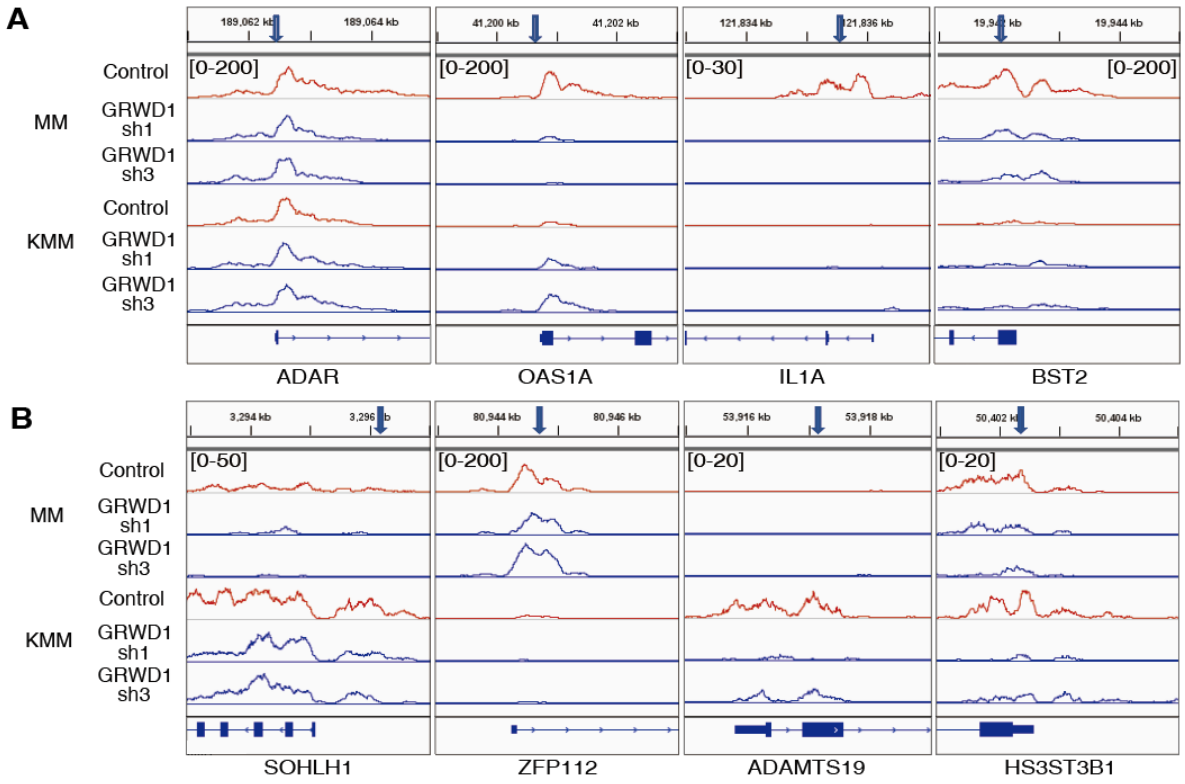

Figure 24: Tracks of H3K4me3 peaks in the promoters of the four candidate GRWD1 targets in MM (A) and KMM (B) cells. The same H3K4me3 peaks were also showed in the other cells for comparison. Primer position was labeled with arrow.

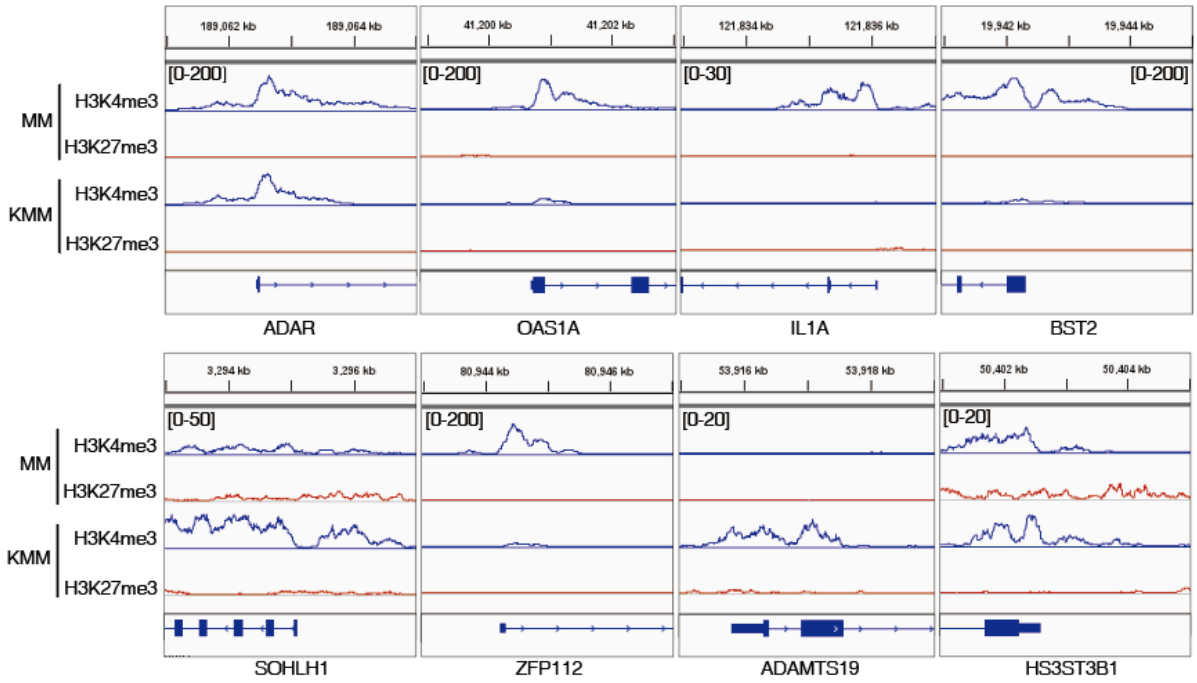

Figure 25: The tracks of H3K4me3 and H3K27me3 marks at the promoter regions of the top target genes from ChIP-seq analysis in MM and KMM cells.

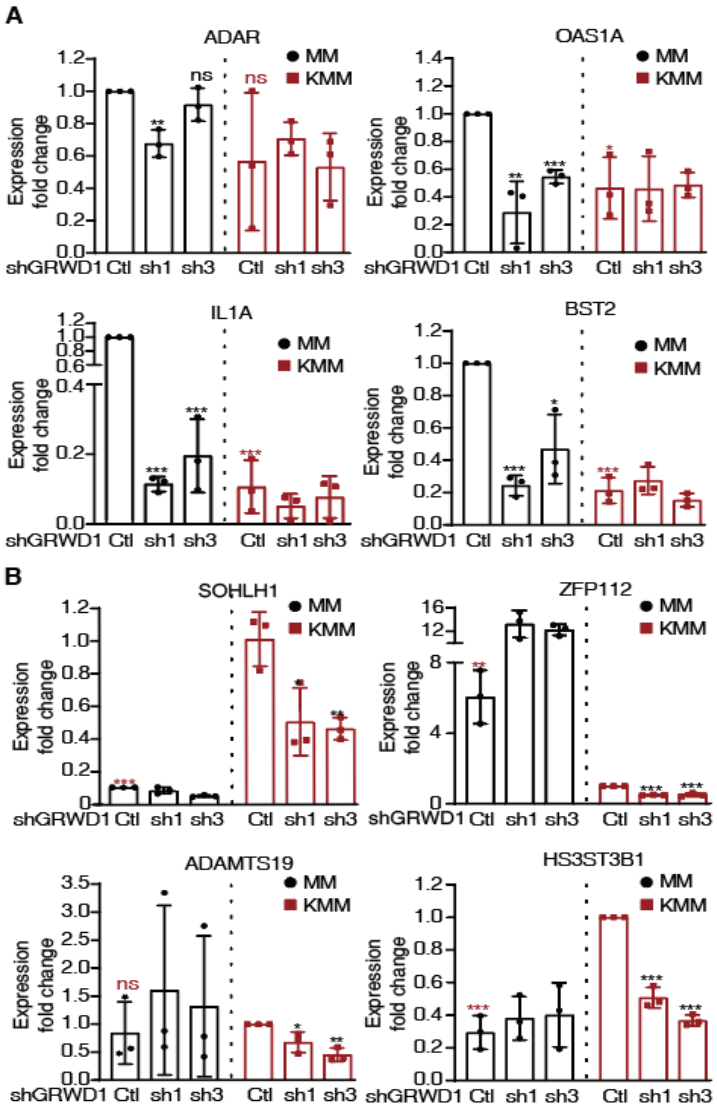

Figure 26: (A)Top four genes with reduction of H3K4me3 peaks at specific gene loci in MM cells after GRWD1 knockdown. The expression levels were normalized to the scrambled control-treated MM cells. **(B) Top four genes with reduction of H3K4me3 peaks at specific gene loci in KMM cells after GRWD1 knockdown.** The expression levels were normalized to the scrambled control-treated KMM cells. P values are from comparisons between each of the shRNA-treated groups (sh1, sh2, and sh3) and the scrambled control (Ctl). Asterisks represent significant results.

2.3.4 GRWD1 interacts with WDR5, the core protein of the H3K4 methyltransferase complex

To investigate the mechanism of GRWD1 regulation of H3K4me3 modification, we searched the protein interaction databases IntAct (169) and BioGRID (170, 171). Among the potential binding partners of GRWD1, WDR5 mediates the assembly of MLL and SET1 histone methyltransferase complexes to regulate histone H3 methylation at lysine 4 (H3K4) (16, 21). WDR5 knockdown reduced the total H3K4 methylation level (24, 25). Hence, WDR5 might mediate GRWD1 regulation of histone H3K4 trimethylation. Indeed, confocal microscopy and proximity ligation assay (PLA) examination revealed that GRWD1 colocalized with WDR5 in both MM and KMM cells (Fig. 27 and 28). In coimmunoprecipitation (co-IP), FLAG-GRWD1 specifically pulled down endogenous WDR5 (Fig. 29A) while FLAG-WDR5 specifically pulled down GRWD1 (Fig. 29B). Furthermore, in vitro pulldown assay revealed the direct interaction between GRWD1 and WDR5 proteins (Fig. 29C). Like GRWD1 knockdown, WDR5 knockdown also reduced the global H3K4me3 level in MM and KMM cells (Fig. 30). These results indicate that GRWD1 and WDR5 physically interact with each other, and both regulate the H3K4me3 modifications.

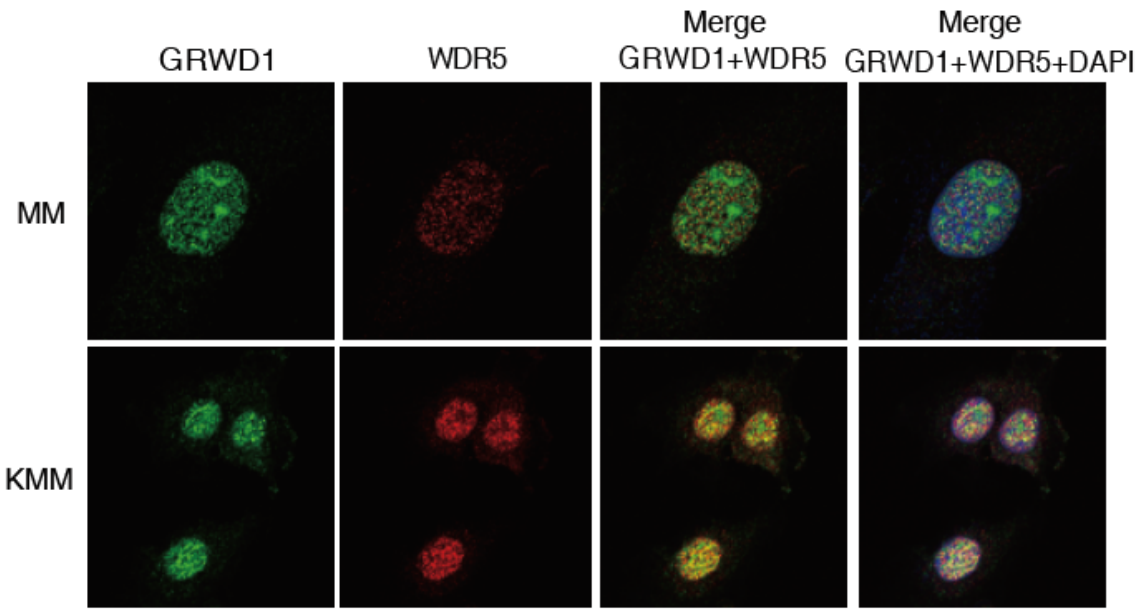

Figure 27: Confocal images showing the co-localization of GRWD1 and WDR5 in MM and KMM cells. Immunofluorescence assays (IFA) were performed using mouse anti-GRWD1 antibodies (green), and rabbit anti-WDR5 (red).

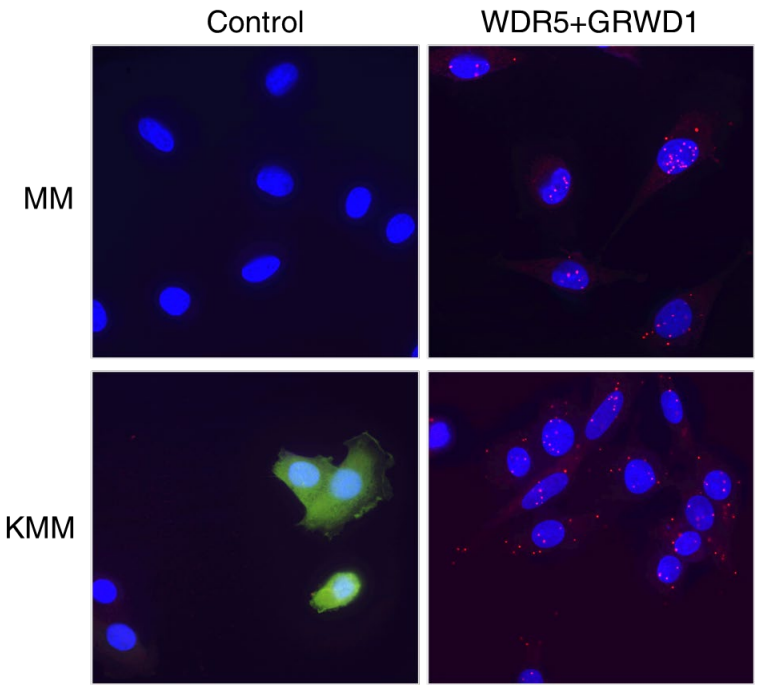

Figure 28: Proximity ligation assay (PLA) showing the co-localization of GRWD1 and WDR5 in MM and KMM cells. PLA reaction was shown in red.

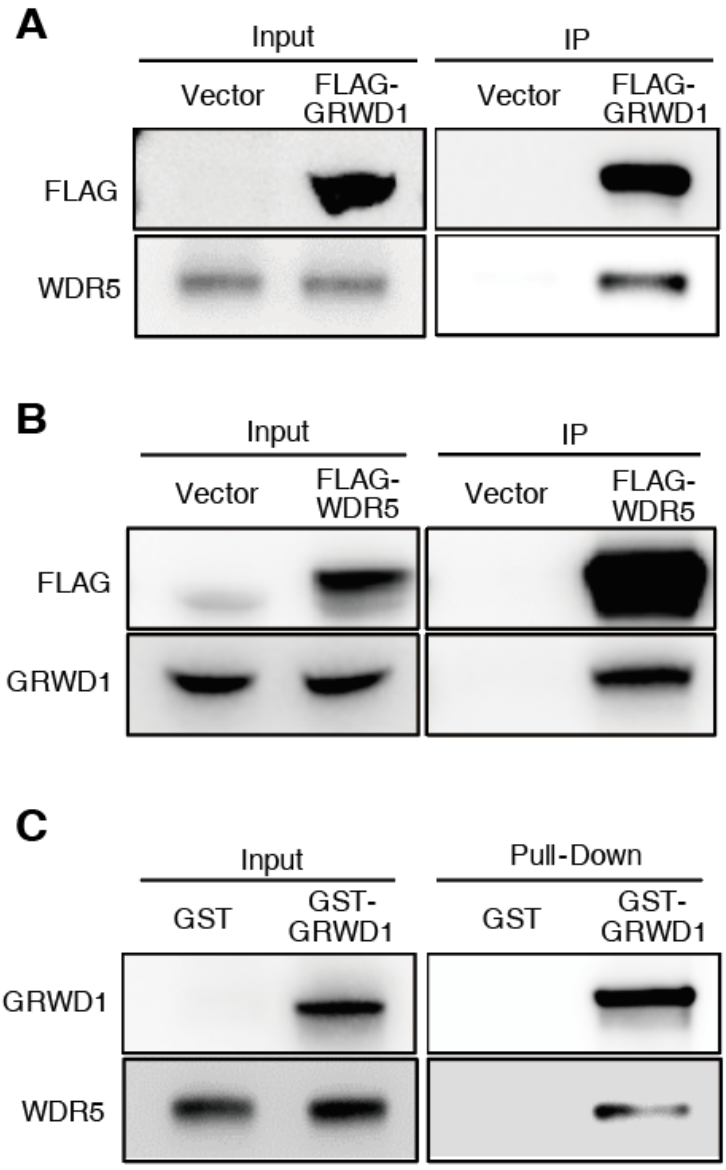

Figure 29: GRWD1 directly interacts with WDR5. (A) FLAG-GRWD1 immunoprecipitated endogenous WDR5 in 293T cells. (B) FLAG-WDR5 immunoprecipitated endogenous GRWD1 in 293T cells. (C) Purified recombinant GST-GRWD1 physically pulled down WDR5 *in vitro*. 293T cells were transfected with the construct coding for FLAG-GRWD1, FLAG-WDR5 or the vector alone. Immunoprecipitation (IP) was performed using anti-FLAG antibody. GST-pull down was performed using anti-GST antibody.

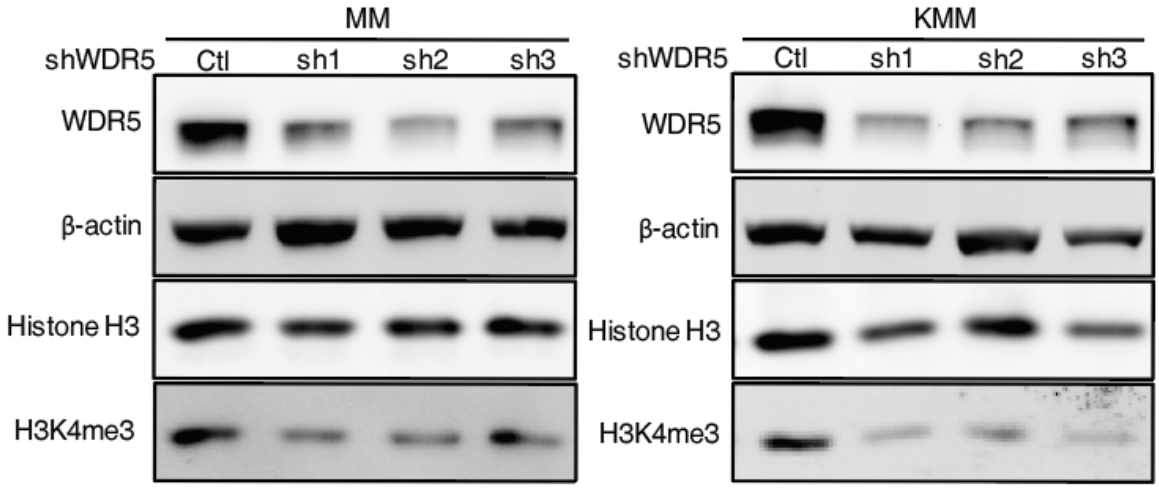

Figure 30: WDR5 knockdown reduced the level of H3K4me3 in MM and KMM cells.

2.3.5 WDR5 knockdown phenocopies GRWD1 knockdown

Since GRWD1 and WDR5 are in the same complex, the loss of WDR5 should affect cells similar to the loss of GRWD1. We performed shRNA-mediated WDR5 knockdown in MM and KMM cells (Fig. 31). Indeed, WDR5 knockdown inhibited the proliferation of both MM and KMM cells with a more profound effect observed in KMM than in MM cells (Fig. 32). WDR5 knockdown also induced cell cycle arrest but had minimal effect on apoptosis in both MM and KMM cells (Fig. 33 and 34). Furthermore, WDR5 knockdown abolished colony formation of KMM cells in a soft agar assay (Fig. 35). Together, these results show that the knockdown of WDR5 affects MM and KMM cells similar to that of GRWD1 knockdown, suggesting that the two proteins might regulate similar sets of genes.

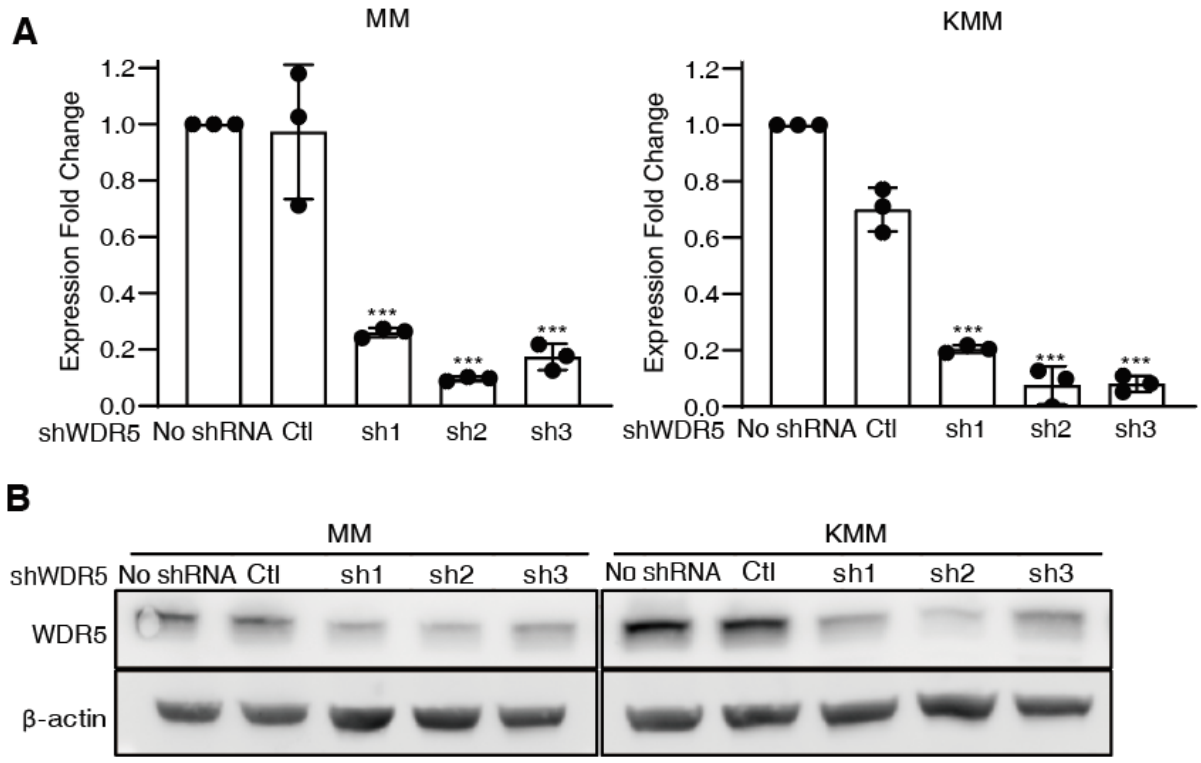

Figure 31: Knockdown efficiencies of WDR5 shRNAs examined by RT-qPCR (A) and Western-blotting (B). WDR5 knockdown greater than 60% was confirmed after 48hrs post-transduction.

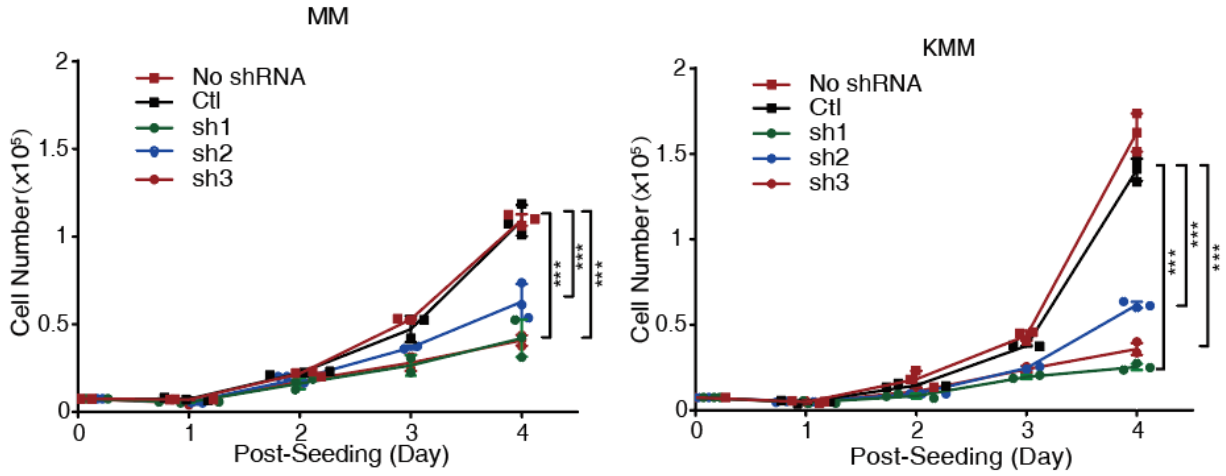

Figure 32 The effects of WDR5 knockdown on cell proliferation. The growth curve was calculated from day 1 to day 4 post-transduction. The data of three or more independent biological replicates were calculated. The values which are statistically significant are indicated with asterisks.

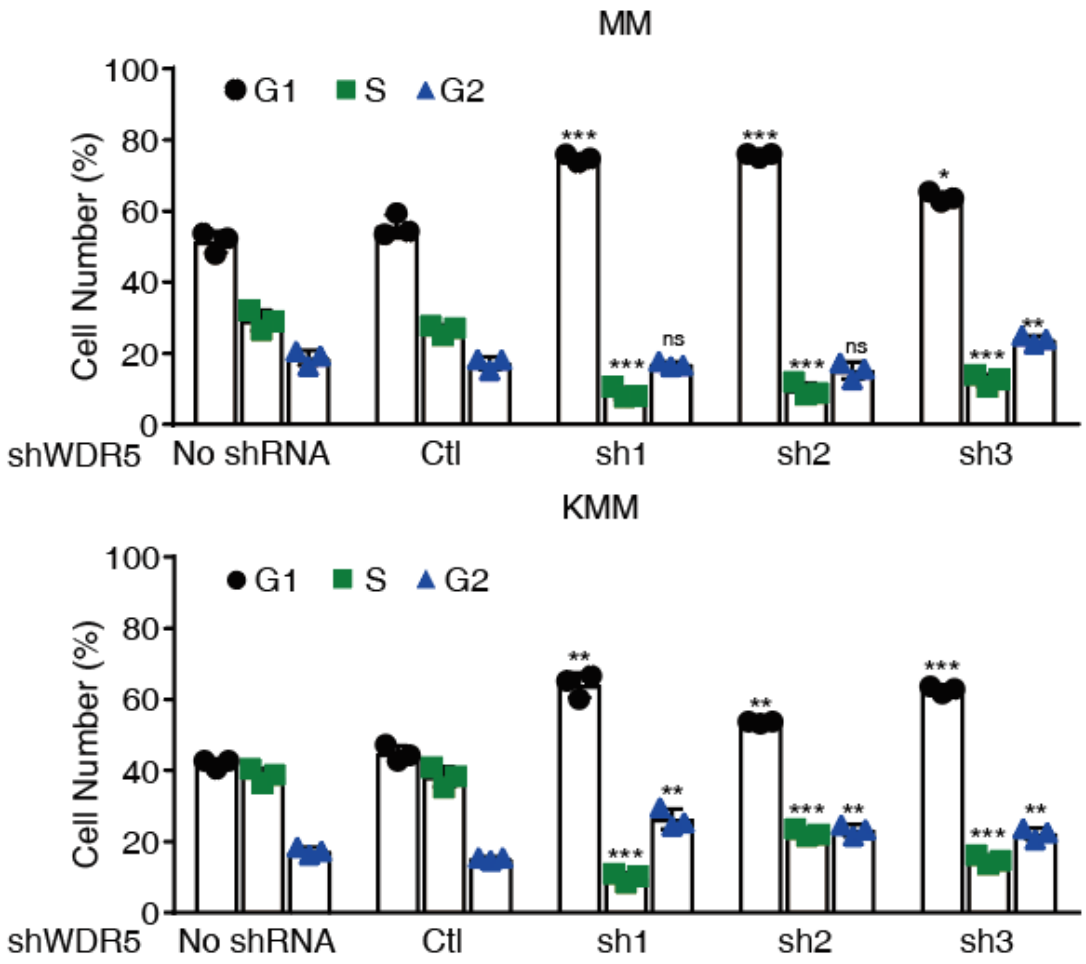

Figure 33: The effects of WDR5 knockdown on cell cycle progression. Bar graph representing the percentage of cells in G1, S and G2. Bars represent an average of three measurements. Asterisks represent significant result.

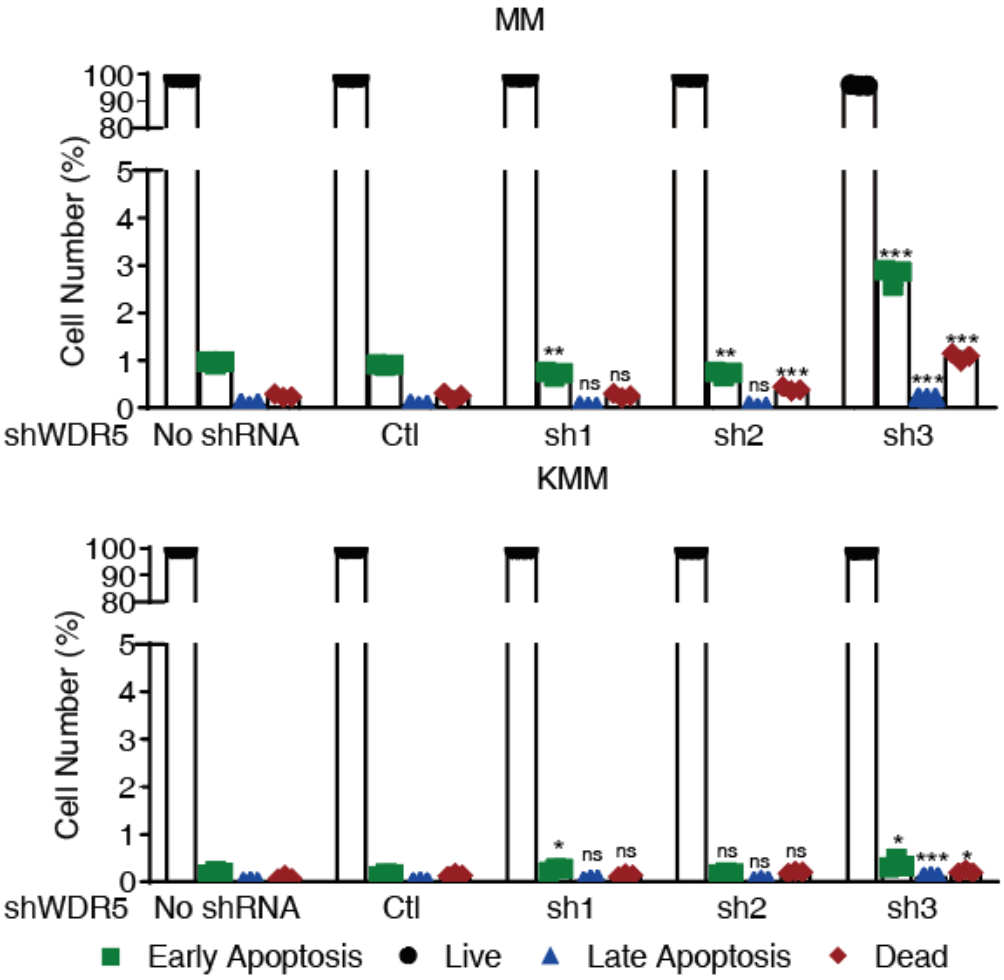

Figure 34: The effects of WDR5 knockdown on apoptosis. Bar graph representing the percentage of cells in live, early apoptosis, late apoptosis, and dead. Bars represent an average of three measurements. Asterisks represent significant results.

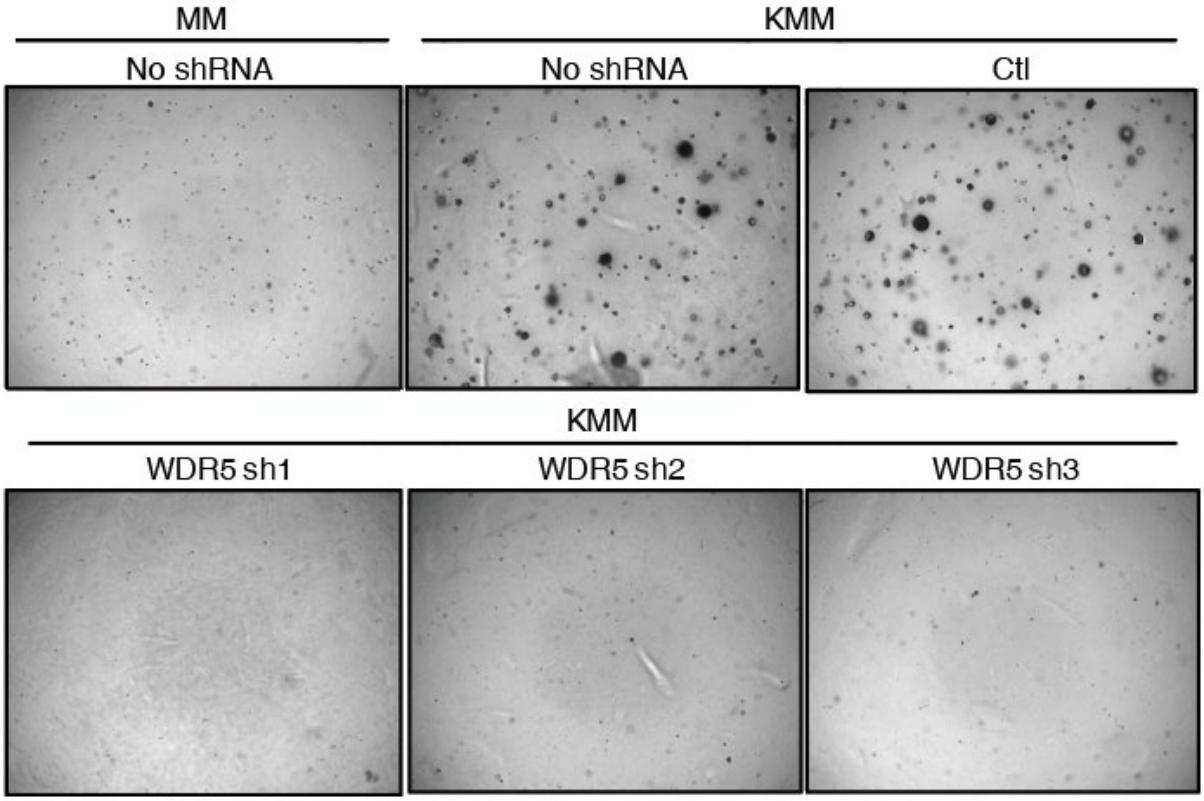

Figure 35: WDR5 knockdown reduced the efficiency of colony formation on soft agar of KMM cells. Picture showed the representative images of colonies in soft agar.

2.3.6 GRWD1 interacts with MLL2, andMLL2 knockdown phenocopies GRWD1 knockdown

Since WDR5 was required for the assembly of MLLs and SET1 histone methyltransferase complexes, we examined the interaction of GRWD1 with this complex. GRWD1 immunoprecipitated MLL2, SET1A, and MLL1 with MLL2 having the strongest interaction (Fig. 36) Co-IP further showed the interaction between GRWD1 and MLL2 (Fig. 37). Therefore, MLL2 is likely one of the major methyltransferases in the GRWD1 complexes.

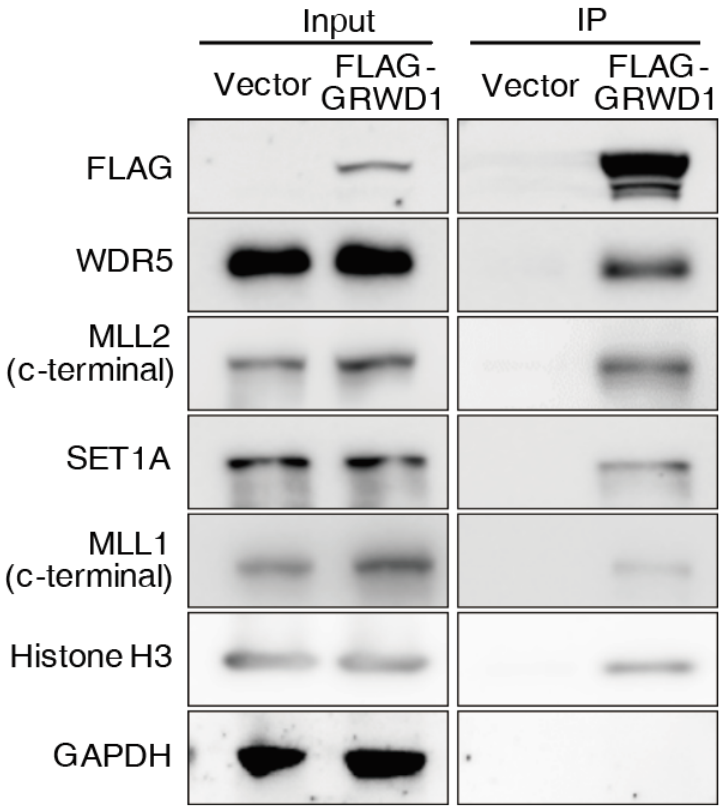

Figure 36: FLAG-GRWD1 immunoprecipitated endogenous methyltransferases MLL1, MLL2 and SET1A. 293T cells were transfected with the construct coding for FLAG-tagged GRWD1 or the vector alone. Immunoprecipitation (IP) was performed using anti-FLAG antibody.

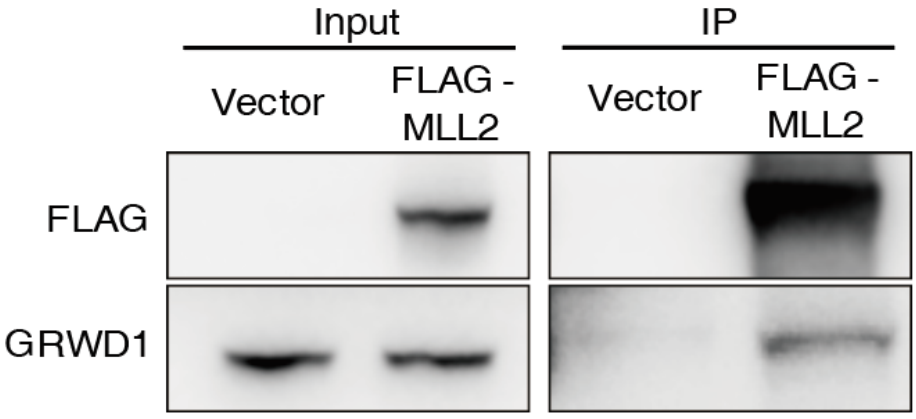

Figure 37: FLAG-MLL2 immunoprecipitated endogenous GRWD1 in 293T cells. 293T cells were transfected with the construct coding for FLAG-MLL2 (c-terminal) or the vector alone. Immunoprecipitation (IP) was performed using anti-FLAG antibody.

To confirm if MLL2 is important to maintain the global level of H3K4me3 in our model, we examined the H3K4me3 mark following the MLL2 knockdown. Like GRWD1 and WDR5, MLL2 knockdown reduced the level of H3K4me3 in both MM and KMM cells (Fig. 38). Consistent with these results, MLL2 knockdown reduced cell proliferation of both MM and KMM cells with a stronger effect observed in KMM than MM cells (Fig. 39). Similarly, MLL2 knockdown induced cell cycle arrest but had a minimal effect on apoptosis in both MM and KMM cells (Fig. 40 and 40). MLL2 knockdown also abolished colony formation of KMM cells in soft agar (Fig. 42). Hence, MLL2 knockdown shared the same phenotype as that of GRWD1 or WDR5 knockdown.

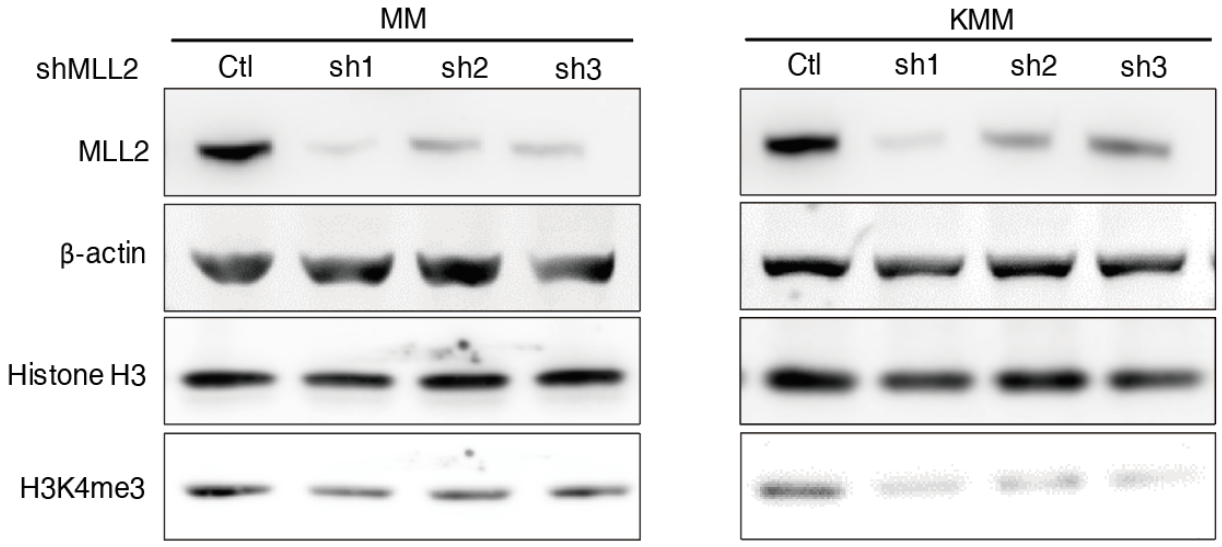

Figure 38: MLL2 knockdown reduced the level of H3K4me3 in MM and KMM cells.

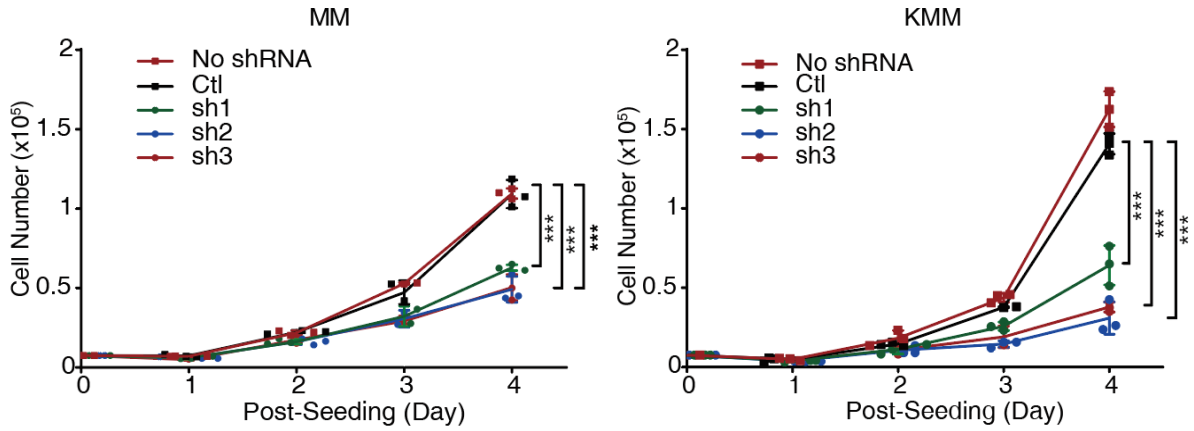

Figure 39: The effects of MLL2 knockdown on cell proliferation. Growth curve was calculated from day 1 to day 4 post-transduction. The data of three or more independent biological replicates were calculated. The values which are statistically significant are indicated with asterisks.

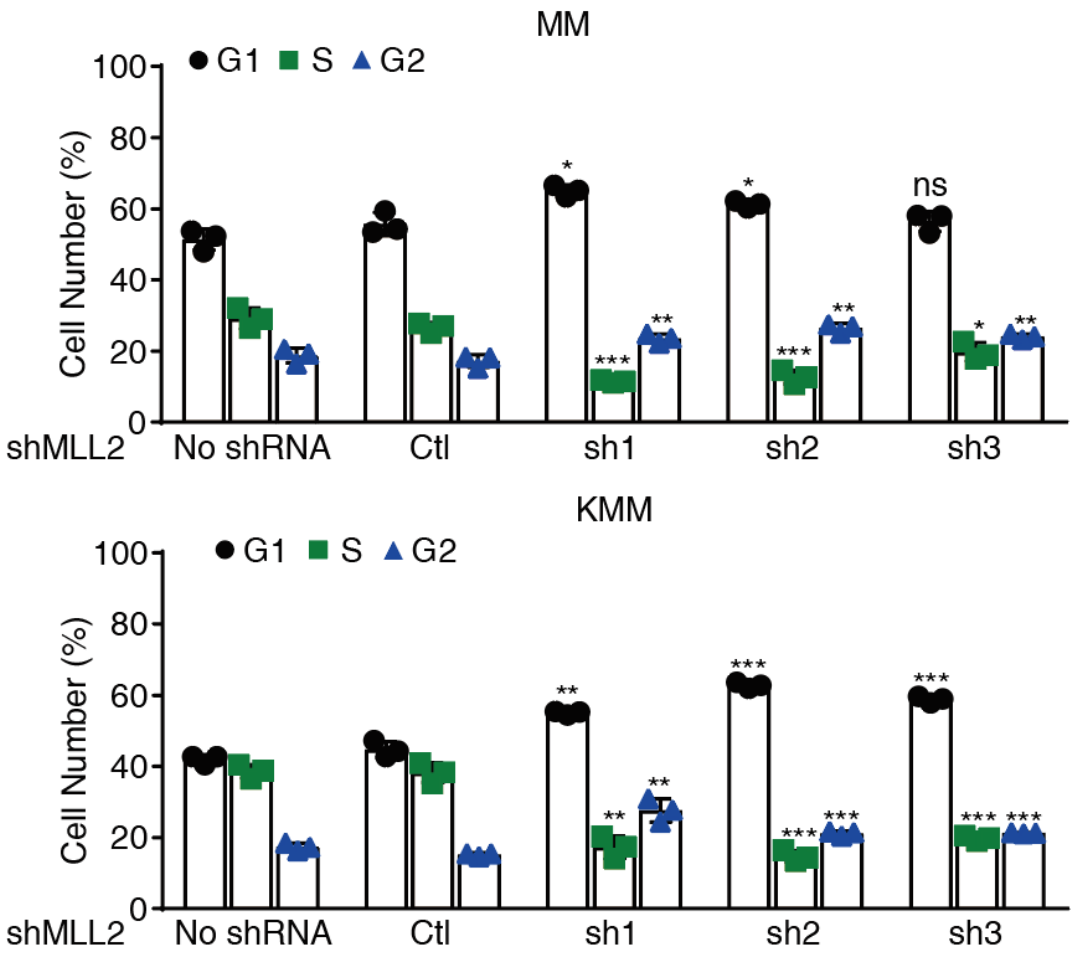

Figure 40: The effects of MLL2 knockdown on cell cycle progression. Bar graph representing the percentage of cells in G1, S and G2. Bars represent an average of three measurements. Asterisks represent significant results.

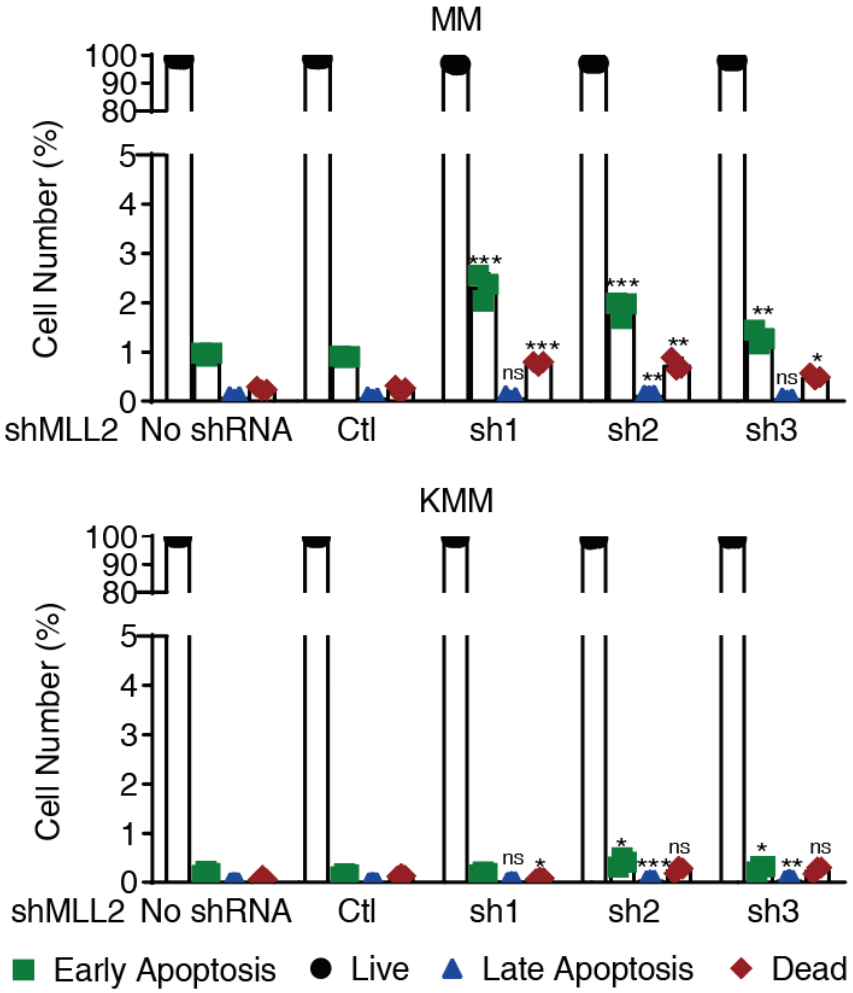

Figure 41: The effects of MLL2 knockdown on apoptosis. Bar graph representing the percentage of cells in live, early apoptosis, late apoptosis and dead. Bars represent an average of three measurements. Asterisks represent significant result.

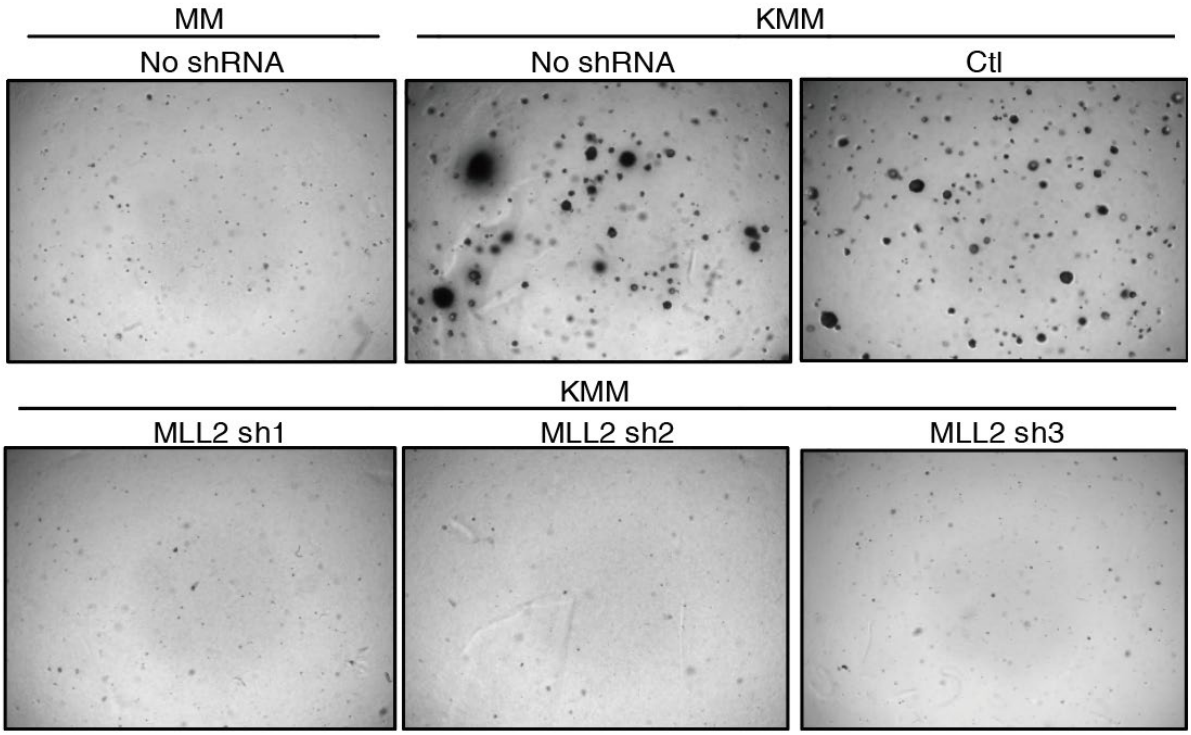

Figure 42: MLL2 knockdown reduced the efficiency of colony formation on soft agar of KMM cells. Picture showed the representative images of colonies in soft agar.

2.3.7 GRWD1, WDR5, and MLL2 share the same complex to regulate specific sets of genes in primary and KSHV-transformed cells

Because GRWD1, WDR5, and MLL2 interacted with one another and regulated the H3K4me3 mark and cell proliferation, we examined the role of GRWD1 in the complex. In co-IP, GRWD1 knockdown reduced the amount of MLL2 protein pulled down by WDR5 (Fig. 43). Conversely, overexpression of GRWD1 increased the amount of MLL2 protein pulled down by WDR5 in a dose-dependent manner (Fig. 44). However, the ability of WDR5 to bind to histone

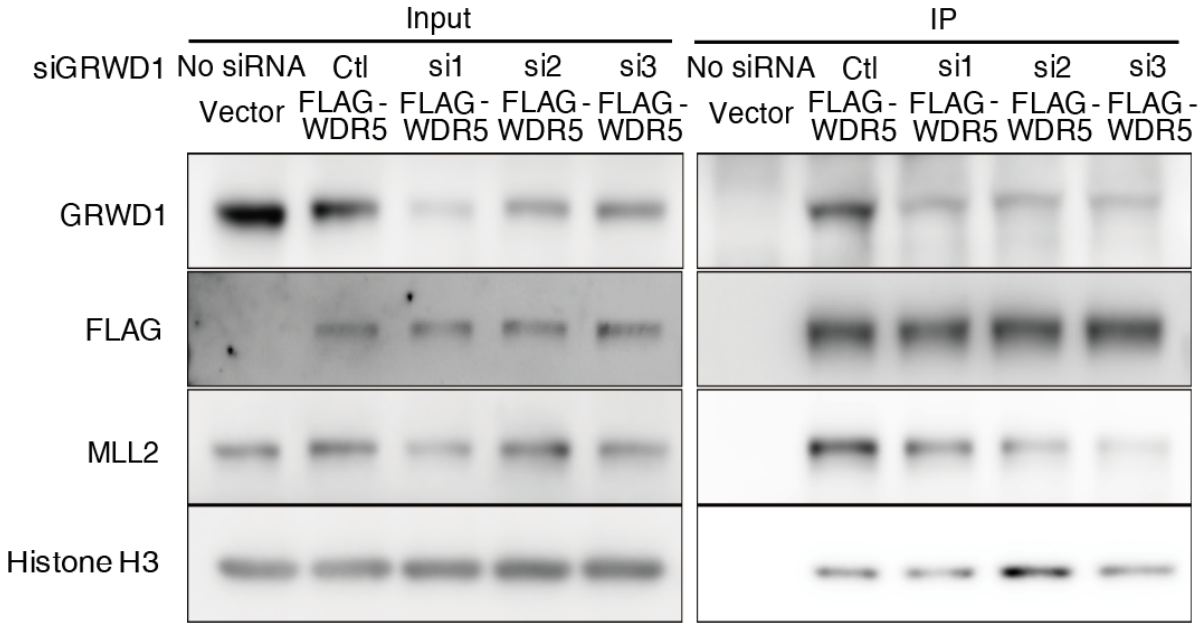

Figure 43: GRWD1 knockdown reduced the efficiency of WDR5 immunoprecipitation of MLL2 but not Histone H3. 293T cells were treated with siGRWD1 and transfected with the construct coding for FLAG-WDR5 or the vector alone. Samples were collected three days post-transfection. Immunoprecipitation (IP) was performed using anti-FLAG antibody.

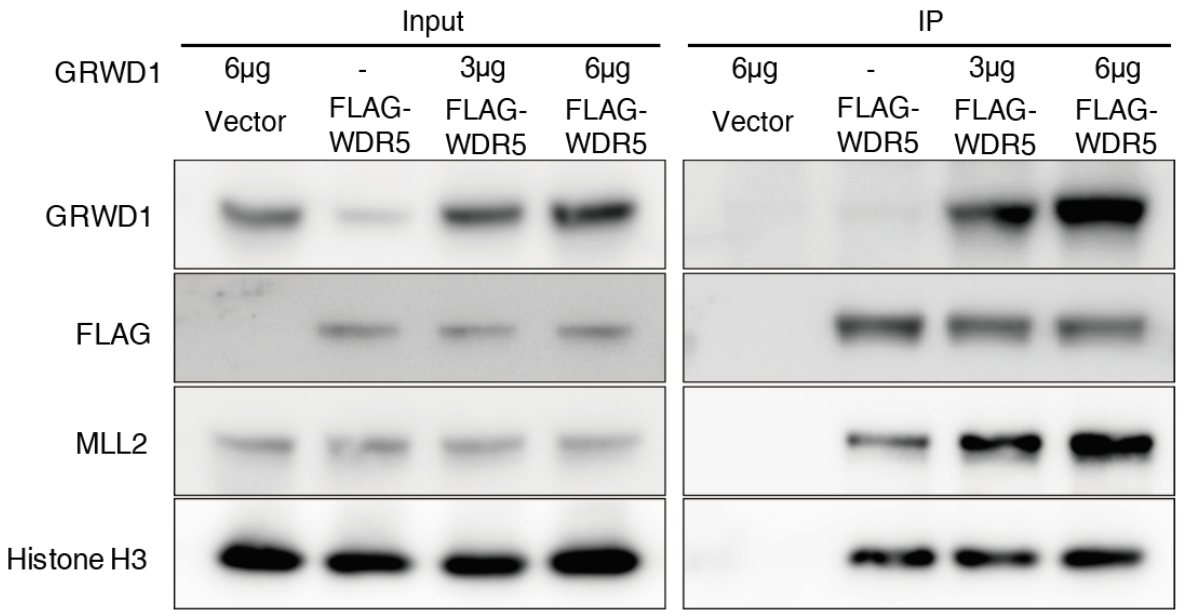

Figure 44: After GRWD1 overexpression increased the efficiency of WDR5 immunoprecipitation of MLL2 but not Histone H3. 293T cells were transfected with the construct coding for FLAG-WDR5 or the vector alone with different doses of untagged GRWD1 vector. Samples were collected three days post-transfection. Immunoprecipitation (IP) was performed using anti-FLAG antibody.

H3 was not affected under both conditions (Fig. 43 and 44). These results indicate that GRWD1 protein is essential for maintaining the interaction between WDR5 and MLL2 and hence the stability of the GRWD1- WDR5-MLL2 complex. We performed RNA-seq after shRNA-mediated knockdown of GRWD1, WDR5, or MLL2 and identified genes that were regulated by the GRWD1-WDR5-MLL2 complex using $P<0.05$ and >1.3-fold change as filters. The heatmaps indeed showed that GRWD1, WDR5, and MLL2 coregulated subsets of genes in MM and KMM cells, respectively (Fig. 45 and 46; see also appendix Table S2A and B). However, GRWD1, WDR5, and MLL2 alone or in combination also regulated distinct sets of genes, respectively (Fig.

45 and 46; see also appendix Table S3A to F), suggesting that these proteins might form different complexes with or independent of one another. As WDR5 coexists in all MLL2 methyltransferase complexes (16, 21), we observed more common genes shared between WDR5 and MLL2 than between GRWD1 and WDR5 or MLL2 in both MM and KMM cells (Fig. 46). Of the 304 and 141 genes that were coregulated by GRWD1, WDR5, and MLL2 in MM and KMM cells, respectively, 119 genes are shared between the two types of cells (Fig. 47; see also appendix Table S2A and B). We identified different subsets of genes that were regulated by GRWD1, WDR5, or MLL2 alone, or coregulated by one another shared by MM and KMM cells (Fig. 48; see also appendix Table S2A and B and Appendix Table S3A to F), which supported the common and distinct phenotypes of the two types of cells observed following knockdown of each of these genes.

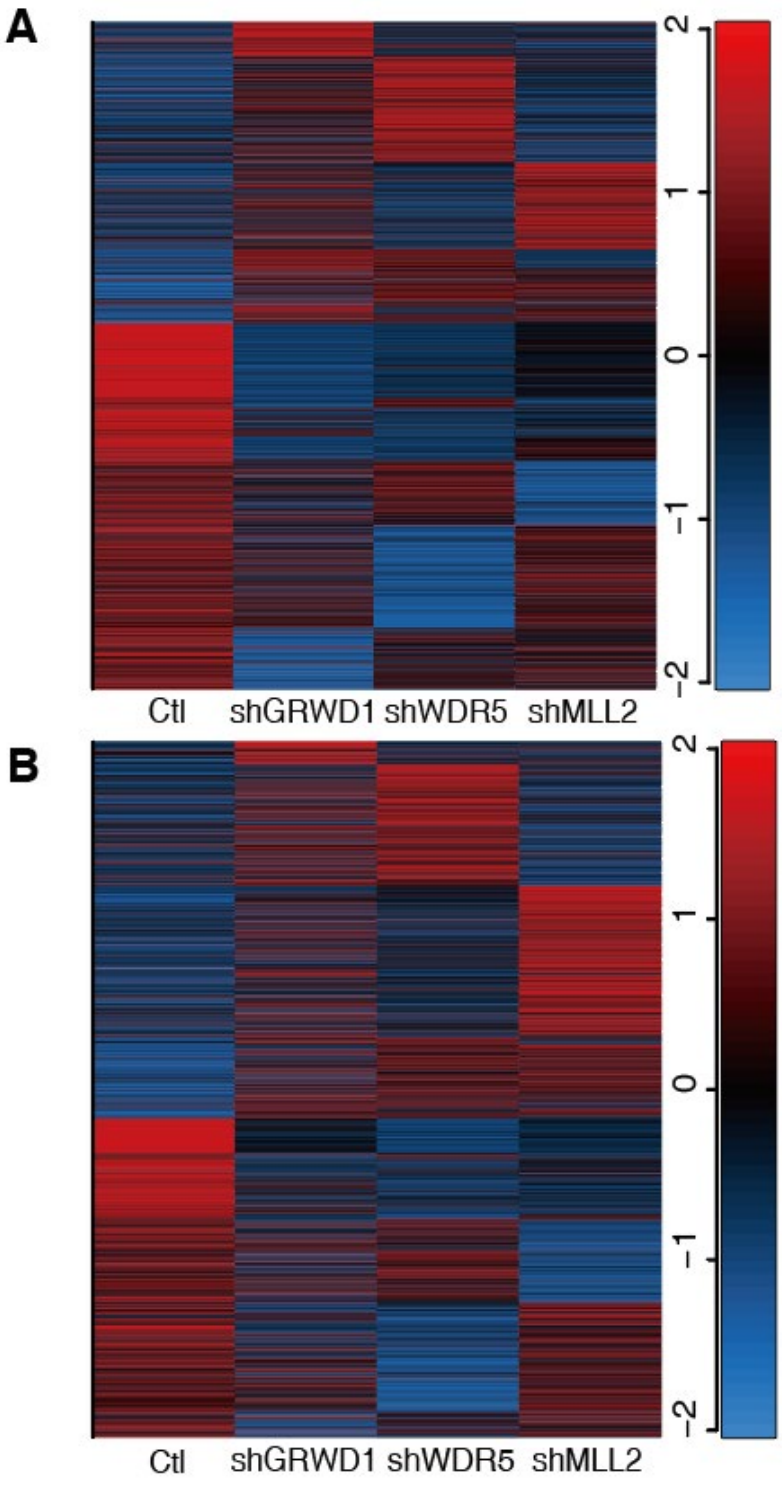

Figure 45: Heatmap of differential gene expression after GRWD1, WDR5, or MLL2 knockdown in MM (A) and KMM (B) cells. Red indicates upregulation and blue indicates downregulation.

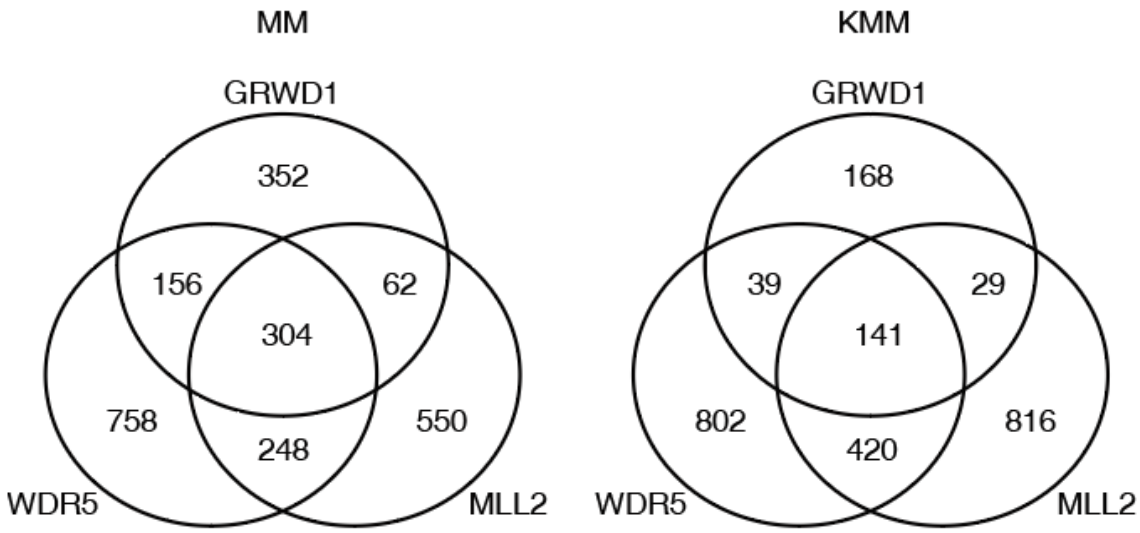

Figure 46: Common and unique gene sets altered following GRWD1, WDR5, or MLL2 knockdown. Numbers of genes under each subgroup were labelled.

We performed Ingenuity Pathway Analysis (IPA) to identify the pathways of the coregulated genes of GRWD1, WDR5, and MLL2 in MM and KMM cells (Fig 49 and Appendix Table S4A and B). Among the top 11 enriched pathways identified in MM cells, 10 were also enriched in KMM cells, many of which participated in cell cycle progression, cytokinesis, and DNA repair (Fig. 49), explaining the common phenotypes observed in these two types of cells. However, we also observed numerous enriched pathways in one cell type but not the other, for example, cell cycle regulation by BTG family proteins and Myc-mediated apoptosis signaling. We confirmed the changes of four cell cycle-related genes, CDK1, CDK2, CDT1, and PCNA, as the commonly downregulated genes following GRWD1, WDR1, or MLL2 knockdown in both MM and KMM cells (Fig. 50 and 51). Together, these results indicate that the GRWD1- WDR5-MLL2 complex mediates cell proliferation by regulating the expression of key cell cycle genes.

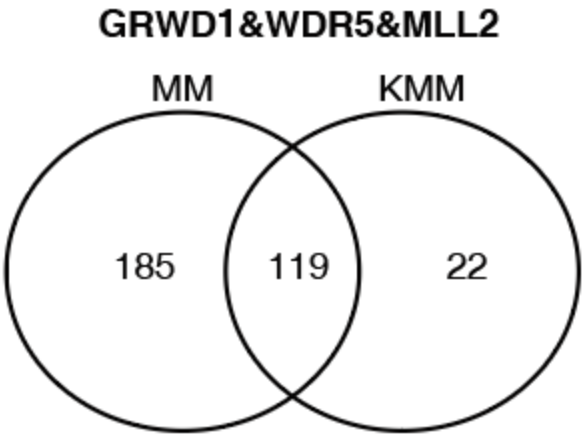

Figure 47: Shared and distinct common genes altered following GRWD1, WDR5, or MLL2 knockdown in MM and KMM cells. Numbers of genes under each subgroup were labelled.

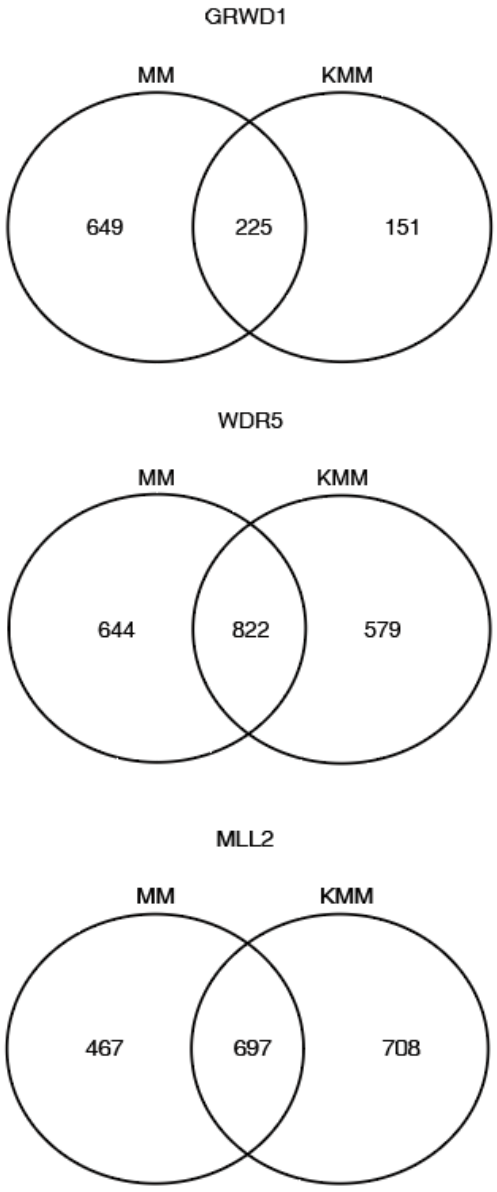

Figure 48: Common and distinct genes altered in MM and KMM cells following GRWD1, WDR5, or MLL2 knockdown. Numbers of genes under each subgroup were labelled.

Ingenuity Canonical Pathways	Rank (KMM)	Rank (MM)
Mitotic Roles of Polo-Like Kinase	1	2
Cell Cycle Control of Chromosomal Replication	2	1
Cell Cycle: G2/M DNA Damage Checkpoint Regulation	3	4
ATM Signaling	4	7
GADD45 Signaling	5	6
Role of BRCA1 in DNA Damage Response	6	5
Estrogen-mediated S-phase Entry	7	10
Role of CHK Proteins in Cell Cycle Checkpoint Control	8	3
Cyclins and Cell Cycle Regulation	9	8
Hereditary Breast Cancer Signaling	10	14
NER Pathway	11	9

Figure 49: The rank of the top enriched pathways of common genes altered following GRWD1, WDR5, or MLL2 knockdown in MM and KMM cells.

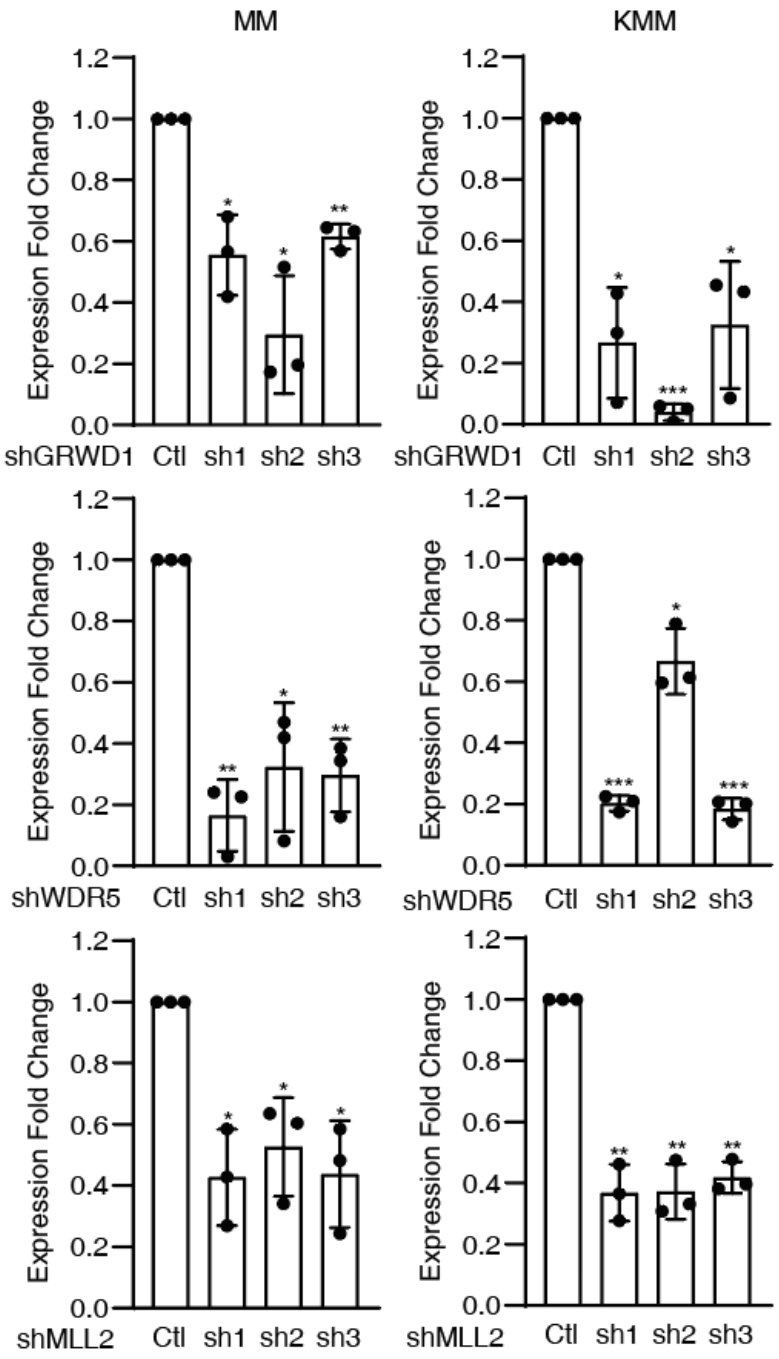

Figure 50: RT-qPCR validation of CDK1 expression in MM and KMM cells after GRWD1, WDR5, or MLL2 knockdown. P values are from comparisons between each of the shRNA-treated groups (sh1, sh2, and sh3) and the scrambled control (Ctl). Asterisks represent significant results.

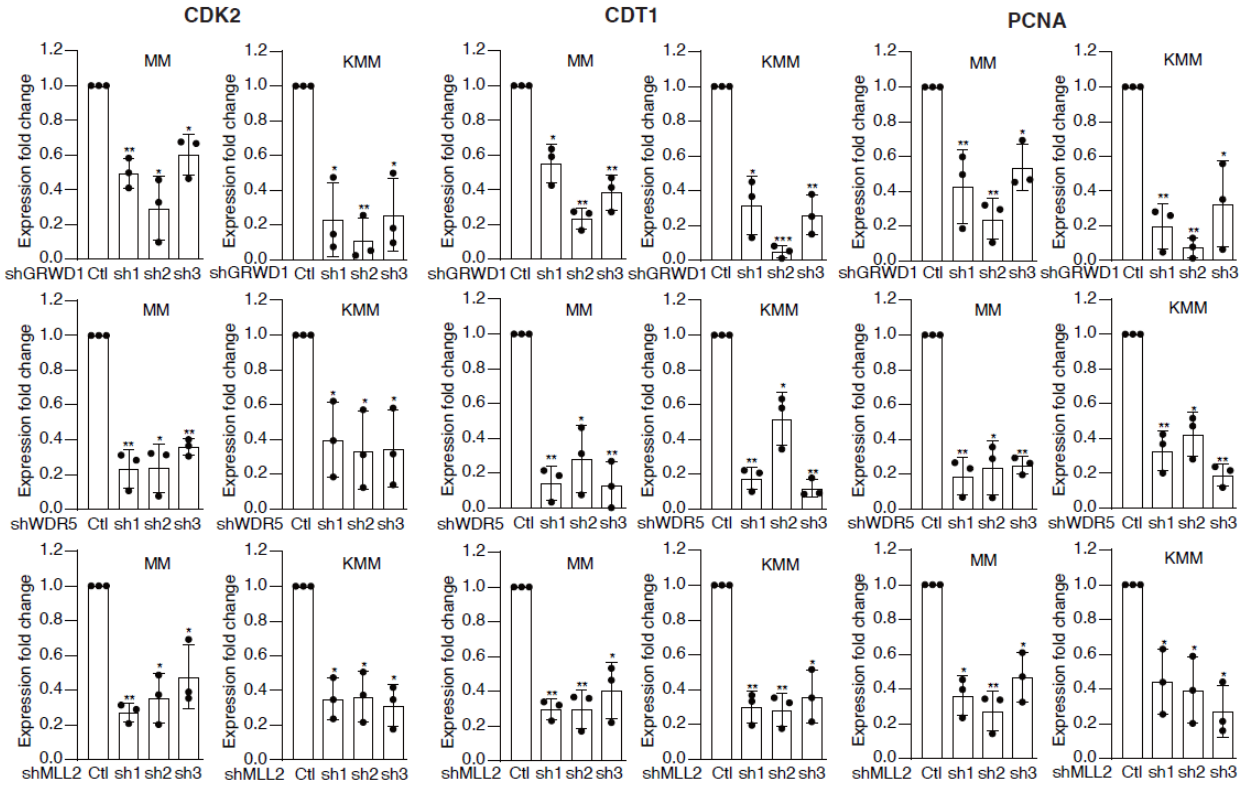

Figure 51: RT-qPCR validation of CDK2, CDT1, and PCNA expression after GRWD1, WDR5, or MLL2 knockdown in MM and KMM cells. P values are from comparisons between each of the shRNA-treated groups (sh1, sh2, and sh3) and the scrambled control (Ctl). Asterisks represent significant results.

2.4 Discussion

It has been well known that the KSHV episome is subjected to epigenetic modifications, including DNA methylation and histone methylation, and acetylation (111-116). KSHV utilizes the epigenetic machinery of the host cell to control its life cycle (113-116). On the other hand, multiple KSHV viral genes can also act as epigenetic regulators to manipulate the expression of

cellular genes (95, 112, 116, 172). For example, KSHV LANA has been reported to interact with both DNA and histone methyltransferase complexes and is associated with promoters of multiple cellular genes (111, 131). In this study, we have shown alterations of H3K4me3 and H3K27me3 marks in the predominantly latent KSHV-transformed KMM cells, providing direct evidence that KSHV latent products might alter the global histone methylation pattern of the host genome (34). Indeed, we have previously shown that KSHV latent products vFLIP and LANA enhance KSHV-induced angiogenesis by upregulating an epigenetic regulator, enhancer of zeste homolog 2 (EZH2), through the NF-kB pathway (128). These results suggest that KSHV might induce cellular transformation by reprograming the cellular epigenome.

In a CRISPR-Cas9 screening, we have previously identified cellular epigenetic regulators that are essential for the survival of KSHV-transformed cells (34, 110). We speculated that these epigenetic factors might mediate KSHV reprogramming of the cellular epigenome. Among the top genes, GRWD1 is an oncogene (145) and has been speculated on as a potential epigenetic regulator (26). Interestingly, GRWD1 is upregulated in KSHV-transformed cells (Fig. 11B), and high expression of GRWD1 predicts poor patient survival outcomes in numerous types of cancer (Fig. 10). Similarly, we have identified 8 other epigenetic regulators that have been reported to play important roles in cancer (145, 173-178) and their expression levels predict the survival of various types of cancer patients (Fig. S1). For example, NFYB was reported to induce the high expression of E2F1 in colorectal cancer and mediate oxaliplatin resistance (173). Thus, the KSHV-induced cellular transformation system is useful for identifying essential genes not only for KSHV-induced cancers but also for other types of cancer.

Although GRWD1 has been identified as a histone-binding protein (139), its role in epigenetic modification remains unclear. A previous study showed that it was pulled down by

CUL4–DDB1 ubiquitin ligase together with several methyltransferase core proteins, suggesting its potential role in histone methylation (25). In this study, we have shown that knockdown of GRWD1 leads to a global reduction of H3K4me3 marks by Western blotting and ChIP-seq, confirming an essential role of GRWD1 in maintaining cellular H3K4me3 marks. We have identified the GRWD1-regulated H3K4me3 peaks in the promoters of specific genes in both KSHV-transformed cells and primary cells (Fig. 21 to 24; see also Table S2A and B).

To understand the mechanism of GRWD1 mediating epigenetic modification, we have confirmed the direct interaction of GRWD1 with the histone H3 lysine 4 (H3K4) methyltransferase core protein WDR5. Since WDR5 is a core protein of human MLL and SET1 H3K4 methyltransferase complexes (16, 21), GRWD1 can potentially regulate H3K4me3 peaks by interacting with these complexes. Indeed, we have identified MLL2 as the major GRWD1-interacting H3K4 methyltransferase. Using both knockdown and overexpression approaches, we have found GRWD1 is directly involved in the interaction of WDR5 and MLL2, possibly by serving as a bridging factor to connect these two proteins in the GRWD1-WDR5-MLL2 complex and affecting the recruitment of MLL2 to WDR5. Although the absence of MLL2 did not show global bulk downregulation of H3K4 methylation in mouse embryonic stem cells or fibroblasts (31, 32), other studies revealed the reduction of H3K4me3 marks by ChIP-seq and H3K4me3 levels by Western blotting after MLL2 knockdown (18, 33), which are consistent with our observations. In agreement with the report that MLL2 is essential for maintaining the H3K4me3 level on bivalent promoters of genes with low expression levels (18, 30, 31), we have also identified a set of GRWD1 targets located at bivalent promoters of genes by ChIP-seq, including SOHLH1 and HS3ST3B1 shared by MM and KMM cells (Fig. 23B, 24B and 25). However, many H3K4me3 peaks affected by GRWD1 knockdowns, such as those of the ADAR gene, were not at

bivalent promoters (Fig. 23 to 25), suggesting potential GRWD1 interactions with other methyltransferases in addition to MLL2. Indeed, we have found genes that are coregulated by GRWD1 and WDR5 but not MLL2, which could be downstream targets of other methyltransferases (Fig. 46). Similarly, we have identified genes that are coregulated by GRWD1 and MLL2 but not WDR5 and genes that are coregulated by WDR5 and MLL2 but not GRWD1 (Fig. 46). Furthermore, we have identified genes that are regulated by GRWD1, WDR5, or MLL2 alone. These results indicate that these proteins might also independently form complexes with other proteins without involving one another.

Among the common pathways that are enriched following knockdown of GRWD1, WDR5, or MLL2, most of them are involved in cell cycle progression (Fig. 49), suggesting the important role of the GRWD1-WDR5-MLL2 complex in this pathway. Consistent with these results, the knockdown of any of the three proteins caused cell cycle arrest (Fig. 13A, 33, and 40). Hence, the GRWD1-WDR5-MLL2 complex might mediate KSHV reprogramming of the epigenome and contribute to cell cycle progression and cellular transformation. Among the KSHV products that can alter epigenetic modifications, LANA is associated with human H3K4 methyltransferase complexes (111) and can directly bind to viral and cellular genomes. LANA might interact with the GRWD1-WDR5-MLL2 complex to regulate specific epigenetic loci on the genome. Further investigation of KSHV hijacking of the host machinery to alter the specific epigenetic marks on both viral and cellular genomes could provide insights into the mechanism of KSHV-induced oncogenesis.

Taken together, we have identified an epigenetic complex that mediates KSHV-induced cellular transformation and cell cycle progression by reprogramming the cellular epigenome and

gene expression. This complex represents a potential novel therapeutic target for KSHV-induced cancers, which could be extended to other types of cancers.

2.5 Acknowledgments

This work was supported by grants from the National Institutes of Health (CA096512, CA124332, CA132637, CA213275, DE025465, and CA197153 to S.-J. Gao). This work was supported in part by award P30CA047904.

We thank members of Dr. Shou-Jiang Gao's laboratory for technical assistance and helpful discussions.

3.0 Summary and Future Perspectives

3.1 KSHV hijacks the host epigenetic machinery during cellular transformation

The concept that the host epigenetic machinery is a target of viruses has been widely reported and extensively studied (179). For KSHV, the regulation of its life cycle requires dynamic epigenetic modifications on its episome, which is important for both viral latent and lytic replication (68, 113). Besides regulating its life cycle to avoid the surveillance of host immune systems, KSHV also exploits the cellular epigenome to regulate the expression of host genes and enhance cell survival, which directly contributes to KSHV-induced tumorigenesis (180, 181). The cellular epigenome is modified by several KSHV latent products. The most well-reported viral epigenetic regulator is KSHV LANA. In addition to interacting and recruiting several epigenetic modification enzymes (111, 131), LANA can also indirectly regulate epigenetic regulators (128) or target cellular pathways by altering the epigenetic modifications of key proteins (182).

Our study has shown the landscape of H3K4me3 and H3K27me3 marks is extensively altered during the KSHV-induced cellular transformation (Fig. 6). Additionally, we have found the transcriptional activation mark H3K4me3 is significantly reduced in KMM cells following LANA knockout (Fig. 52). Since LANA is critical for maintaining the stability of KSHV episome in the cells, LANA knockout could lead to the loss of the KSHV genome from KMM cells. The reduction of H3K4me3 marks following the loss of LANA suggests the importance of epigenetic regulation in KSHV latency and cellular transformation.

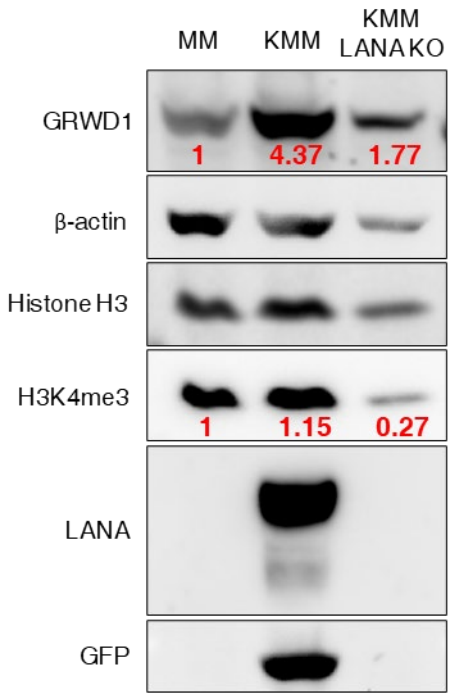

Figure 52: The global level of H3K4me3 marks reduced significantly after knocking out the KSHV episome from the transformed cells. Protein quantification of GRWD1 normalized to β-actin and H3K4me3 normalized to Histone H3 was labeled in red.

Understanding how KSHV reprograms cellular epigenome is important for revealing the mechanism of KSHV-induced oncogenesis. Identification of the specific epigenetic modifications and the regulatory pathways that are essential for cellular transformation could provide insights into the molecular basis of KSHV-induced tumorigenesis.

3.2 GRWD1 is upregulated by KSHV

Our results indicated that GRWD1 was upregulated in KMM cells compared to MM cells (Fig. 11). KSHV upregulation of GRWD1 was also observed in human cells. For example, the levels of GRWD1 protein were about 2.5-fold in BCP1 and BCBL1 compared to BJAB cells (Fig. 53).

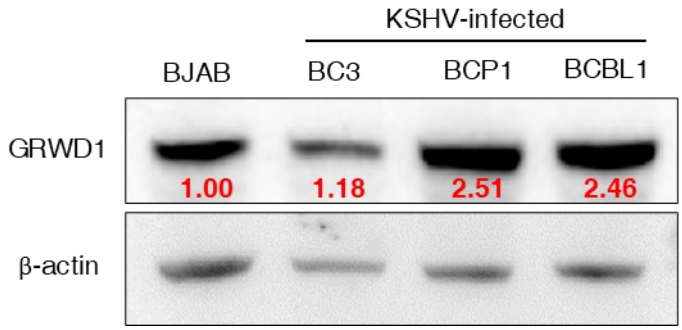

Figure 53: GRWD1 was upregulated in BCP1 and BCBL1 compared to BJAB cells. Protein quantification of GRWD1 normalized to β-actin was labeled in red.

To investigate the upstream viral regulator(s) of GRWD1, we examined the expression of GRWD1 in the MM cells infected by KSHV mutants of latent products including vCyclin, vFLIP, and the miRNA cluster. We did not find any significant alterations of GRWD1 in MM cells infected by any of these mutants (Fig. 54). The KSHV latent product LANA is associated with human H3K4 methyltransferase complexes (111).

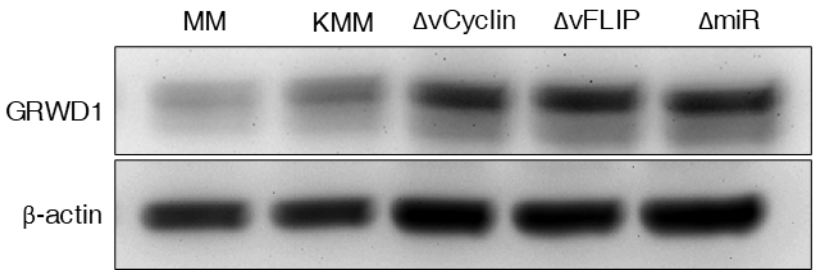

Figure 54: The upregulated GRWD1 expression in KMM cells could not be eliminated by single deletion of KSHV latent products.

However, LANA overexpression did not alter the expression of GRWD1 (Fig. 55). Based on these results, we speculate that the upregulation of GRWD1 in KMM cells may be caused by multiple viral latent products involving a complication mechanism during the KSHV-induced cellular transformation process.

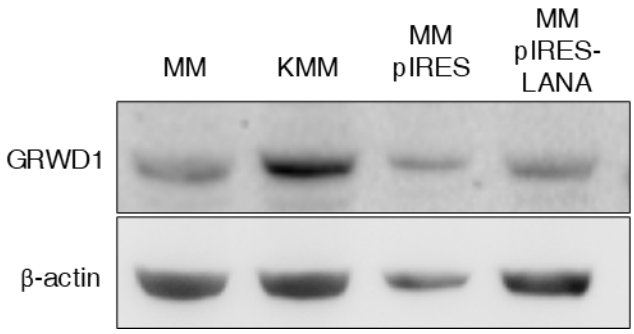

Figure 55: LANA overexpression in MM cells cannot increase the expression of GRWD1.

However, we observed the interaction between LANA and the GRWD1-WDR5-MLL2 complex by co-IP (Fig. 56). Since GRWD1 is essential for the survival of KSHV-transformed cells, KSHV might have used GRWD1 to promote the H3K4me3 mark in its host cells. Indeed, we have observed distinct H3K4me3 peaks of GRWD1 targets in KMM but not MM cells, suggesting that

KSHV might have hijacked GRWD1 to facilitate the recruitment of the GRWD1-WDR5-MLL2 complex to specific genomic loci to regulate gene expression. LANA may serve as the potential binding partner and viral regulator of the GRWD1-WDR5-MLL2 complex. Future ChIP-seq experiments are needed to provide detailed evidence that the overlapped bindings of LANA to the cellular genome with those of the GRWD1-WDR5-MLL2 complex. Further investigations would be needed to reveal the mechanism of LANA hijacking of the GRWD1-WDR5-MLL2 complex, which might alter the H3K4me3 pattern on both viral and cellular genomes.

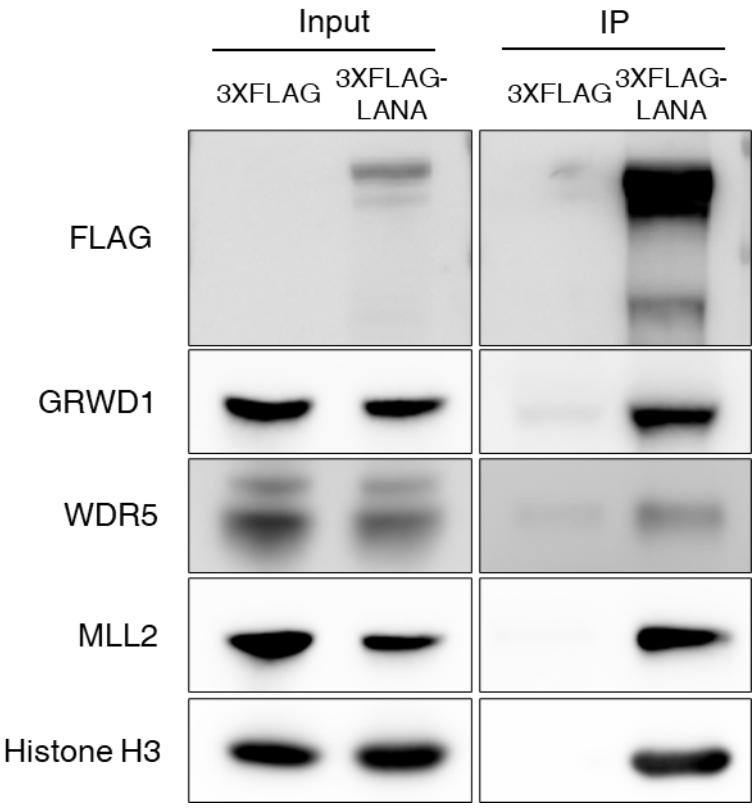

Figure 56: 3×FLAG-LANA immunoprecipitated GRWD1, WDR5 and MLL2. 293T cells were transfected with the construct coding for 3XFLAG-LANA or vector alone. Immunoprecipitation (IP) was performed using anti-FLAG antibody.

3.3 GRWD1, a novel epigenetic-regulated ribosomal protein

Although GRWD1 has been reported to be a multifunctional protein, its fundamental function as a ribosomal protein inside the nucleolus is largely unknown. Its yeast homolog Rrb1 has been shown to interact with rpL3, a highly conserved ribosomal protein, to regulate its expression and localization (141, 142). We have observed that GRWD1 can interact with human RPL3 (Fig. 57), indicating the evolutionary conservation of the GRWD1-RPL3 complex and confirming the likely involvement of GRWD1 in ribosomal biogenesis. Because of the essential role of ribosomal biogenesis, further investigations to reveal how GRWD1 regulates RPL3 in human cells and the role of GRWD1 in ribosomal biogenesis might help illustrate its cellular functions.

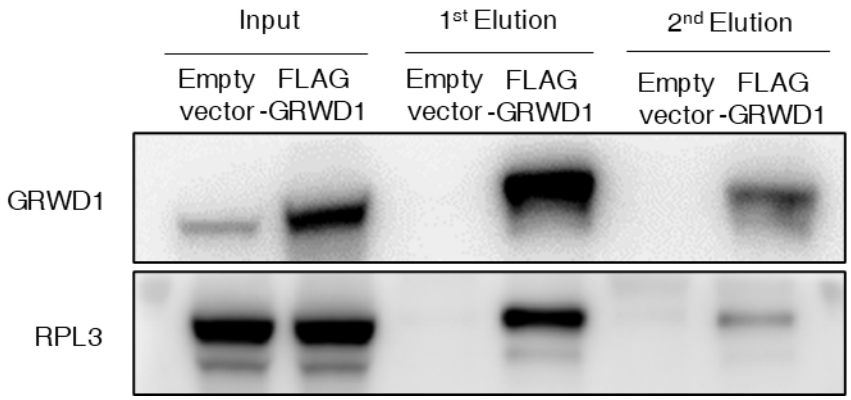

Figure 57: FLAG-GRWD1 immunoprecipitated RPL3. 293T cells were transfected with the construct coding for FLAG-GRWD1 or vector alone. Immunoprecipitation (IP) was performed using anti-FLAG antibody.

Multiple ribosomal proteins have been reported to have functions beyond the ribosome, such as the involvement in tumorigenesis (146, 154, 183-188). For example, ribosomal proteins including RPL5 and RPL11 inhibit the function of MDM2, a RING-type E3 ubiquitin ligase that targets the tumor suppresser p53 for degradation, thus stabilizing p53 and regulates its activity (189-191). GRWD1 has been identified as a novel oncogenic ribosomal protein by inhibiting the function of RPL11 to inhibit MDM2 as well as directly interacting with p53 (143-146). In our study, we have demonstrated that GRWD1 is a novel epigenetic regulator of H3K4me3 and forms a complex with the methyltransferase core proteins WDR5 and MLL2. Our finding has provided additional evidence that ribosomal proteins might be involved in epigenetic regulation. Ribosomal proteins might not just be regulated by the epigenetic machinery but also directly take part in the regulation process of epigenetic remodeling.

3.4 Summary and limitations of the study

GRWD1 is an evolutionary conservative protein and was first described as a ribosomal protein. We have identified the role of GRWD1 as a novel epigenetic factor in the GRWD1-WDR5-MLL2 complex that regulates the expression of key cell cycle genes to modulate cell proliferation. A set of genes are specifically regulated by the GRWD1-WDR5-MLL2 complex, in the meanwhile, GRWD1, WDR5 and MLL2 also regulate distinct sets of genes suggesting that these proteins might form different complexes with or independent of one another. KSHV hijacks the GRWD1-WDR5-MLL2 complex to manipulate the H3K4me3 pattern during the KSHV-induced cellular transformation, leading to the epigenetic alterations in KSHV-transformed cells thus mediating KSHV-induced tumorigenesis.

In our hypothesis, GRWD1 mediates KSHV-induced cellular transformation by recruiting the H3K4 methyltransferase complex to the promotors of growth-promoting genes. The majority of GRWD1 in uninfected cells is located inside the nucleolus and functions in ribosomal biogenesis (Fig. 58A). A portion of GRWD1 binds with histone H3 and promotes H3K4 methylation, and another portion interacts with other binding partners, such as CDT1. In KSHV-transformed cells, the latent protein LANA recruits the GRWD1-WDR5-MLL2 complex through GRWD1 to the promoters of growth-promoting genes and cell cycle related genes, resulting in the increased H3K4me3 level and higher cell proliferation rate (Fig. 58B).

Further investigations are needed to reveal the mechanism of how LANA hijacks the GRWD1-WDR5-MLL2 complex and changes the H3K4me3 pattern on both viral and cellular genomes. Due to the quality of the GRWD1 antibody, we failed to perform GRWD1 ChIP and cannot get very clean bands of the binding partners of GRWD1 by endogenous IP. One possibility to overcome this problem is to knock in a tag to create endogenous tagged GRWD1 with Crispr-Cas9 thus allowing specific and sensitive detection with tag antibody. To perform GRWD1, WDR5, MLL2, and LANA ChIP and map the location of these four proteins on the chromatin can provide further evidence for their interactions. Furthermore, based on the overlaps of GRWD1, WDR5, and MLL2 peaks, the common downstream genes specifically regulated by the GRWD1-WDR5-MLL2 complex could be identified. By comparing the differences in their peak locations in MM cells to KMM cells, the alteration of H3K4me3 peaks mediated by KSHV-hijacked GRWD1-WDR5-MLL2 complex could be identified, and the overlaps of LANA peaks would reveal the regulatory role of LANA on the downstream targets of this complex.

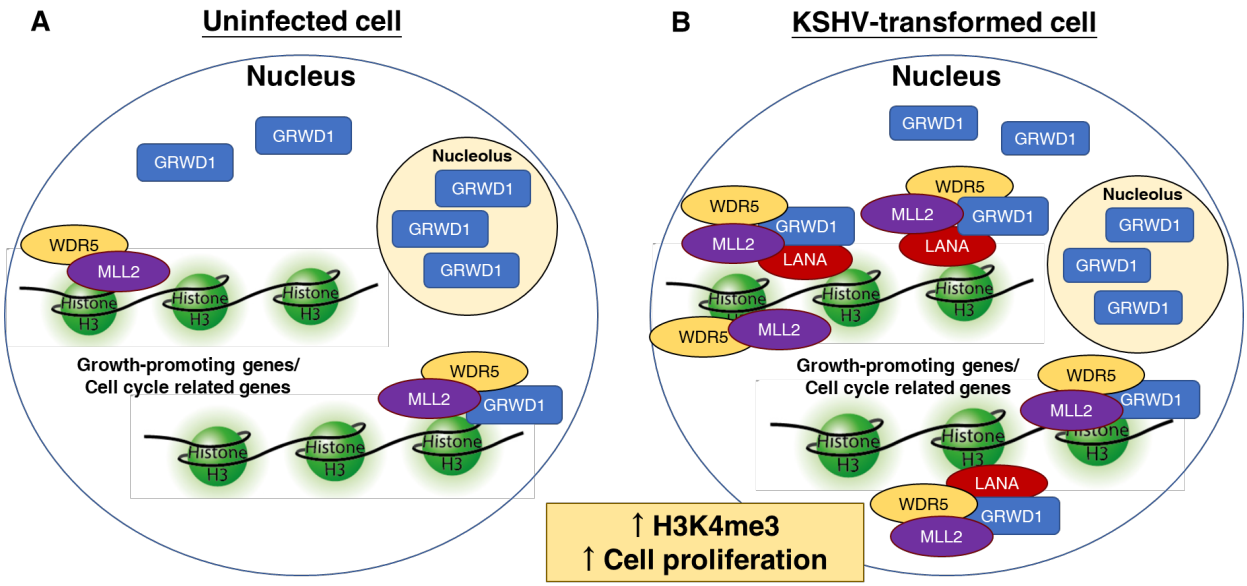

Figure 58: Summary of the model for KSHV-induced cellular transformation mediated by GRWD1. (A) In uninfected cells, GRWD1 is mostly located inside the nucleolus and functions in ribosomal biogenesis, a portion of GRWD1 binds with histone H3 and promotes H3K4 methylation. (B) In KSHV-transformed cells, LANA recruits GRWD1-WDR5-MLL2 complex through GRWD1 to the promoters of growth-promoting genes/cell cycle related genes, resulting in the increased H3K4me3 level and higher cell proliferation rate.

Appendix A Supplementary Tables

Table S1: Altered H3K4me3 peaks and associated genes after GRWD1 knockdown in MM (A) and KMM (B) cells is shown in Table S1.pdf at

https://www.ncbi.nlm.nih.gov/pmc/articles/PMC8689518/bin/mbio.03431-21-st002.pdf.

Table S2: Common and distinct genes altered in MM (A) and KMM (B) cells following knockdown of GRWD1, WDR5, or MLL2 is shown in Table S2.pdf at

https://www.ncbi.nlm.nih.gov/pmc/articles/PMC8689518/bin/mbio.03431-21-st003.pdf

Table S3: Top altered genes following knockdown of GRWD1 (A and D), WDR5 (B and E), and MLL2 (C and F) in MM (A, B, and C) and KMM (D, E, and F) cells is shown in Table S3.pdf at

https://www.ncbi.nlm.nih.gov/pmc/articles/PMC8689518/bin/mbio.03431-21-st004.pdf

Table S4: Top enriched pathways of common genes after GRWD1, WDR5, or MLL2 knockdown in MM (A) and KMM (B) cells is shown in Table S4.pdf at

https://www.ncbi.nlm.nih.gov/pmc/articles/PMC8689518/bin/mbio.03431-21-st005.pdf

Appendix B Supplementary Figures

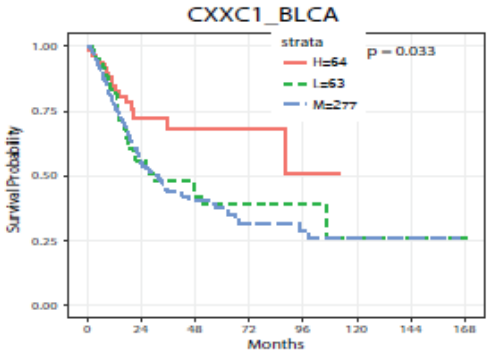

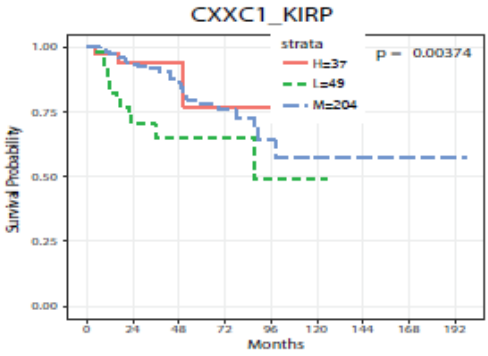

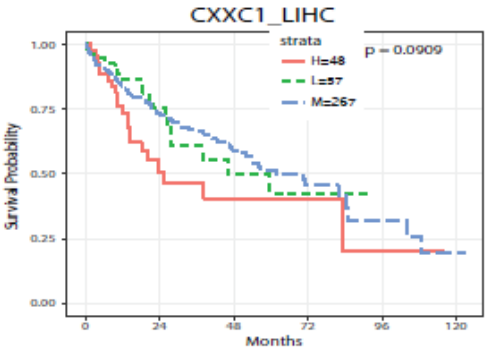

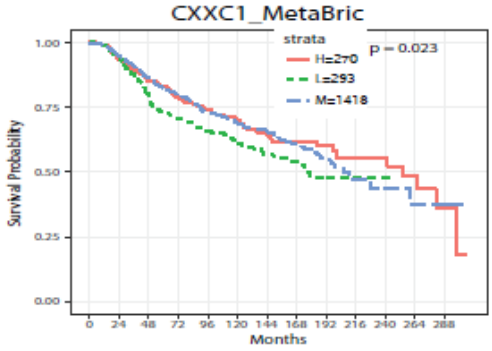

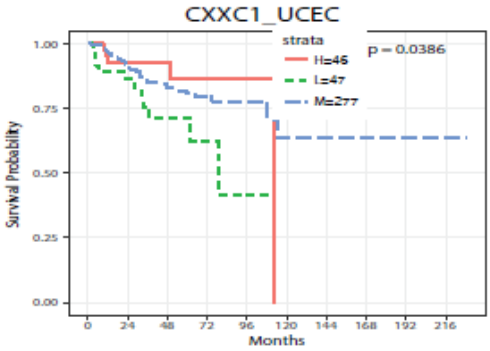

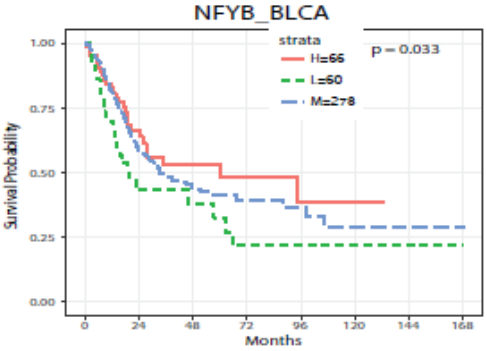

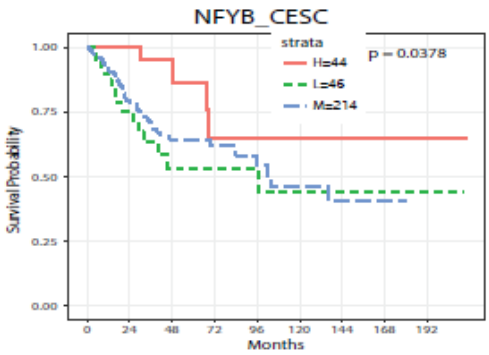

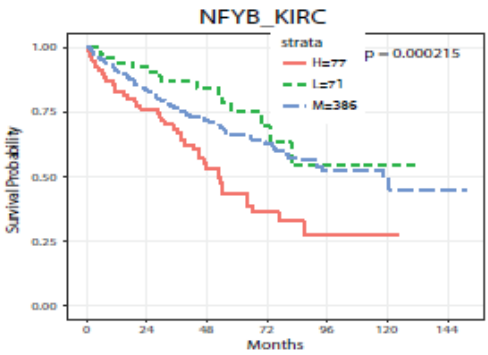

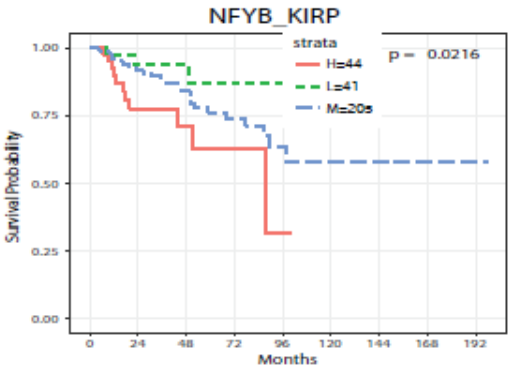
NFYB_KIRP
strata
H=44
L=41
M=205
p = 0.0216
Survival Probability
Months

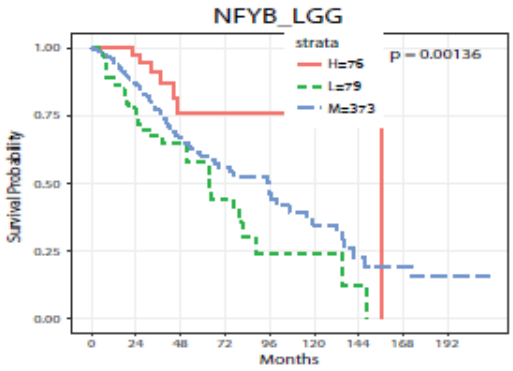
NFYB_LGG
strata
H=76
L=79
M=373
p = 0.00136
Survival Probability
Months

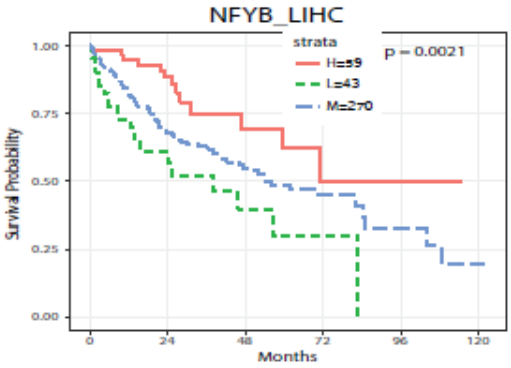
NFYB_LIHC
strata
H=59
L=43
M=270
p = 0.0021
Survival Probability
Months

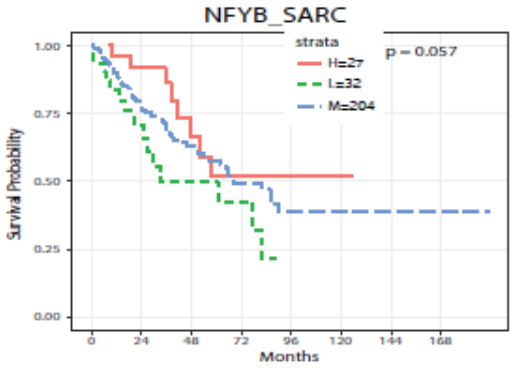
NFYB_SARC
strata
H=27
L=32
M=204
p = 0.057
Survival Probability
Months

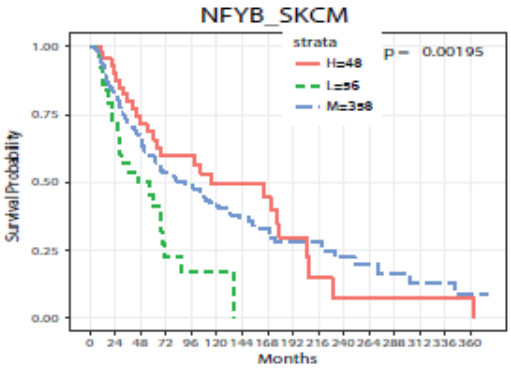
NFYB_SKCM
strata
H=48
L=56
M=358
p = 0.00195
Survival Probability
Months

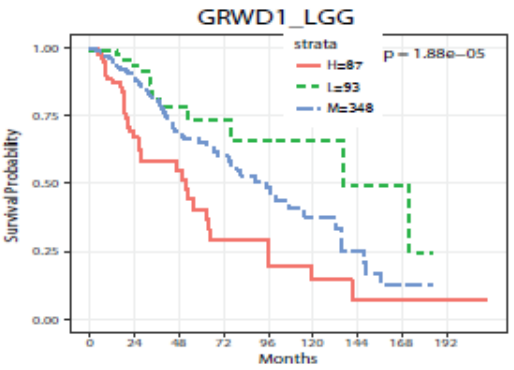
GRWD1_LGG
strata
H=87
L=93
M=348
p = 1.88e−05
Survival Probability
Months

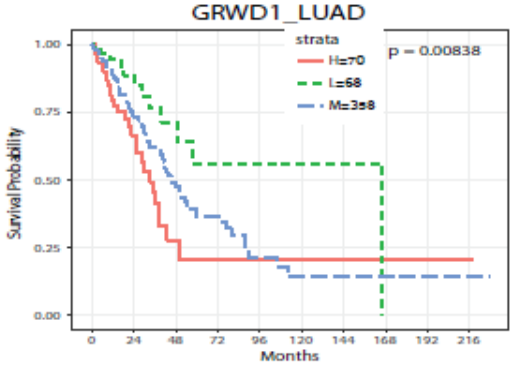
GRWD1_LUAD
strata
H=70
L=68
M=358
p = 0.00838
Survival Probability
Months

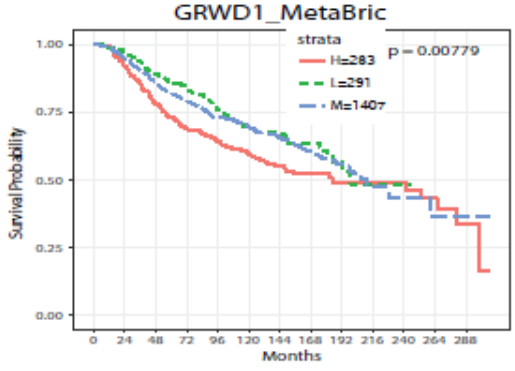
GRWD1_MetaBric
strata
H=283
L=291
M=1407
p = 0.00779
Survival Probability
Months

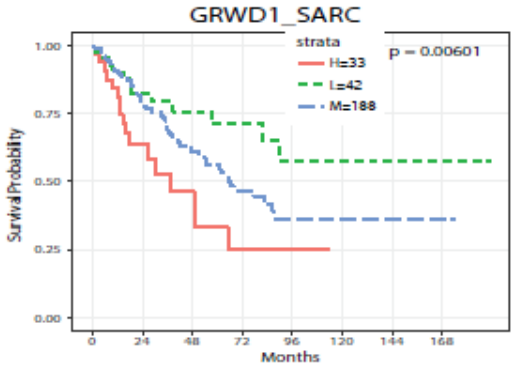
GRWD1_SARC
strata
H=33
L=42
M=188
p = 0.00601
Survival Probability
Months

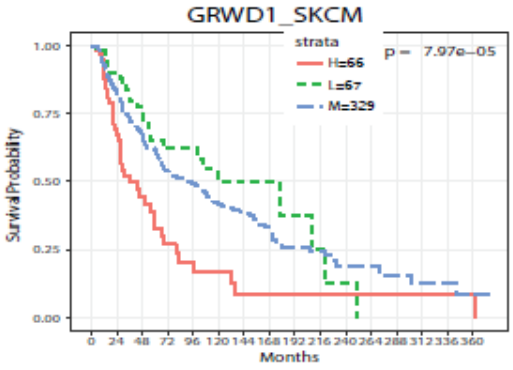
GRWD1_SKCM
strata
H=66
L=67
M=329
p = 7.97e−05
Survival Probability
Months

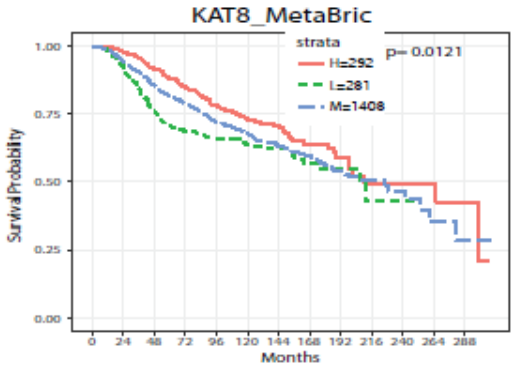
KAT8_MetaBric
strata
H=292
L=281
M=1408
p= 0.0121
Survival Probability
Months

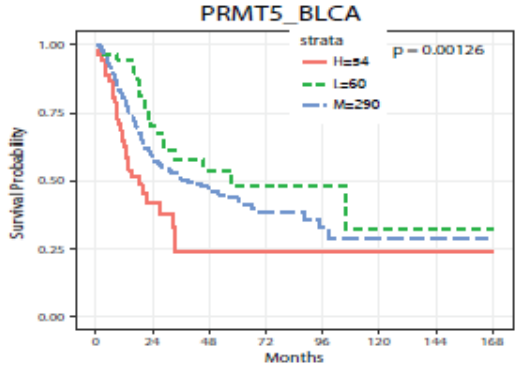
PRMT5_BLCA
strata
H=54
L=60
M=290
p = 0.00126
Survival Probability
Months

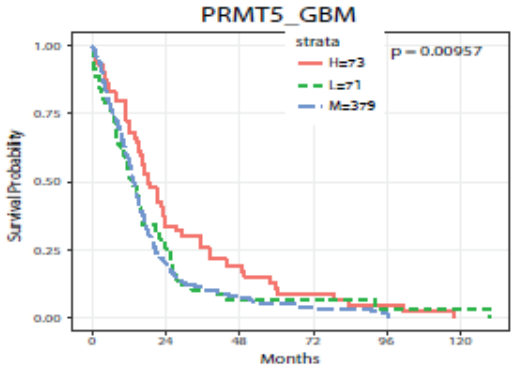
PRMT5_GBM
strata
H=73
L=71
M=379
p = 0.00957
Survival Probability
Months

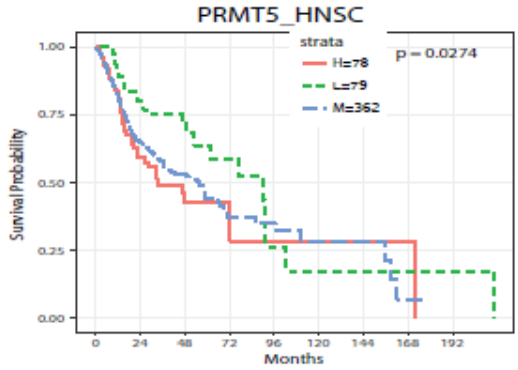
PRMT5_HNSC
strata
H=78
L=79
M=362
p = 0.0274
Survival Probability
Months

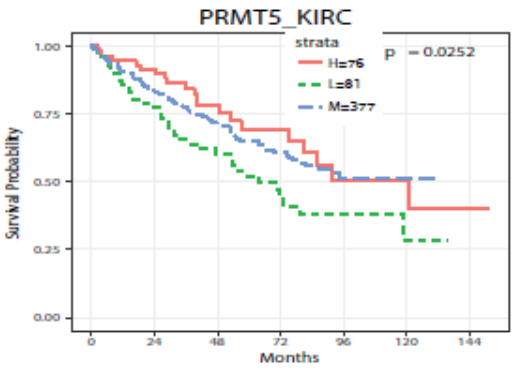
PRMT5_KIRC
strata
H=76
L=81
M=377
p = 0.0252
Survival Probability
Months

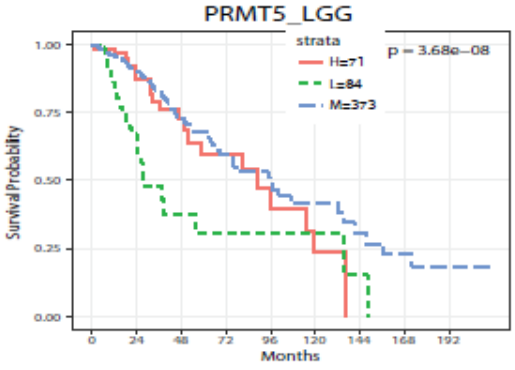
PRMT5_LGG
strata
H=71
L=84
M=373
p = 3.68e−08
Survival Probability
Months

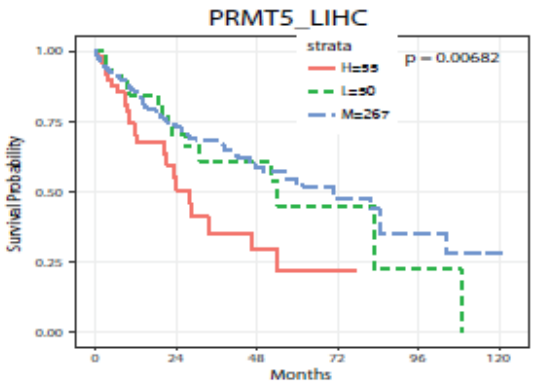
PRMT5_LIHC
strata
H=55
L=90
M=267
p = 0.00682
Survival Probability
Months

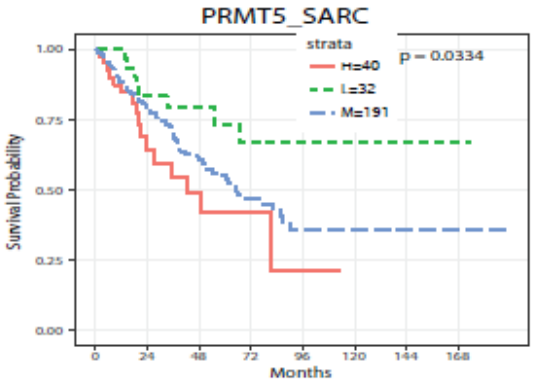
PRMT5_SARC
strata
H=40
L=32
M=191
p = 0.0334
Survival Probability
Months

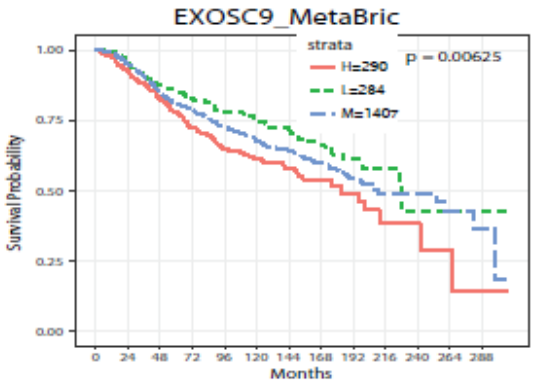
EXOSC9_MetaBric
strata
H=290
L=284
M=1407
p = 0.00625
Survival Probability
Months

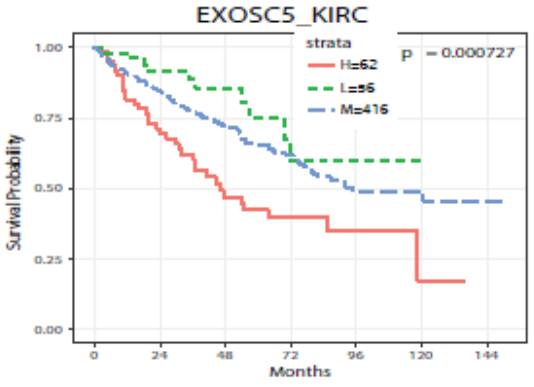
EXOSC5_KIRC
strata
H=62
L=56
M=416
p = 0.000727
Survival Probability
Months

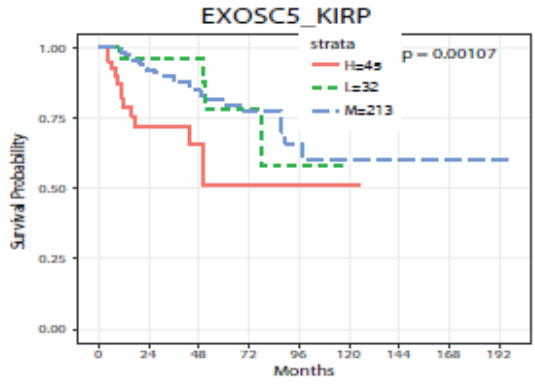
EXOSC5_KIRP
strata
H=45
L=32
M=213
p = 0.00107
Survival Probability
Months

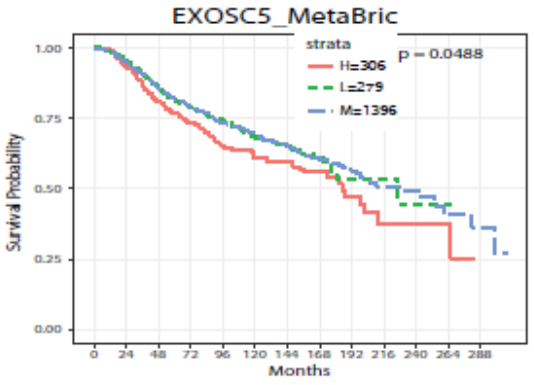
EXOSC5_MetaBric
strata
H=306
L=279
M=1396
p = 0.0488
Survival Probability
Months

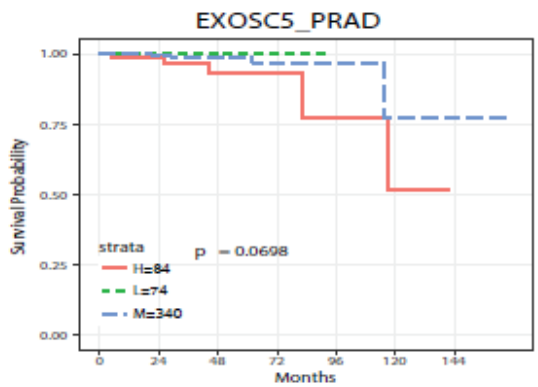
EXOSC5_PRAD
strata
H=84
L=74
M=340
p = 0.0698
Survival Probability
Months

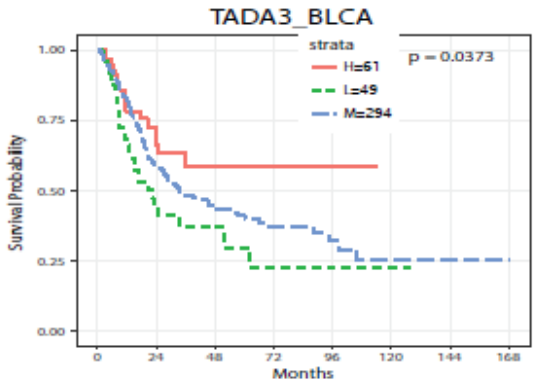
TADA3_BLCA
strata
H=61
L=49
M=294
p = 0.0373
Survival Probability
Months

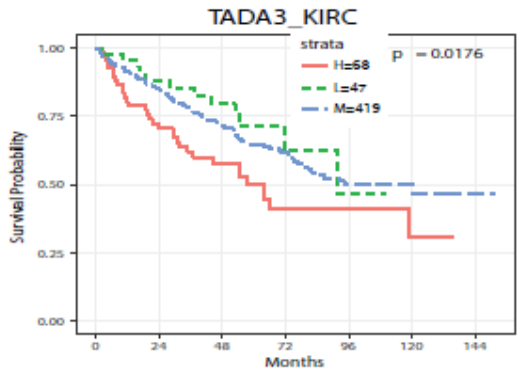
TADA3_KIRC
strata
H=68
L=47
M=419
p = 0.0176
Survival Probability
Months

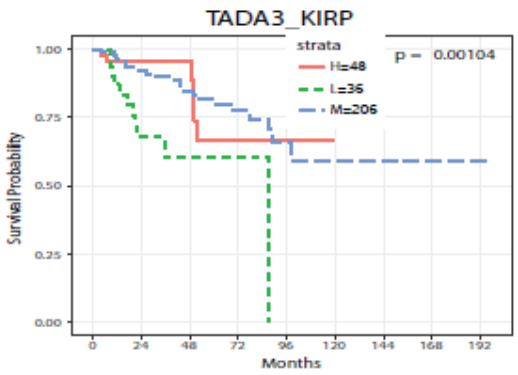
TADA3_KIRP
strata
H=48
L=36
M=206
p = 0.00104
Survival Probability
Months

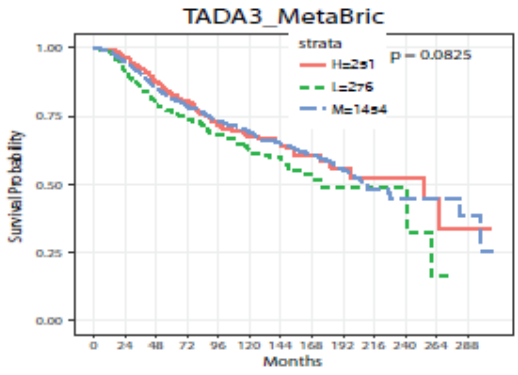
TADA3_MetaBric
strata
H=251
L=276
M=1454
p = 0.0825
Survival Probability
Months

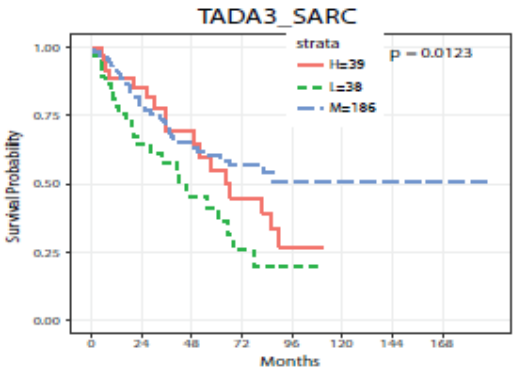
TADA3_SARC
strata
H=39
L=38
M=186
p = 0.0123
Survival Probability
Months

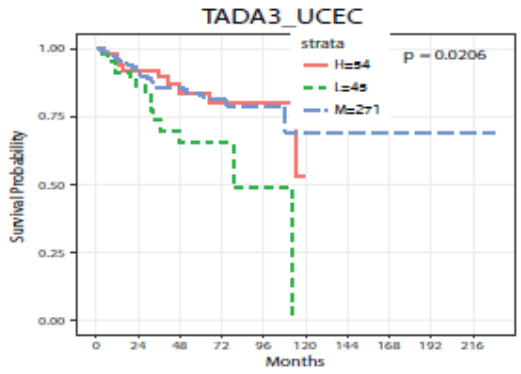
TADA3_UCEC
strata
H=54
L=45
M=271
p = 0.0206
Survival Probability
Months

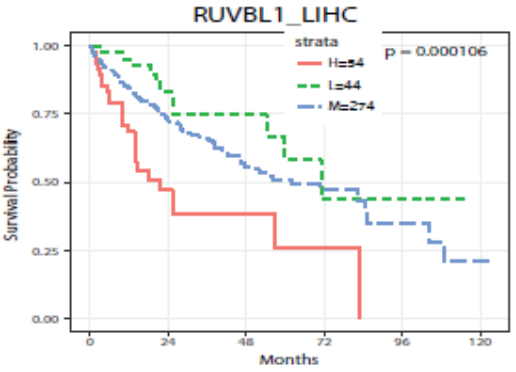
RUVBL1_LIHC
strata
H=54
L=44
M=274
p = 0.000106
Survival Probability
Months

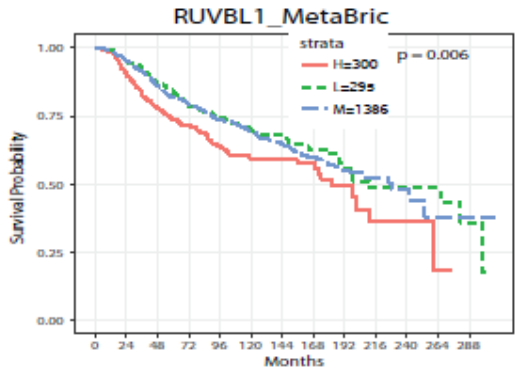
RUVBL1_MetaBric
strata
H=300
L=295
M=1386
p = 0.006
Survival Probability
Months

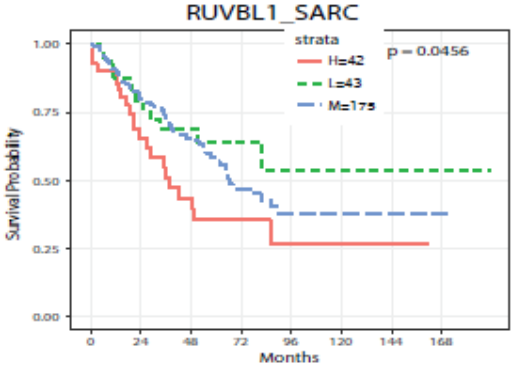
RUVBL1_SARC
strata
H=42
L=43
M=175
p = 0.0456
Survival Probability
Months

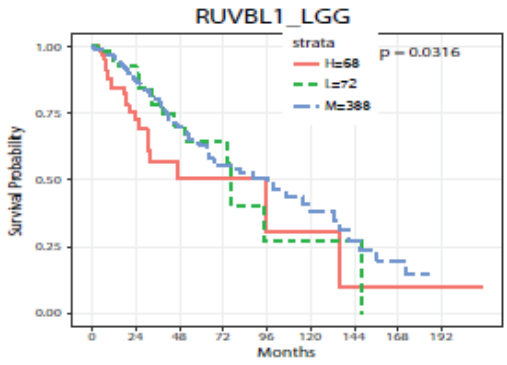

Figure S1 The survival plots for the top 9 epigenetic factors including CXXC1, NFYB, GRWD1, KAT8, PRMT5, EXOSC9, EXOSC5, TADA3, and RUVBL1 with the largest differences in CRISPR scores between MM and KMM cells identified in CRISPR-Cas9 screening in different types of cancer from the TCGA data set. Including bladder urothelial carcinoma (BLCA), kidney renal clear cell carcinoma (KIRC), kidney renal papillary cell carcinoma (KIRP), liver hepatocellular carcinoma (LIHC), breast cancer (MetaBric), sarcoma (SARC), uterine corpus endometrial carcinoma (UCEC), glioblastoma multiforme (GBM), lung squamous cell carcinoma (LUSC), prostate adenocarcinoma (PRAD), brain lower-grade glioma (LGG), lung adenocarcinoma (LUAD), skin cutaneous melanoma (SKCM), cervical squamous cell carcinoma and endocervical adenocarcinoma (CESC), head-neck squamous cell carcinoma (HNSC), and ovarian serous cystadenocarcinoma (OV). Patients were grouped into high (H), medium (M), and low (L) based on the expression of the target gene.

Bibliography

1. Bird A. 2007. Perceptions of epigenetics. Nature 447:396-8.

2. Waddington CH. 2012. The epigenotype. 1942. Int J Epidemiol 41:10-3.

3. Nebbioso A, Tambaro FP, Dell'Aversana C, Altucci L. 2018. Cancer epigenetics: Moving forward. PLoS Genet 14:e1007362.

4. Kanwal R, Gupta K, Gupta S. 2015. Cancer epigenetics: an introduction. Methods Mol Biol 1238:3-25.

5. Bassett SA, Barnett MP. 2014. The role of dietary histone deacetylases (HDACs) inhibitors in health and disease. Nutrients 6:4273-301.

6. Medvedeva YA, Lennartsson A, Ehsani R, Kulakovskiy IV, Vorontsov IE, Panahandeh P, Khimulya G, Kasukawa T, Consortium F, Drablos F. 2015. EpiFactors: a comprehensive database of human epigenetic factors and complexes. Database (Oxford) 2015:bav067.

7. Stoccoro A, Coppede F. 2018. Role of epigenetics in Alzheimer's disease pathogenesis. Neurodegener Dis Manag 8:181-193.

8. Prasher D, Greenway SC, Singh RB. 2020. The impact of epigenetics on cardiovascular disease. Biochem Cell Biol 98:12-22.

9. Sims RJ, 3rd, Nishioka K, Reinberg D. 2003. Histone lysine methylation: a signature for chromatin function. Trends Genet 19:629-39.

10. Black JC, Van Rechem C, Whetstine JR. 2012. Histone lysine methylation dynamics: establishment, regulation, and biological impact. Mol Cell 48:491-507.

11. Dupont C, Armant DR, Brenner CA. 2009. Epigenetics: definition, mechanisms and clinical perspective. Semin Reprod Med 27:351-7.

12. Di Lorenzo A, Bedford MT. 2011. Histone arginine methylation. FEBS Lett 585:2024-31.

13. Takahashi YH, Westfield GH, Oleskie AN, Trievel RC, Shilatifard A, Skiniotis G. 2011. Structural analysis of the core COMPASS family of histone H3K4 methylases from yeast to human. Proc Natl Acad Sci U S A 108:20526-31.

14. Shilatifard A. 2012. The COMPASS family of histone H3K4 methylases: mechanisms of regulation in development and disease pathogenesis. Annu Rev Biochem 81:65-95.

15. Smith E, Lin C, Shilatifard A. 2011. The super elongation complex (SEC) and MLL in development and disease. Genes Dev 25:661-72.

16. Ali A, Tyagi S. 2017. Diverse roles of WDR5-RbBP5-ASH2L-DPY30 (WRAD) complex in the functions of the SET1 histone methyltransferase family. J Biosci 42:155-159.

17. Wu M, Wang PF, Lee JS, Martin-Brown S, Florens L, Washburn M, Shilatifard A. 2008. Molecular regulation of H3K4 trimethylation by Wdr82, a component of human Set1/COMPASS. Mol Cell Biol 28:7337-44.

18. Denissov S, Hofemeister H, Marks H, Kranz A, Ciotta G, Singh S, Anastassiadis K, Stunnenberg HG, Stewart AF. 2014. Mll2 is required for H3K4 trimethylation on bivalent promoters in embryonic stem cells, whereas Mll1 is redundant. Development 141:526-37.

19. Hu D, Gao X, Morgan MA, Herz HM, Smith ER, Shilatifard A. 2013. The MLL3/MLL4 branches of the COMPASS family function as major histone H3K4 monomethylases at enhancers. Mol Cell Biol 33:4745-54.

20. Herz HM, Mohan M, Garruss AS, Liang K, Takahashi YH, Mickey K, Voets O, Verrijzer CP, Shilatifard A. 2012. Enhancer-associated H3K4 monomethylation by Trithorax-related, the Drosophila homolog of mammalian Mll3/Mll4. Genes Dev 26:2604-20.

21. Trievel RC, Shilatifard A. 2009. WDR5, a complexed protein. Nat Struct Mol Biol 16:678-80.

22. Sha L, Ayoub A, Cho US, Dou Y. 2020. Insights on the regulation of the MLL/SET1 family histone methyltransferases. Biochim Biophys Acta Gene Regul Mech 1863:194561.

23. Guarnaccia AD, Tansey WP. 2018. Moonlighting with WDR5: A Cellular Multitasker. J Clin Med 7.

24. Ang YS, Tsai SY, Lee DF, Monk J, Su J, Ratnakumar K, Ding J, Ge Y, Darr H, Chang B, Wang J, Rendl M, Bernstein E, Schaniel C, Lemischka IR. 2011. Wdr5 mediates self-renewal and reprogramming via the embryonic stem cell core transcriptional network. Cell 145:183-97.

25. Higa LA, Wu M, Ye T, Kobayashi R, Sun H, Zhang H. 2006. CUL4-DDB1 ubiquitin ligase interacts with multiple WD40-repeat proteins and regulates histone methylation. Nat Cell Biol 8:1277-83.

26. Lu K, Tao H, Si X, Chen Q. 2018. The Histone H3 Lysine 4 Presenter WDR5 as an Oncogenic Protein and Novel Epigenetic Target in Cancer. Front Oncol 8:502.

27. Krivtsov AV, Armstrong SA. 2007. MLL translocations, histone modifications and leukaemia stem-cell development. Nat Rev Cancer 7:823-33.

28. Sun Y, Bell JL, Carter D, Gherardi S, Poulos RC, Milazzo G, Wong JW, Al-Awar R, Tee AE, Liu PY, Liu B, Atmadibrata B, Wong M, Trahair T, Zhao Q, Shohet JM, Haupt Y, Schulte JH, Brown PJ, Arrowsmith CH, Vedadi M, MacKenzie KL, Huttelmaier S, Perini G, Marshall GM, Braithwaite A, Liu T. 2015. WDR5 Supports an N-Myc Transcriptional

Complex That Drives a Protumorigenic Gene Expression Signature in Neuroblastoma. Cancer Res 75:5143-54.

29. Thomas LR, Wang Q, Grieb BC, Phan J, Foshage AM, Sun Q, Olejniczak ET, Clark T, Dey S, Lorey S, Alicie B, Howard GC, Cawthon B, Ess KC, Eischen CM, Zhao Z, Fesik SW, Tansey WP. 2015. Interaction with WDR5 promotes target gene recognition and tumorigenesis by MYC. Mol Cell 58:440-52.

30. Klonou A, Chlamydas S, Piperi C. 2021. Structure, Activity and Function of the MLL2 (KMT2B) Protein Lysine Methyltransferase. Life (Basel) 11.

31. Hu D, Garruss AS, Gao X, Morgan MA, Cook M, Smith ER, Shilatifard A. 2013. The Mll2 branch of the COMPASS family regulates bivalent promoters in mouse embryonic stem cells. Nat Struct Mol Biol 20:1093-7.

32. Wang P, Lin C, Smith ER, Guo H, Sanderson BW, Wu M, Gogol M, Alexander T, Seidel C, Wiedemann LM, Ge K, Krumlauf R, Shilatifard A. 2009. Global analysis of H3K4 methylation defines MLL family member targets and points to a role for MLL1-mediated H3K4 methylation in the regulation of transcriptional initiation by RNA polymerase II. Mol Cell Biol 29:6074-85.

33. Kim D, Kim Y, Lee BB, Cho EY, Han J, Shim YM, Kim DH. 2021. Metformin Reduces Histone H3K4me3 at the Promoter Regions of Positive Cell Cycle Regulatory Genes in Lung Cancer Cells. Cancers (Basel) 13.

34. Wei S, Lu S, Liang L, Wang X, Li W, Li T, Chen L, Ju E, Zhang X, Lai Z, Huang Y, Lu X, Gao SJ. 2021. GRWD1-WDR5-MLL2 Epigenetic Complex Mediates H3K4me3 Mark and Is Essential for Kaposi's Sarcoma-Associated Herpesvirus-Induced Cellular Transformation. mBio 12:e0343121.

35. Rao RC, Dou Y. 2015. Hijacked in cancer: the KMT2 (MLL) family of methyltransferases. Nat Rev Cancer 15:334-46.

36. Andreu-Vieyra CV, Chen R, Agno JE, Glaser S, Anastassiadis K, Stewart AF, Matzuk MM. 2010. MLL2 is required in oocytes for bulk histone 3 lysine 4 trimethylation and transcriptional silencing. PLoS Biol 8.

37. Glaser S, Lubitz S, Loveland KL, Ohbo K, Robb L, Schwenk F, Seibler J, Roellig D, Kranz A, Anastassiadis K, Stewart AF. 2009. The histone 3 lysine 4 methyltransferase, Mll2, is only required briefly in development and spermatogenesis. Epigenetics Chromatin 2:5.

38. Glaser S, Schaft J, Lubitz S, Vintersten K, van der Hoeven F, Tufteland KR, Aasland R, Anastassiadis K, Ang SL, Stewart AF. 2006. Multiple epigenetic maintenance factors implicated by the loss of Mll2 in mouse development. Development 133:1423-32.

39. Kerimoglu C, Agis-Balboa RC, Kranz A, Stilling R, Bahari-Javan S, Benito-Garagorri E, Halder R, Burkhardt S, Stewart AF, Fischer A. 2013. Histone-methyltransferase MLL2 (KMT2B) is required for memory formation in mice. J Neurosci 33:3452-64.

40. Rous P. 1910. A Transmissible Avian Neoplasm. (Sarcoma of the Common Fowl.). J Exp Med 12:696-705.

41. Rous P. 1911. A Sarcoma of the Fowl Transmissible by an Agent Separable from the Tumor Cells. J Exp Med 13:397-411.

42. Martin D, Gutkind JS. 2008. Human tumor-associated viruses and new insights into the molecular mechanisms of cancer. Oncogene 27 Suppl 2:S31-42.

43. Moore PS, Chang Y. 2010. Why do viruses cause cancer? Highlights of the first century of human tumour virology. Nat Rev Cancer 10:878-89.

44. Duesberg PH, Vogt PK. 1970. Differences between the ribonucleic acids of transforming and nontransforming avian tumor viruses. Proc Natl Acad Sci U S A 67:1673-80.

45. Stehelin D, Varmus HE, Bishop JM, Vogt PK. 1976. DNA related to the transforming gene(s) of avian sarcoma viruses is present in normal avian DNA. Nature 260:170-3.

46. Mirvish ED, Shuda M. 2016. Strategies for Human Tumor Virus Discoveries: From Microscopic Observation to Digital Transcriptome Subtraction. Front Microbiol 7:676.

47. McLaughlin-Drubin ME, Munger K. 2008. Viruses associated with human cancer. Biochim Biophys Acta 1782:127-50.

48. Brown KD, Hostager BS, Bishop GA. 2001. Differential signaling and tumor necrosis factor receptor-associated factor (TRAF) degradation mediated by CD40 and the Epstein-Barr virus oncoprotein latent membrane protein 1 (LMP1). J Exp Med 193:943-54.

49. Kilger E, Kieser A, Baumann M, Hammerschmidt W. 1998. Epstein-Barr virus-mediated B-cell proliferation is dependent upon latent membrane protein 1, which simulates an activated CD40 receptor. EMBO J 17:1700-9.

50. Thomas JT, Laimins LA. 1998. Human papillomavirus oncoproteins E6 and E7 independently abrogate the mitotic spindle checkpoint. J Virol 72:1131-7.

51. Matsuoka M, Jeang KT. 2007. Human T-cell leukaemia virus type 1 (HTLV-1) infectivity and cellular transformation. Nat Rev Cancer 7:270-80.

52. Yoshida M. 2001. Multiple viral strategies of HTLV-1 for dysregulation of cell growth control. Annu Rev Immunol 19:475-96.

53. Sarid R, Olsen SJ, Moore PS. 1999. Kaposi's sarcoma-associated herpesvirus: epidemiology, virology, and molecular biology. Adv Virus Res 52:139-232.

54. Szajerka T, Jablecki J. 2007. Kaposi's sarcoma revisited. AIDS Rev 9:230-6.

55. Ye F, Lei X, Gao SJ. 2011. Mechanisms of Kaposi's Sarcoma-Associated Herpesvirus Latency and Reactivation. Adv Virol 2011.

56. Ahmed MM, Cushman CH, DeCaprio JA. 2021. Merkel Cell Polyomavirus: Oncogenesis in a Stable Genome. Viruses 14.

57. Arora R, Chang Y, Moore PS. 2012. MCV and Merkel cell carcinoma: a molecular success story. Curr Opin Virol 2:489-98.

58. Cheng J, Park DE, Berrios C, White EA, Arora R, Yoon R, Branigan T, Xiao T, Westerling T, Federation A, Zeid R, Strober B, Swanson SK, Florens L, Bradner JE, Brown M, Howley PM, Padi M, Washburn MP, DeCaprio JA. 2017. Merkel cell polyomavirus recruits MYCL to the EP400 complex to promote oncogenesis. PLoS Pathog 13:e1006668.

59. Cheng J, Rozenblatt-Rosen O, Paulson KG, Nghiem P, DeCaprio JA. 2013. Merkel cell polyomavirus large T antigen has growth-promoting and inhibitory activities. J Virol 87:6118-26.

60. Gaglia MM, Munger K. 2018. More than just oncogenes: mechanisms of tumorigenesis by human viruses. Curr Opin Virol 32:48-59.

61. Hanahan D. 2022. Hallmarks of Cancer: New Dimensions. Cancer Discov 12:31-46.

62. Hanahan D, Weinberg RA. 2000. The hallmarks of cancer. Cell 100:57-70.

63. Hanahan D, Weinberg RA. 2011. Hallmarks of cancer: the next generation. Cell 144:646-74.

64. Klein G. 2002. Perspectives in studies of human tumor viruses. Front Biosci 7:d268-74.

65. Morales-Sanchez A, Fuentes-Panana EM. 2014. Human viruses and cancer. Viruses 6:4047-79.

66. Radu O, Pantanowitz L. 2013. Kaposi sarcoma. Arch Pathol Lab Med 137:289-94.

67. Goncalves PH, Uldrick TS, Yarchoan R. 2017. HIV-associated Kaposi sarcoma and related diseases. AIDS 31:1903-1916.

68. Uppal T, Jha HC, Verma SC, Robertson ES. 2015. Chromatinization of the KSHV Genome During the KSHV Life Cycle. Cancers (Basel) 7:112-42.

69. Boshoff C. 2002. Kaposi's sarcoma biology. IUBMB Life 53:259-61.

70. Moore PS, Chang Y. 1998. Kaposi's sarcoma (KS), KS-associated herpesvirus, and the criteria for causality in the age of molecular biology. Am J Epidemiol 147:217-21.

71. Chang Y, Cesarman E, Pessin MS, Lee F, Culpepper J, Knowles DM, Moore PS. 1994. Identification of herpesvirus-like DNA sequences in AIDS-associated Kaposi's sarcoma. Science 266:1865-9.

72. Chen YB, Rahemtullah A, Hochberg E. 2007. Primary effusion lymphoma. Oncologist 12:569-76.

73. Gaidano G, Carbone A. 2001. Primary effusion lymphoma: a liquid phase lymphoma of fluid-filled body cavities. Adv Cancer Res 80:115-46.

74. Gessain A. 1997. [Human herpesvirus 8 and associated diseases: Kaposi's sarcoma, body cavity based lymphoma and multicentric Castleman disease: clinical and molecular epidemiology]. Bull Acad Natl Med 181:1023-34.

75. Kaplan LD. 2013. Human herpesvirus-8: Kaposi sarcoma, multicentric Castleman disease, and primary effusion lymphoma. Hematology Am Soc Hematol Educ Program 2013:103-8.

76. Ye X, Zhao Y, Karijolich J. 2019. The landscape of transcription initiation across latent and lytic KSHV genomes. PLoS Pathog 15:e1007852.

77. Purushothaman P, Dabral P, Gupta N, Sarkar R, Verma SC. 2016. KSHV Genome Replication and Maintenance. Front Microbiol 7:54.

78. Qin J, Li W, Gao SJ, Lu C. 2017. KSHV microRNAs: Tricks of the Devil. Trends Microbiol 25:648-661.

79. Komatsu T, Ballestas ME, Barbera AJ, Kaye KM. 2002. The KSHV latency-associated nuclear antigen: a multifunctional protein. Front Biosci 7:d726-30.

80. Uppal T, Banerjee S, Sun Z, Verma SC, Robertson ES. 2014. KSHV LANA--the master regulator of KSHV latency. Viruses 6:4961-98.

81. Ueda K. 2018. KSHV Genome Replication and Maintenance in Latency. Adv Exp Med Biol 1045:299-320.

82. Staudt MR, Dittmer DP. 2003. Viral latent proteins as targets for Kaposi's sarcoma and Kaposi's sarcoma-associated herpesvirus (KSHV/HHV-8) induced lymphoma. Curr Drug Targets Infect Disord 3:129-35.

83. Arvanitakis L, Mesri EA, Nador RG, Said JW, Asch AS, Knowles DM, Cesarman E. 1996. Establishment and characterization of a primary effusion (body cavity-based) lymphoma cell line (BC-3) harboring kaposi's sarcoma-associated herpesvirus (KSHV/HHV-8) in the absence of Epstein-Barr virus. Blood 88:2648-54.

84. Cannon JS, Ciufo D, Hawkins AL, Griffin CA, Borowitz MJ, Hayward GS, Ambinder RF. 2000. A new primary effusion lymphoma-derived cell line yields a highly infectious Kaposi's sarcoma herpesvirus-containing supernatant. J Virol 74:10187-93.

85. Komanduri KV, Luce JA, McGrath MS, Herndier BG, Ng VL. 1996. The natural history and molecular heterogeneity of HIV-associated primary malignant lymphomatous effusions. J Acquir Immune Defic Syndr Hum Retrovirol 13:215-26.

86. Menezes J, Leibold W, Klein G, Clements G. 1975. Establishment and characterization of an Epstein-Barr virus (EBC)-negative lymphoblastoid B cell line (BJA-B) from an exceptional, EBV-genome-negative African Burkitt's lymphoma. Biomedicine 22:276-84.

87. McAllister SC, Moses AV. 2007. Endothelial cell- and lymphocyte-based in vitro systems for understanding KSHV biology. Curr Top Microbiol Immunol 312:211-44.

88. An FQ, Folarin HM, Compitello N, Roth J, Gerson SL, McCrae KR, Fakhari FD, Dittmer DP, Renne R. 2006. Long-term-infected telomerase-immortalized endothelial cells: a model for Kaposi's sarcoma-associated herpesvirus latency in vitro and in vivo. J Virol 80:4833-46.

89. Lagunoff M, Bechtel J, Venetsanakos E, Roy AM, Abbey N, Herndier B, McMahon M, Ganem D. 2002. De novo infection and serial transmission of Kaposi's sarcoma-associated herpesvirus in cultured endothelial cells. J Virol 76:2440-8.

90. Moses AV, Fish KN, Ruhl R, Smith PP, Strussenberg JG, Zhu L, Chandran B, Nelson JA. 1999. Long-term infection and transformation of dermal microvascular endothelial cells by human herpesvirus 8. J Virol 73:6892-902.

91. Ciufo DM, Cannon JS, Poole LJ, Wu FY, Murray P, Ambinder RF, Hayward GS. 2001. Spindle cell conversion by Kaposi's sarcoma-associated herpesvirus: formation of colonies and plaques with mixed lytic and latent gene expression in infected primary dermal microvascular endothelial cell cultures. J Virol 75:5614-26.

92. Flore O, Rafii S, Ely S, O'Leary JJ, Hyjek EM, Cesarman E. 1998. Transformation of primary human endothelial cells by Kaposi's sarcoma-associated herpesvirus. Nature 394:588-92.

93. Hong YK, Foreman K, Shin JW, Hirakawa S, Curry CL, Sage DR, Libermann T, Dezube BJ, Fingeroth JD, Detmar M. 2004. Lymphatic reprogramming of blood vascular endothelium by Kaposi sarcoma-associated herpesvirus. Nat Genet 36:683-5.

94. Naranatt PP, Krishnan HH, Svojanovsky SR, Bloomer C, Mathur S, Chandran B. 2004. Host gene induction and transcriptional reprogramming in Kaposi's sarcoma-associated herpesvirus (KSHV/HHV-8)-infected endothelial, fibroblast, and B cells: insights into modulation events early during infection. Cancer Res 64:72-84.

95. Wang HW, Trotter MW, Lagos D, Bourboulia D, Henderson S, Makinen T, Elliman S, Flanagan AM, Alitalo K, Boshoff C. 2004. Kaposi sarcoma herpesvirus-induced cellular reprogramming contributes to the lymphatic endothelial gene expression in Kaposi sarcoma. Nat Genet 36:687-93.

96. Mutlu AD, Cavallin LE, Vincent L, Chiozzini C, Eroles P, Duran EM, Asgari Z, Hooper AT, La Perle KM, Hilsher C, Gao SJ, Dittmer DP, Rafii S, Mesri EA. 2007. In vivo-restricted and reversible malignancy induced by human herpesvirus-8 KSHV: a cell and animal model of virally induced Kaposi's sarcoma. Cancer Cell 11:245-58.

97. Jones T, Ye F, Bedolla R, Huang Y, Meng J, Qian L, Pan H, Zhou F, Moody R, Wagner B, Arar M, Gao SJ. 2012. Direct and efficient cellular transformation of primary rat mesenchymal precursor cells by KSHV. J Clin Invest 122:1076-81.

98. Parsons CH, Szomju B, Kedes DH. 2004. Susceptibility of human fetal mesenchymal stem cells to Kaposi sarcoma-associated herpesvirus. Blood 104:2736-8.

99. Wu W, Vieira J, Fiore N, Banerjee P, Sieburg M, Rochford R, Harrington W, Jr., Feuer G. 2006. KSHV/HHV-8 infection of human hematopoietic progenitor (CD34+) cells: persistence of infection during hematopoiesis in vitro and in vivo. Blood 108:141-51.

100. Jones T, Ramos da Silva S, Bedolla R, Ye F, Zhou F, Gao SJ. 2014. Viral cyclin promotes KSHV-induced cellular transformation and tumorigenesis by overriding contact inhibition. Cell Cycle 13:845-58.

101. Gruffaz M, Vasan K, Tan B, Ramos da Silva S, Gao SJ. 2017. TLR4-Mediated Inflammation Promotes KSHV-Induced Cellular Transformation and Tumorigenesis by Activating the STAT3 Pathway. Cancer Res 77:7094-7108.

102. He M, Yuan H, Tan B, Bai R, Kim HS, Bae S, Che L, Kim JS, Gao SJ. 2016. SIRT1-mediated downregulation of p27Kip1 is essential for overcoming contact inhibition of Kaposi's sarcoma-associated herpesvirus transformed cells. Oncotarget 7:75698-75711.

103. Ju E, Li T, Ramos da Silva S, Markazi A, Gao SJ. 2021. Reversible switching of primary cells between normal and malignant state by oncogenic virus KSHV and CRISPR/Cas9-mediated targeting of a major viral latent protein. J Med Virol 93:5065-5075.

104. Zhu Y, Ramos da Silva S, He M, Liang Q, Lu C, Feng P, Jung JU, Gao SJ. 2016. An Oncogenic Virus Promotes Cell Survival and Cellular Transformation by Suppressing Glycolysis. PLoS Pathog 12:e1005648.

105. Li T, Zhu Y, Cheng F, Lu C, Jung JU, Gao SJ. 2019. Oncogenic Kaposi's Sarcoma-Associated Herpesvirus Upregulates Argininosuccinate Synthase 1, a Rate-Limiting Enzyme of the Citrulline-Nitric Oxide Cycle, To Activate the STAT3 Pathway and Promote Growth Transformation. J Virol 93.

106. Liang D, Hu H, Li S, Dong J, Wang X, Wang Y, He L, He Z, Gao Y, Gao SJ, Lan K. 2014. Oncogenic herpesvirus KSHV Hijacks BMP-Smad1-Id signaling to promote tumorigenesis. PLoS Pathog 10:e1004253.

107. Moody R, Zhu Y, Huang Y, Cui X, Jones T, Bedolla R, Lei X, Bai Z, Gao SJ. 2013. KSHV microRNAs mediate cellular transformation and tumorigenesis by redundantly targeting cell growth and survival pathways. PLoS Pathog 9:e1003857.

108. Li T, Ju E, Gao SJ. 2019. Kaposi sarcoma-associated herpesvirus miRNAs suppress CASTOR1-mediated mTORC1 inhibition to promote tumorigenesis. J Clin Invest 129:3310-3323.

109. Zhu Y, Li T, Ramos da Silva S, Lee JJ, Lu C, Eoh H, Jung JU, Gao SJ. 2017. A Critical Role of Glutamine and Asparagine gamma-Nitrogen in Nucleotide Biosynthesis in Cancer Cells Hijacked by an Oncogenic Virus. mBio 8.

110. Gruffaz M, Yuan H, Meng W, Liu H, Bae S, Kim JS, Lu C, Huang Y, Gao SJ. 2019. CRISPR-Cas9 Screening of Kaposi's Sarcoma-Associated Herpesvirus-Transformed Cells Identifies XPO1 as a Vulnerable Target of Cancer Cells. mBio 10.

111. Hu J, Yang Y, Turner PC, Jain V, McIntyre LM, Renne R. 2014. LANA binds to multiple active viral and cellular promoters and associates with the H3K4methyltransferase hSET1 complex. PLoS Pathog 10:e1004240.

112. Pei Y, Wong JH, Robertson ES. 2020. Herpesvirus Epigenetic Reprogramming and Oncogenesis. Annu Rev Virol 7:309-331.

113. Campbell M, Yang WS, Yeh WW, Kao CH, Chang PC. 2020. Epigenetic Regulation of Kaposi's Sarcoma-Associated Herpesvirus Latency. Front Microbiol 11:850.

114. Gunther T, Grundhoff A. 2010. The epigenetic landscape of latent Kaposi sarcoma-associated herpesvirus genomes. PLoS Pathog 6:e1000935.

115. Toth Z, Maglinte DT, Lee SH, Lee HR, Wong LY, Brulois KF, Lee S, Buckley JD, Laird PW, Marquez VE, Jung JU. 2010. Epigenetic analysis of KSHV latent and lytic genomes. PLoS Pathog 6:e1001013.

116. Lu F, Day L, Gao SJ, Lieberman PM. 2006. Acetylation of the latency-associated nuclear antigen regulates repression of Kaposi's sarcoma-associated herpesvirus lytic transcription. J Virol 80:5273-82.

117. Chen HS, Lu F, Lieberman PM. 2013. Epigenetic regulation of EBV and KSHV latency. Curr Opin Virol 3:251-9.

118. Broussard G, Damania B. 2020. Regulation of KSHV Latency and Lytic Reactivation. Viruses 12.

119. Tan M, Li S, Juillard F, Chitas R, Custodio TF, Xue H, Szymula A, Sun Q, Liu B, Alvarez AL, Chen S, Huang J, Simas JP, McVey CE, Kaye KM. 2021. MLL1 is regulated by KSHV LANA and is important for virus latency. Nucleic Acids Res 49:12895-12911.

120. Toth Z, Brulois K, Lee HR, Izumiya Y, Tepper C, Kung HJ, Jung JU. 2013. Biphasic euchromatin-to-heterochromatin transition on the KSHV genome following de novo infection. PLoS Pathog 9:e1003813.

121. Naik NG, Nguyen TH, Roberts L, Fischer LT, Glickman K, Golas G, Papp B, Toth Z. 2020. Epigenetic factor siRNA screen during primary KSHV infection identifies novel host restriction factors for the lytic cycle of KSHV. PLoS Pathog 16:e1008268.

122. Geng Z, Gao Z. 2020. Mammalian PRC1 Complexes: Compositional Complexity and Diverse Molecular Mechanisms. Int J Mol Sci 21.

123. Toth Z, Papp B, Brulois K, Choi YJ, Gao SJ, Jung JU. 2016. LANA-Mediated Recruitment of Host Polycomb Repressive Complexes onto the KSHV Genome during De Novo Infection. PLoS Pathog 12:e1005878.

124. Lu F, Stedman W, Yousef M, Renne R, Lieberman PM. 2010. Epigenetic regulation of Kaposi's sarcoma-associated herpesvirus latency by virus-encoded microRNAs that target Rta and the cellular Rbl2-DNMT pathway. J Virol 84:2697-706.

125. Yang WS, Campbell M, Chang PC. 2017. SUMO modification of a heterochromatin histone demethylase JMJD2A enables viral gene transactivation and viral replication. PLoS Pathog 13:e1006216.

126. Yang WS, Hsu HW, Campbell M, Cheng CY, Chang PC. 2015. K-bZIP Mediated SUMO-2/3 Specific Modification on the KSHV Genome Negatively Regulates Lytic Gene Expression and Viral Reactivation. PLoS Pathog 11:e1005051.

127. Aneja KK, Yuan Y. 2017. Reactivation and Lytic Replication of Kaposi's Sarcoma-Associated Herpesvirus: An Update. Front Microbiol 8:613.

128. He M, Zhang W, Bakken T, Schutten M, Toth Z, Jung JU, Gill P, Cannon M, Gao SJ. 2012. Cancer angiogenesis induced by Kaposi sarcoma-associated herpesvirus is mediated by EZH2. Cancer Res 72:3582-92.

129. Kim KY, Huerta SB, Izumiya C, Wang DH, Martinez A, Shevchenko B, Kung HJ, Campbell M, Izumiya Y. 2013. Kaposi's sarcoma-associated herpesvirus (KSHV) latency-associated nuclear antigen regulates the KSHV epigenome by association with the histone demethylase KDM3A. J Virol 87:6782-93.

130. Sakakibara S, Ueda K, Nishimura K, Do E, Ohsaki E, Okuno T, Yamanishi K. 2004. Accumulation of heterochromatin components on the terminal repeat sequence of Kaposi's sarcoma-associated herpesvirus mediated by the latency-associated nuclear antigen. J Virol 78:7299-310.

131. Shamay M, Krithivas A, Zhang J, Hayward SD. 2006. Recruitment of the de novo DNA methyltransferase Dnmt3a by Kaposi's sarcoma-associated herpesvirus LANA. Proc Natl Acad Sci U S A 103:14554-9.

132. Xu C, Min J. 2011. Structure and function of WD40 domain proteins. Protein Cell 2:202-14.

133. Li D, Roberts R. 2001. WD-repeat proteins: structure characteristics, biological function, and their involvement in human diseases. Cell Mol Life Sci 58:2085-97.

134. Fong HK, Hurley JB, Hopkins RS, Miake-Lye R, Johnson MS, Doolittle RF, Simon MI. 1986. Repetitive segmental structure of the transducin beta subunit: homology with the CDC4 gene and identification of related mRNAs. Proc Natl Acad Sci U S A 83:2162-6.

135. Smith TF, Gaitatzes C, Saxena K, Neer EJ. 1999. The WD repeat: a common architecture for diverse functions. Trends Biochem Sci 24:181-5.

136. Gratenstein K, Heggestad AD, Fortun J, Notterpek L, Pestov DG, Fletcher BS. 2005. The WD-repeat protein GRWD1: potential roles in myeloid differentiation and ribosome biogenesis. Genomics 85:762-73.

137. Weinstein J. 1997. Cell cycle-regulated expression, phosphorylation, and degradation of p55Cdc. A mammalian homolog of CDC20/Fizzy/slp1. J Biol Chem 272:28501-11.

138. Rots NY, Liu M, Anderson EC, Freedman LP. 1998. A differential screen for ligand-regulated genes: identification of HoxA10 as a target of vitamin D3 induction in myeloid leukemic cells. Mol Cell Biol 18:1911-8.

139. Aizawa M, Sugimoto N, Watanabe S, Yoshida K, Fujita M. 2016. Nucleosome assembly and disassembly activity of GRWD1, a novel Cdt1-binding protein that promotes pre-replication complex formation. Biochim Biophys Acta 1863:2739-2748.

140. Sugimoto N, Maehara K, Yoshida K, Yasukouchi S, Osano S, Watanabe S, Aizawa M, Yugawa T, Kiyono T, Kurumizaka H, Ohkawa Y, Fujita M. 2015. Cdt1-binding protein GRWD1 is a novel histone-binding protein that facilitates MCM loading through its influence on chromatin architecture. Nucleic Acids Res 43:5898-911.

141. Iouk TL, Aitchison JD, Maguire S, Wozniak RW. 2001. Rrb1p, a yeast nuclear WD-repeat protein involved in the regulation of ribosome biosynthesis. Mol Cell Biol 21:1260-71.

142. Killian A, Le Meur N, Sesboue R, Bourguignon J, Bougeard G, Gautherot J, Bastard C, Frebourg T, Flaman JM. 2004. Inactivation of the RRB1-Pescadillo pathway involved in ribosome biogenesis induces chromosomal instability. Oncogene 23:8597-602.

143. Fujiyama H, Tsuji T, Hironaka K, Yoshida K, Sugimoto N, Fujita M. 2020. GRWD1 directly interacts with p53 and negatively regulates p53 transcriptional activity. J Biochem 167:15-24.

144. Ichikawa MK, Saitoh M. 2022. Direct and indirect roles of GRWD1 in the inactivation of p53 in cancer. J Biochem doi:10.1093/jb/mvac010.

145. Kayama K, Watanabe S, Takafuji T, Tsuji T, Hironaka K, Matsumoto M, Nakayama KI, Enari M, Kohno T, Shiraishi K, Kiyono T, Yoshida K, Sugimoto N, Fujita M. 2017. GRWD1 negatively regulates p53 via the RPL11-MDM2 pathway and promotes tumorigenesis. EMBO Rep 18:123-137.

146. Takafuji T, Kayama K, Sugimoto N, Fujita M. 2017. GRWD1, a new player among oncogenesis-related ribosomal/nucleolar proteins. Cell Cycle 16:1397-1403.

147. Tomczak K, Czerwinska P, Wiznerowicz M. 2015. The Cancer Genome Atlas (TCGA): an immeasurable source of knowledge. Contemp Oncol (Pozn) 19:A68-77.

148. Tada S. 2007. Cdt1 and geminin: role during cell cycle progression and DNA damage in higher eukaryotes. Front Biosci 12:1629-41.

149. Zhang H. 2021. Regulation of DNA Replication Licensing and Re-Replication by Cdt1. Int J Mol Sci 22.

150. Pozo PN, Cook JG. 2016. Regulation and Function of Cdt1; A Key Factor in Cell Proliferation and Genome Stability. Genes (Basel) 8.

151. Sugimoto N, Kitabayashi I, Osano S, Tatsumi Y, Yugawa T, Narisawa-Saito M, Matsukage A, Kiyono T, Fujita M. 2008. Identification of novel human Cdt1-binding proteins by a proteomics approach: proteolytic regulation by APC/CCdh1. Mol Biol Cell 19:1007-21.

152. Du YC, Stillman B. 2002. Yph1p, an ORC-interacting protein: potential links between cell proliferation control, DNA replication, and ribosome biogenesis. Cell 109:835-48.

153. Levine AJ, Oren M. 2009. The first 30 years of p53: growing ever more complex. Nat Rev Cancer 9:749-58.

154. Miliani de Marval PL, Zhang Y. 2011. The RP-Mdm2-p53 pathway and tumorigenesis. Oncotarget 2:234-8.

155. Bursac S, Brdovcak MC, Donati G, Volarevic S. 2014. Activation of the tumor suppressor p53 upon impairment of ribosome biogenesis. Biochim Biophys Acta 1842:817-30.

156. Moll UM, Petrenko O. 2003. The MDM2-p53 interaction. Mol Cancer Res 1:1001-8.

157. Li C, Wong WH. 2001. Model-based analysis of oligonucleotide arrays: expression index computation and outlier detection. Proc Natl Acad Sci U S A 98:31-6.

158. Kazachenka A, Bertozzi TM, Sjoberg-Herrera MK, Walker N, Gardner J, Gunning R, Pahita E, Adams S, Adams D, Ferguson-Smith AC. 2018. Identification, Characterization, and Heritability of Murine Metastable Epialleles: Implications for Non-genetic Inheritance. Cell 175:1259-1271 e13.

159. Langmead B, Salzberg SL. 2012. Fast gapped-read alignment with Bowtie 2. Nat Methods 9:357-9.

160. Ross-Innes CS, Stark R, Teschendorff AE, Holmes KA, Ali HR, Dunning MJ, Brown GD, Gojis O, Ellis IO, Green AR, Ali S, Chin SF, Palmieri C, Caldas C, Carroll JS. 2012. Differential oestrogen receptor binding is associated with clinical outcome in breast cancer. Nature 481:389-93.

161. McCarthy DJ, Chen Y, Smyth GK. 2012. Differential expression analysis of multifactor RNA-Seq experiments with respect to biological variation. Nucleic Acids Res 40:4288-97.

162. Yu G, Wang LG, He QY. 2015. ChIPseeker: an R/Bioconductor package for ChIP peak annotation, comparison and visualization. Bioinformatics 31:2382-3.

163. Masuda Y, Takahashi H, Sato S, Tomomori-Sato C, Saraf A, Washburn MP, Florens L, Conaway RC, Conaway JW, Hatakeyama S. 2015. TRIM29 regulates the assembly of DNA repair proteins into damaged chromatin. Nat Commun 6:7299.

164. Paquin KL, Mamrak NE, Garzon JL, Cantres-Velez JA, Azzinaro PA, Vuono EA, Lima KE, Camberg JL, Howlett NG. 2019. FANCD2 Binding to H4K20me2 via a Methyl-Binding Domain Is Essential for Efficient DNA Cross-Link Repair. Mol Cell Biol 39.

165. Higgs MR, Sato K, Reynolds JJ, Begum S, Bayley R, Goula A, Vernet A, Paquin KL, Skalnik DG, Kobayashi W, Takata M, Howlett NG, Kurumizaka H, Kimura H, Stewart GS. 2018. Histone Methylation by SETD1A Protects Nascent DNA through the Nucleosome Chaperone Activity of FANCD2. Mol Cell 71:25-41 e6.

166. Hunt LC, Stover J, Haugen B, Shaw TI, Li Y, Pagala VR, Finkelstein D, Barton ER, Fan Y, Labelle M, Peng J, Demontis F. 2019. A Key Role for the Ubiquitin Ligase UBR4 in Myofiber Hypertrophy in Drosophila and Mice. Cell Rep 28:1268-1281 e6.

167. Palmbos PL, Wang L, Yang H, Wang Y, Leflein J, Ahmet ML, Wilkinson JE, Kumar-Sinha C, Ney GM, Tomlins SA, Daignault S, Kunju LP, Wu XR, Lotan Y, Liebert M, Ljungman ME, Simeone DM. 2015. ATDC/TRIM29 Drives Invasive Bladder Cancer Formation through miRNA-Mediated and Epigenetic Mechanisms. Cancer Res 75:5155-66.

168. Enot DP, Vacchelli E, Jacquelot N, Zitvogel L, Kroemer G. 2018. TumGrowth: An open-access web tool for the statistical analysis of tumor growth curves. Oncoimmunology 7:e1462431.

169. Orchard S, Ammari M, Aranda B, Breuza L, Briganti L, Broackes-Carter F, Campbell NH, Chavali G, Chen C, del-Toro N, Duesbury M, Dumousseau M, Galeota E, Hinz U, Iannuccelli M, Jagannathan S, Jimenez R, Khadake J, Lagreid A, Licata L, Lovering RC, Meldal B, Melidoni AN, Milagros M, Peluso D, Perfetto L, Porras P, Raghunath A, Ricard-Blum S, Roechert B, Stutz A, Tognolli M, van Roey K, Cesareni G, Hermjakob H. 2014. The MIntAct project--IntAct as a common curation platform for 11 molecular interaction databases. Nucleic Acids Res 42:D358-63.

170. Oughtred R, Stark C, Breitkreutz BJ, Rust J, Boucher L, Chang C, Kolas N, O'Donnell L, Leung G, McAdam R, Zhang F, Dolma S, Willems A, Coulombe-Huntington J, Chatr-Aryamontri A, Dolinski K, Tyers M. 2019. The BioGRID interaction database: 2019 update. Nucleic Acids Res 47:D529-D541.

171. Oughtred R, Rust J, Chang C, Breitkreutz BJ, Stark C, Willems A, Boucher L, Leung G, Kolas N, Zhang F, Dolma S, Coulombe-Huntington J, Chatr-Aryamontri A, Dolinski K, Tyers M. 2021. The BioGRID database: A comprehensive biomedical resource of curated protein, genetic, and chemical interactions. Protein Sci 30:187-200.

172. Flanagan JM. 2007. Host epigenetic modifications by oncogenic viruses. Br J Cancer 96:183-8.

173. Fang Z, Gong C, Yu S, Zhou W, Hassan W, Li H, Wang X, Hu Y, Gu K, Chen X, Hong B, Bao Y, Chen X, Zhang X, Liu H. 2018. NFYB-induced high expression of E2F1 contributes to oxaliplatin resistance in colorectal cancer via the enhancement of CHK1 signaling. Cancer Lett 415:58-72.

174. Zhu H, Wang Y, Wei T, Zhao X, Li F, Li Y, Wang F, Cai Y, Jin J. 2021. KAT8/MOF-Mediated Anti-Cancer Mechanism of Gemcitabine in Human Bladder Cancer Cells. Biomol Ther (Seoul) 29:184-194.

175. Kim JY, Yu J, Abdulkadir SA, Chakravarti D. 2016. KAT8 Regulates Androgen Signaling in Prostate Cancer Cells. Mol Endocrinol 30:925-36.

176. Kim H, Ronai ZA. 2020. PRMT5 function and targeting in cancer. Cell Stress 4:199-215.

177. Yenerall P, Das AK, Wang S, Kollipara RK, Li LS, Villalobos P, Flaming J, Lin YF, Huffman K, Timmons BC, Gilbreath C, Sonavane R, Kinch LN, Rodriguez-Canales J, Moran C, Behrens C, Hirasawa M, Takata T, Murakami R, Iwanaga K, Chen BPC, Grishin NV, Raj GV, Wistuba, II, Minna JD, Kittler R. 2020. RUVBL1/RUVBL2 ATPase Activity Drives PAQosome Maturation, DNA Replication and Radioresistance in Lung Cancer. Cell Chem Biol 27:105-121 e14.

178. Yoshino S, Matsui Y, Fukui Y, Seki M, Yamaguchi K, Kanamori A, Saitoh Y, Shimamura T, Suzuki Y, Furukawa Y, Kaneko S, Seiki M, Murakami Y, Inoue JI, Sakamoto T. 2020. EXOSC9 depletion attenuates P-body formation, stress resistance, and tumorigenicity of cancer cells. Sci Rep 10:9275.

179. Silmon de Monerri NC, Kim K. 2014. Pathogens hijack the epigenome: a new twist on host-pathogen interactions. Am J Pathol 184:897-911.

180. Gunther T, Grundhoff A. 2017. Epigenetic manipulation of host chromatin by Kaposi sarcoma-associated herpesvirus: a tumor-promoting factor? Curr Opin Virol 26:104-111.

181. Lee HR, Brulois K, Wong L, Jung JU. 2012. Modulation of Immune System by Kaposi's Sarcoma-Associated Herpesvirus: Lessons from Viral Evasion Strategies. Front Microbiol 3:44.

182. Di Bartolo DL, Cannon M, Liu YF, Renne R, Chadburn A, Boshoff C, Cesarman E. 2008. KSHV LANA inhibits TGF-beta signaling through epigenetic silencing of the TGF-beta type II receptor. Blood 111:4731-40.

183. Goudarzi KM, Lindstrom MS. 2016. Role of ribosomal protein mutations in tumor development (Review). Int J Oncol 48:1313-24.

184. Pecoraro A, Pagano M, Russo G, Russo A. 2021. Ribosome Biogenesis and Cancer: Overview on Ribosomal Proteins. Int J Mol Sci 22.

185. Zhou X, Liao WJ, Liao JM, Liao P, Lu H. 2015. Ribosomal proteins: functions beyond the ribosome. J Mol Cell Biol 7:92-104.

186. Cho J, Park J, Shin SC, Kim JH, Kim EE, Song EJ. 2020. Ribosomal protein S2 interplays with MDM2 to induce p53. Biochem Biophys Res Commun 523:542-547.

187. Dong Z, Jiang H, Liang S, Wang Y, Jiang W, Zhu C. 2019. Ribosomal Protein L15 is involved in Colon Carcinogenesis. Int J Med Sci 16:1132-1141.

188. Deisenroth C, Franklin DA, Zhang Y. 2016. The Evolution of the Ribosomal Protein-MDM2-p53 Pathway. Cold Spring Harb Perspect Med 6.

189. Zhang Y, Wolf GW, Bhat K, Jin A, Allio T, Burkhart WA, Xiong Y. 2003. Ribosomal protein L11 negatively regulates oncoprotein MDM2 and mediates a p53-dependent ribosomal-stress checkpoint pathway. Mol Cell Biol 23:8902-12.

190. Lohrum MA, Ludwig RL, Kubbutat MH, Hanlon M, Vousden KH. 2003. Regulation of HDM2 activity by the ribosomal protein L11. Cancer Cell 3:577-87.

191. Dai MS, Lu H. 2004. Inhibition of MDM2-mediated p53 ubiquitination and degradation by ribosomal protein L5. J Biol Chem 279:44475-82.